Sphingolipids Modulate the Inflammatory Response and Muscle Function in Mdx Mice

Jonathan Adam Doering

Thesis to the faculty of the Virginia Polytechnic Institute and State University in partial fulfillment of the requirements for the degree of

Master of Science

In

Human Nutrition, Foods, and Exercise

Robert W. Grange, Committee Chair

Eva M. Schmelz

Klaus D. Elgert

June 20, 2013

Blacksburg, Virginia

Keywords: Duchenne Muscular Dystrophy, mdx, inflammation, sphingolipids, muscle function

Sphingolipids Modulate the Inflammatory Response and Muscle Function in Mdx Mice

Jonathan Adam Doering

Abstract

Duchenne Muscular Dystrophy (DMD) is characterized by progressive muscle degeneration and a chronic inflammatory response. Sphingolipid metabolites are associated with the generation or perpetuation of low-grade chronic inflammation critical in atherosclerosis, obesity and cancer. Dietary sphingolipids, however, can suppress intestinal inflammation. We hypothesized that dietary sphingomyelin (SM) from bovine milk can modulate the inflammatory signature and improve muscle function in mdx mice, a model of DMD. C57BL10 (WT) and mdx mice were fed AIN 76A diet ± 0.1% SM for 7 weeks starting at age 4 weeks (n=10/group: WT, WT + S, mdx, mdx + S). At ages 5, 7, and 9 weeks, ankle flexor torque was determined *in vivo*. Mice were euthanized at 11 wks. Serum creatine kinase and extensor digitorum longus (EDL) contractile properties *in vitro* were determined; Tibialis Anterior (TA) inflammatory markers were profiled by qRT-PCR; TA sections were stained with H&E and immunohistochemistry for p-Akt was performed. At age 9 weeks, *in vivo* ankle flexor torque at stimulation frequencies 50-150 Hz was greater in mdx+S vs. mdx ($P=0.0160$) and WT ($P<0.0001$). At 11 wks, only WT+S EDL stress *in vitro* was greater than all other groups at 50-150 Hz. The *in vitro* relative stress-frequency relationship of mdx+S EDL was left shifted from the other treatment groups. Inflammatory genetic markers were increased in mdx+S mice. These data suggest treatment of mdx mice with 0.1% SM improves ankle flexor torque *in vivo*, causes a left shift of the stress-frequency relationship *in vitro*, and modulates the inflammatory gene signature.

Acknowledgements

"There is nothing either good or bad, but thinking makes it so"-William Shakespeare

First and foremost, I would like to thank my family: my parents, Mark and Gretta Doering for their unconditional love and support through all the challenges and difficulties throughout my life, especially when times were the worst (and all the money that came with the challenges!); my brother Andrew, for being a best friend, rival and someone I can always talk with; and lastly, my brother Bradley for being a constant inspiration and such an integral part of my pursuits in academia.

Next, I would like to thank my committee: my teacher, advisor, and friend Dr. Robert Grange for not only giving me the opportunity to pursue my goals, but for always providing the right push and advice when I needed it the most (and your seemingly unlimited patience!); Dr. Eva Schmelz, for your great insights and instruction on laboratory techniques and your great sense of humor which always cheered me up when things were difficult. Finally, Dr. Klaus Elgert for instilling in me your appreciation for scientific inquiry and exploration, as well as your kind suggestions and advice. My thanks to all of you for your patience and support during my studies!

Special thanks go to all the undergraduate students who have assisted in the lab. Alex, Becky, Sarah, Greg, Brittany (you know who you are), you made the days pass quickly and your assistance with all the procedures (especially that microarray analysis) was invaluable and it was truly a pleasure to get to know each of you and your goals. I hope to watch as you too develop your personal careers.

Special thanks go to Michele Lewis, my first and only TA advisor during my thesis studies. I learned much during my time as your TA and I greatly appreciated the opportunities you provided me to teach class and interact with students. It was a wonderful experience that I will carry fondly through my academic career.

Finally, and most importantly, I would like to thank my wonderful wife, Nichole. You have stood by me and supported me through each step of this process. You never let me quit and you continue to push me every day to be a better person. This first year of marriage has been a wonderful experience, and I cannot wait for our next stage in life!

Table of Contents

List of Figures

List of Tables

Chapter 1: Introduction

Duchenne muscular dystrophy (DMD) is a severe muscle wasting disease that affects 1 in 3500 males [6]. The disease is characterized by loss of the protein dystrophin from the cytosolic surface of the sarcolemma of muscle cells. In addition, other proteins of the dystrophin-glycoprotein complex (DGC) are absent [6]. In the absence of the DGC, muscle cells undergo cycles of degeneration and regeneration, and are susceptible to contraction-induced injury [7, 8]. Prolonged cycles of degeneration and regeneration leads to progressive loss of muscle function, Ultimately, afflicted boys are unable to walk by adolescence, and death occurs by the mid-20s due to cardiac or respiratory failure [7]. While the primary genetic mutations causing the lack of dystrophin and associated proteins have been elucidated, the mechanisms of disease onset and progression are not well understood [9]. Understanding these mechanisms would assist in the development of novel treatment strategies that could slow or halt the disease.

Loss of dystrophin results from spontaneous mutations of its gene, one of the largest sequenced to date [10]. The dystrophin gene is located at locus p21 of the X-chromosome, and yields several different isoforms, each of which may be present in different tissues [11]. In DMD, loss of the skeletal muscle isoform and DGC lead to severe pathophysiology [6]. The association of dystrophin and the DGC with the sarcolemma provides a stabilizing link between the extracellular matrix and the cytoskeletal surface of the sarcolemma [6]. The predominant theory of disease onset suggests the lack of dystrophin and the DGC disrupts the mechanical linkage between the sarcolemma and the cellular cytoskeleton, which impairs sarcolemmal strength [6]. Loss of this mechanical linkage is considered to cause tears along the sarcolemmal surface and the unregulated exchange of ions between the muscle and the extracellular matrix. In response, the immune system is activated for repair [9]. Although damaged muscle fibers undergo repair by satellite cells, dystrophin is not replaced, and repair is never complete. This absence leads to prolonged cycles of degeneration and regeneration. Eventually, satellite cells used to replace damaged muscle fibers are

exhausted and damaged muscle tissue is eventually replaced by fatty and connective tissue [12].

While dystrophin deficiency is the primary cause of DMD, secondary mechanisms may explain why loss of dystrophin in humans leads to death but not in mdx mice, a model of DMD [13]. Inflammation responds as a natural repair mechanism; however, its precise role in the pathophysiology of DMD is unclear. Current immunosuppression therapy with corticosteroids (i.e., prednisone) prolongs ambulation in DMD patients and improves muscle strength, but does not reduce inflammatory cell infiltration [14]; this effect is not typically observed in non-DMD patients. A better understanding of the inflammatory signaling pathways could facilitate specific therapies for DMD.

Inflammatory cytokines such as TNF-alpha and transcription factors like NF-kB have been well described in mdx mice [13, 15, 16]. Investigators have reported on the basis of gene microarray studies, a clear inflammatory response that is defined by elevated levels of cytokines, chemokines, and other inflammatory genetic markers [13]. One aim of this study was to determine the activation of Akt, a common secondary messenger, and the subsequent signal cascade that increases activity of NF-kB and the inflammatory response [17, 18].

A potential treatment option to ameliorate the inflammatory response may be evident in the family of bioactive lipids known as sphingolipids. Previously thought to provide only structure to cell membranes, sphingolipids also drive cell signaling [19]. Metabolized dietary sphingolipids represent a distinct family of molecules with both pro- and anti-inflammatory properties [19, 20]. From an anti-inflammatory perspective, sphingolipid metabolites within the cell may inhibit Akt (Protein kinase B), an activator of NF-kB, and thereby reduce the overall inflammatory response [20, 21]. Meanwhile, pro-inflammatory sphingolipid metabolites within the cell can activate Akt, or act upon their own receptors on the cell surface [19]. Normally, the interaction of pro- and anti-inflammatory sphingolipids are highly regulated [22]. However, when increased levels of sphingolipids are introduced into the diet, anti-inflammatory metabolites are elevated until they are broken down into their pro-inflammatory counterparts, or degraded.

Current research exploring this interplay shows that in a variety of cancers, the inflammatory response is slowed so that earlier less severe stages of the disease last longer [23, 24]. This beneficial modulation of the inflammatory response by sphingolipids may also be advantageous in DMD.

Statement of Problem

DMD is caused by mutations in the gene that encodes the protein dystrophin, resulting in cycles of muscle fiber degeneration and regeneration, with the outcome that muscle function is severely compromised. The mechanisms behind the pathophysiology of the disease are unclear, but an inflammatory response likely contributes, both positively and negatively. Dietary sphingolipids readily available in many foods could potentially suppress the inflammatory response. Furthermore, the attenuated inflammatory response could improve muscle function. The potential modulatory effects of dietary sphingolipids on the pathophysiology of DMD have not been examined. The purpose of this study was to determine if dietary sphingolipids could attenuate the inflammatory response and subsequently improve muscle function in the mdx male mouse, a common model of DMD.

Specific Aims

1. To determine if male mdx mice aged 80 days (~11 weeks) exhibit a decreased inflammatory response if fed chow supplemented with dietary sphingolipids. Primary method: qRT-PCR was used to quantify specific genetic inflammatory markers previously identified in a preliminary study (Appendix A).
2. To determine if activation of Akt (by phosphorylation) is decreased by sphingolipid treatment. Primary method: immunohistochemistry was used to identify localization of activated Akt.
3. To determine if sphingolipid treatment improves muscle contractile function, decreases sarcolemmal membrane leakiness, and decreases the number of regenerating fibers. Primary methods: determine contractile properties *in vivo* during the 4 weeks of feeding and then *in vitro* at sacrifice; determine serum creatine kinase content by commercial kit; determine the numbers of centralized nuclei by H&E staining.

Main Hypotheses

1. Sphingolipid treatment will reduce the inflammatory response by promoting expression of anti-inflammatory molecules, while reducing those that are pro-inflammatory.
2. Sphingolipid treatment will inhibit phosphorylation of Akt, reducing p-Akt content.
3. Sphingolipid treatment will reduce the inflammatory response such that contractile/mechanical properties of the EDL muscles will improve over time, and serum CK levels and numbers of centralized nuclei will be reduced.

Specific Null Hypotheses

H_{01}: Tibialis Anterior (TA) mRNA expression profiles will not differ between muscles of control (C57/BL10) and mdx mice fed normal chow (AIN 76A).

H_{02}: TA mRNA expression profiles will not differ between control fed normal chow and control fed chow supplemented with sphingolipids.

H_{03}: TA mRNA expression profiles will not differ between mdx mice fed normal chow and mdx mice fed chow supplemented with sphingolipids.

H_{04}: TA mRNA expression profiles will not differ between normal chow fed mice and normal chow supplemented with sphingolipids.

H_{05}: Percent centralized nuclei will not differ between muscles of control and mdx mice fed normal chow

H_{06}: Percent centralized nuclei will not differ between control fed normal chow and control fed normal chow supplemented with sphingolipids

H_{07}: Percent centralized nuclei will not differ between mdx mice fed normal chow and mdx mice fed normal chow supplemented with sphingolipids.

H_{08}: Percent centralized nuclei will not differ between mice fed normal chow and mice fed normal chow supplemented with sphingolipids.

H_{09}: *In vivo* lower limb flexor contractile responses will not differ between muscles of control and mdx mice fed normal chow.

H_{10}: *In vivo* lower limb flexor contractile responses will not differ between control fed normal chow and control fed normal chow supplemented with sphingolipids.

H_{11}: *In vivo* lower limb flexor contractile responses will not differ between mdx mice fed normal chow and mdx mice fed normal chow supplemented with sphingolipids.

H_{12}: *In vivo* lower limb flexor contractile responses will not differ between mice fed normal chow and mice fed normal chow supplemented with sphingolipids

H_{13}: *In vivo* lower limb flexor contractile responses will not differ between ages of mice (at 5, 7, and 9 weeks of age).

H_{14}: *In vitro* EDL contractile responses will not differ between muscles of control and mdx mice fed normal chow.

H_{15}: *In vitro* EDL contractile responses will not differ between control fed normal chow and control fed normal chow supplemented with sphingolipids.

H_{16}: *In vitro* EDL contractile responses will not differ between mdx mice fed normal chow and mdx mice fed normal chow supplemented with sphingolipids.

H_{17}: *In vitro* EDL contractile responses will not differ between mice fed normal chow and mice fed normal chow supplemented with sphingolipids.

H_{18}: *In vitro* EDL contractile responses will not differ between in vivo stimulated leg and the non-stimulated leg.

Chapter 2: Literature Review

Section A: Fundamental Contractile Properties

A.1- Introduction

This thesis seeks to determine if dietary sphingolipids can decrease the inflammatory response and improve skeletal muscle contractile function in mdx male mice, a model of Duchenne Muscular Dystrophy (DMD). The literature review is organized in the order of data collection. In Section A, properties of non-diseased skeletal muscle will be reviewed. In Section B, the changes in these properties in dystrophic muscles of humans and mice, and effects of muscle injury will be reviewed. In Section C, a basic review of the inflammatory response will be presented. Finally, in Section D, dietary sphingolipids and their role in modulating the inflammatory response will be examined.

A.2- Skeletal Muscle Hierarchy

Humans contain three types of muscle: Skeletal, smooth, and cardiac. Both smooth and cardiac muscles are regulated by the autonomic nervous system, independent of conscious control. Functions include a regular heart beat (cardiac), peristalsis (smooth), sphincter control (smooth), viscoelasticity of blood vessels (smooth), and a variety of other responses. Skeletal muscle is controlled by the somatic nervous system, which provides conscious control. Contraction of skeletal muscle provides locomotion, posture, and heat regulation. In a disease such as DMD, skeletal muscles lose contractile function because there are inherent changes in the muscle, independent of nervous regulation. Simply put: the muscles can be activated but they do not respond normally.

Skeletal muscle is made of individual component muscle cells known as muscle fibers. In humans, fibers are multinucleated cylindrical cells that can vary in diameter from 10µm to over 60µm [25]. Many fibers can be arranged to form a fascicle (not

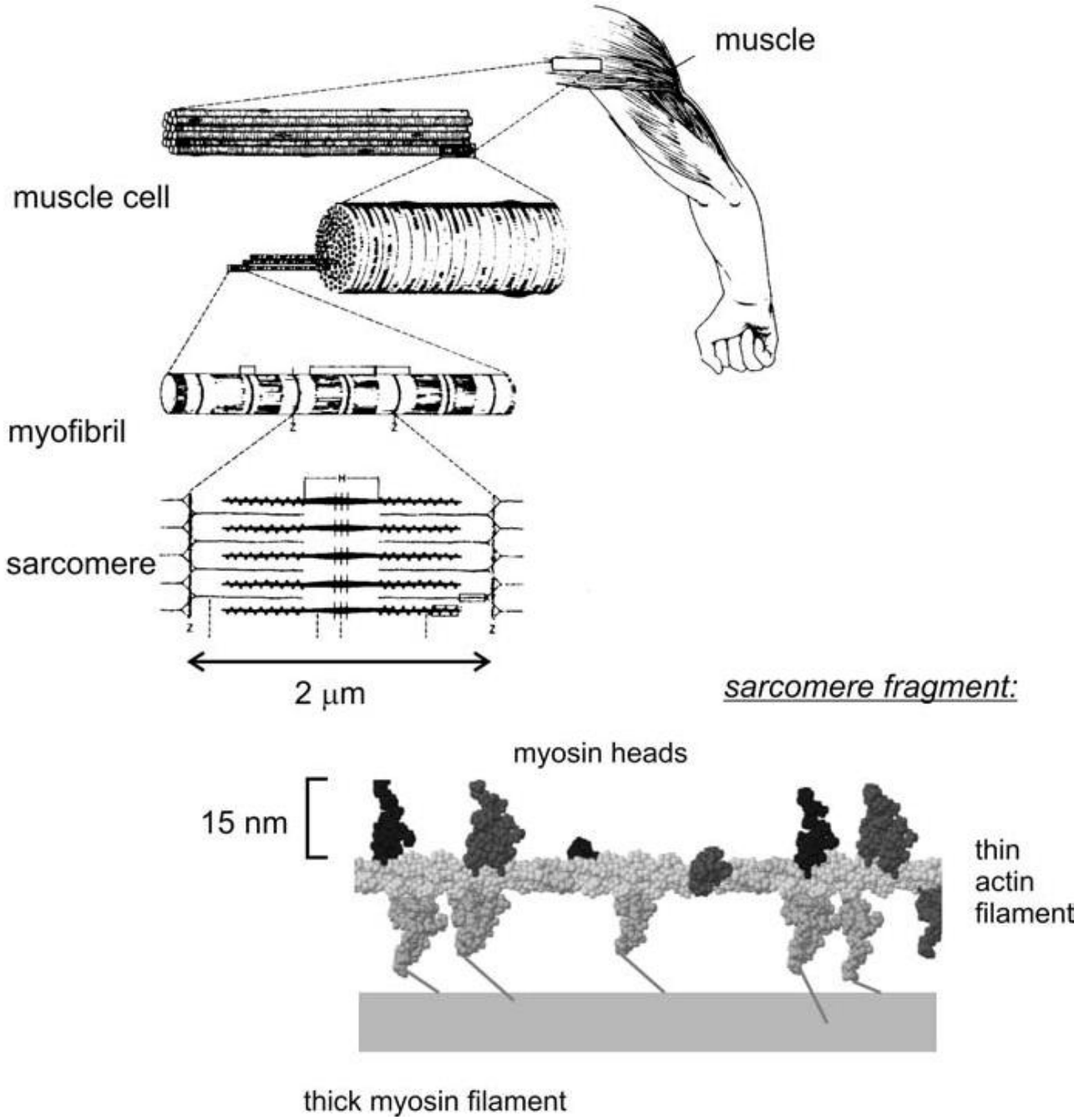

Figure 2.1 Basic structure of skeletal muscle. Reprinted with permission from SpringerLink, Koubassova, N.A, Molecular Mechanism of actin-myosin motor in muscle [3]

shown), with multiple fascicles making up the whole skeletal muscle. The fiber, fascicle and whole muscle are sheathed with connective tissue. The nuclei of each fiber are found at the periphery of each fiber. Fibers are comprised of myofibrils, which contain the functional contractile unit, the sarcomere (Fig 2.1). The sarcomeres are connected in series within the myofibril, with the total number of sarcomeres determining the length (sarcomeres in series) and diameter (myofibrils and therefore, sarcomeres in parallel) of the fiber. Sarcomeres contain a geometric arrangement of thick and thin filaments which result from polymerization of the proteins myosin and actin, respectively [26]. If the myofibril is seen in cross section, these filaments form a hexagonal structure, with one myosin associating with 6 actin filaments [27]. A sarcomere is composed of these thick and thin filaments, the protein titin (discussed below), and other proteins important for contraction (discussed below). A sarcomere is described by its various regions of interacting thick and thin filaments. Located at the connection point between two sarcomeres is the Z-band (line or disc), followed by the location of primarily the thick filaments, the A-band, and finally the I-band is the region comprised of thin filaments, spanning between two sarcomeres (Fig 2.2, 2.3) [27]. Where the thick and thin filaments do not overlap is the H-zone, and the A-band is the location of myosin with some overlap of actin. Each sarcomere, bounded by the Z-lines, is approximately 2 to 3.65µm long, and appears by light microscopy as alternating light (I-Band) and dark (A-band) regions associated with the previously described areas[28] (Fig 2.3).

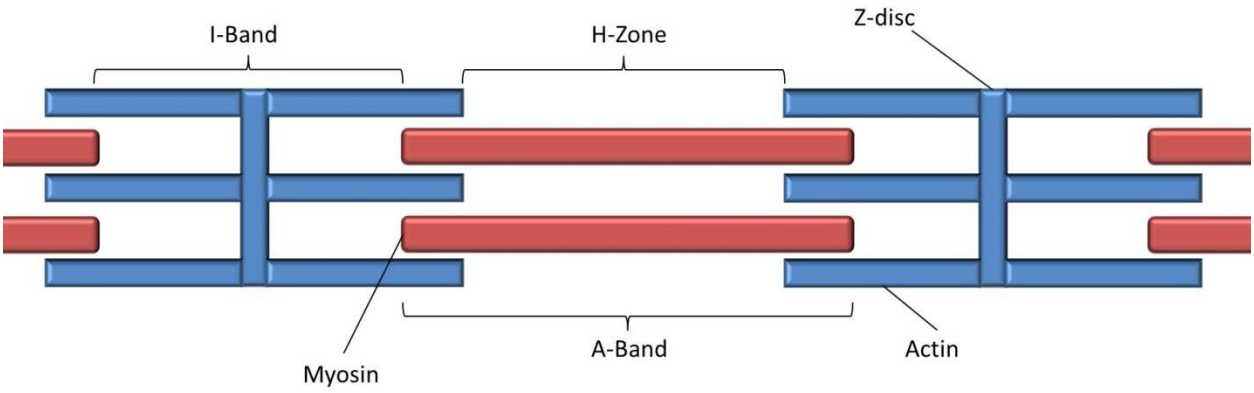

Figure 2.2 Schematic of the sarcomere.

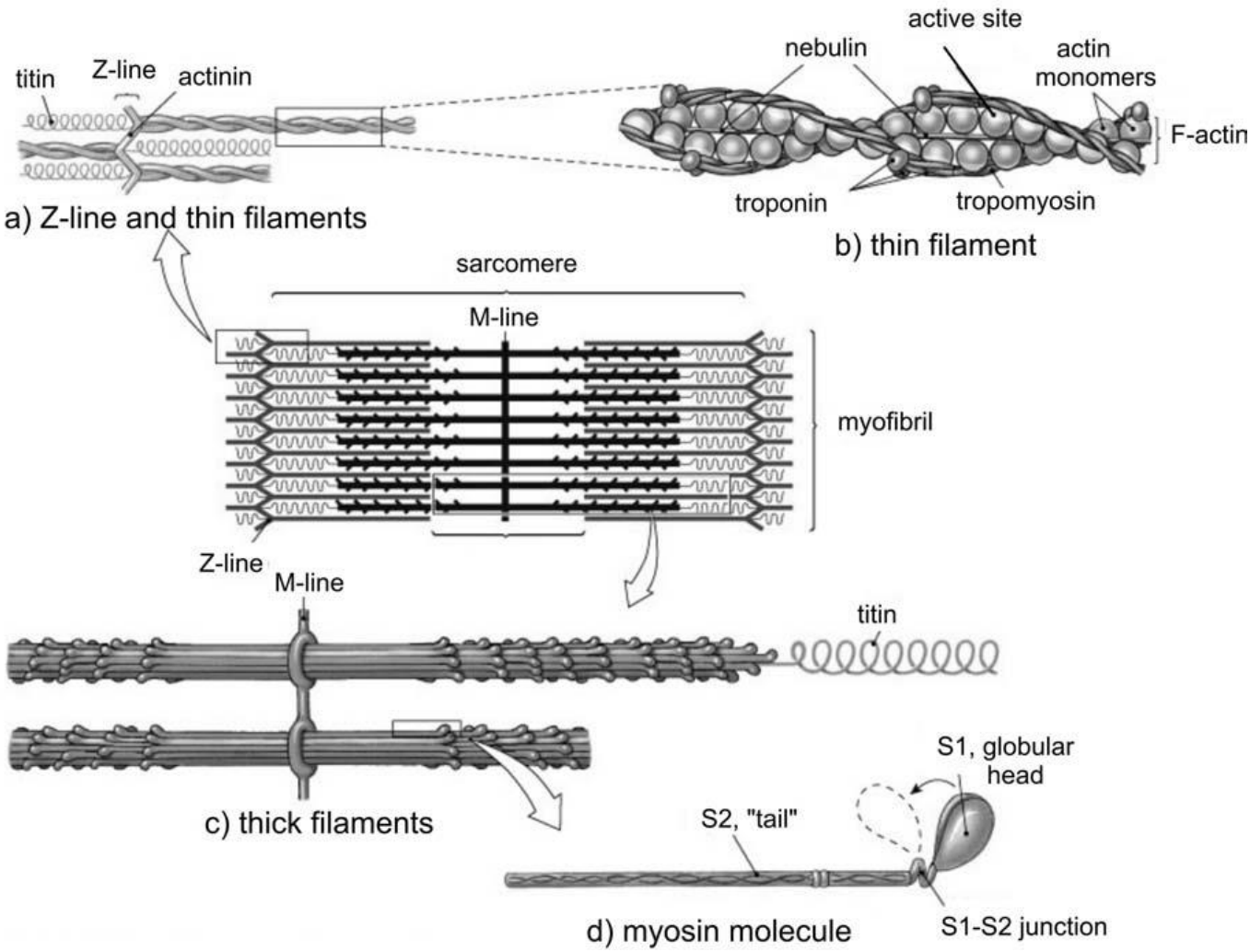

Figure 2.3 Structure of the sarcomere. Reprinted with permission from SpringerLink, Koubassova, N.A, Molecular Mechanism of actin-myosin motor in muscle [3]

The thin filaments, primarily comprised of actin, regulate tension generation during muscle contraction (see section A.4). Globular actin (G-actin) polymerizes in a helical fashion to create filamentous actin (F-actin), the primary component of the filament [29]. Troponin and tropomyosin bind to actin as a regulatory complex (described in Section A.4, skeletal muscle contraction). The thick filaments are known as myosin and appear as a long tail with two globular heads [3]. Myosin is created through the formation of 6 polypeptide chains; 2 heavy chains (M.W. of 200,000 Da) and 4 light chains (M.W. ≤25,000 Da). When myosin is cleaved by the enzyme trypsin, two fragments the heavy and light meromyosin result. Heavy meromyosin (HMM) is the head portion and a short associated tail, and is responsible for generating muscle tension through its interaction with actin (see Section A.4) [3]. HMM can be further split

into sub fragment 1 and sub fragment 2 (S1 and S2, respectively, Fig 2.3). Light meromyosin (LMM) is the longer tail portion (to the left of S2 in Fig 2.3) and associates with other tails of myosin molecules to form the thick filament backbone. The myosin heads project out from the backbone radially to (Fig 2.3) [3]. Myosin is an adenosine triphosphatase (ATPase) that hydrolyzes adenosine triphosphate (ATP) to provide energy for muscle contraction. Hydrolysis occurs at the head of myosin. Titin is responsible for maintaining the passive elasticity of muscle. Titin acts as a spring spanning from the Z-band to the M-band, and assists with force transduction along the Z-band and helps to maintain resting tension along the I-band [30] (Fig 2.3).

A.3- Spatial Arrangement of Filaments

The force generated by muscles is directly correlated to the distance between thick and thin filaments in the sarcomere. In diseased muscle, spacing of filaments may be altered to diminish force production [31, 32]. Many images do not adequately represent the 3-dimensional structure of the filaments; however, X-ray diffraction studies have provided a more complete representation of the filament lattice [33, 34]. When the filament lattice spacing is reduced, a diminished force output is observed [35]. At a specific spacing, the skeletal muscle can produce the optimal amount of force - this will be further examined in Section A.4. The geometric order of the structural lattice is maintained by Z-line and M-line spacing, and titin [36, 37]. If any of these components are compromised, filament spacing may be altered, resulting in reduced force output.

A.4- Muscle Contraction

Contraction is the result of biochemical energy from ATP hydrolysis converted to mechanical energy. The theory of sarcomere contraction was developed by researchers from two laboratories in 1984: Andrew Huxley and Rolf Niedergerke[38] and by Hugh Huxley and Jean Hanson [39]. This theory was known as the sliding filament model of contraction and suggests that myosin thick filaments slide along actin thin filaments shortening the sarcomere and producing force. Based on microscopy studies, the I-band and H-zone shorten during muscle contraction, while the A-band remains unchanged [39]. As sarcomeres within a fiber shorten, the fiber also shortens. As more fibers contract, eventually the entire muscle undergoes contraction. This endpoint of

sarcomere contraction is a complex process beginning with the activation of an action potential, a rapid change in electrical activity initiated within the cell body of a motor neuron.

A.4.1- Excitation-Contraction Coupling and Muscle Contraction

Excitation-contraction coupling (E-C coupling) is the process by which an electrical signal, known as an action potential (AP) is transmitted to fibers within a target muscle. Signals originating in the motor cortex and other areas of the brain provide the signals to the muscles via the α-motor neuron (α-MN) pools in the spinal cord. An α-MN and all the muscle fibers it innervates are known as a motor unit. The AP that originates in the α-MN propagates down its axon by voltage-gated sodium channels until it reaches the neuromuscular junction (NMJ), which is the synapse between an α-MN and the muscle fiber. As the AP reaches the axon terminal or button, voltage-gated calcium channels open and the influx of calcium binds to the protein synaptotagamin on vesicles that contain the neurotransmitter acetylcholine (Ach); the vesicles then fuse with the plasma membrane of the axonal button by soluble N-ethylmaleimide-sensitive factor (NSF) attachment proteins (SNAREs) [28], and exocytose Ach into the synaptic cleft. The Ach diffuses to the post synaptic membrane (motor end plate) and binds to nicotinic Ach receptors on the post synaptic membrane of the muscle fiber. The fiber at rest has a negative potential (from -70 to -90 mV) inside with respect to the outside that is maintained by the distribution of positive and negative ions within and outside the fiber. For example, sodium is at high concentration outside and low inside the fiber at rest. Activation of the Ach receptors opens sodium/potassium channels allowing sodium to enter the fiber. The excess sodium moving into the fiber causes a net depolarization (fiber becomes positive inside with respect to the outside) or AP that propagates over the fiber's sarcolemmal membrane. The AP spreads into the fiber's network of T-tubules which extend transversely into the center of the fiber. Depolarization within the T-tubule activates the dihydropyridine receptor (DHPR) a voltage sensor localized in the T-tubule membrane. The DHPR physically interacts with the ryanodine receptor (RyR) localized in the membrane of the sarcoplasmic reticulum (SR). Calcium is then released from the SR to trigger contraction in the sarcomere. [40]. RyRs are activated by the release of calcium at low intracellular calcium concentrations, and deactivated with higher

intracellular calcium concentrations. The negative and positive feedback mechanisms of the RyR provide further regulation of muscle contraction.

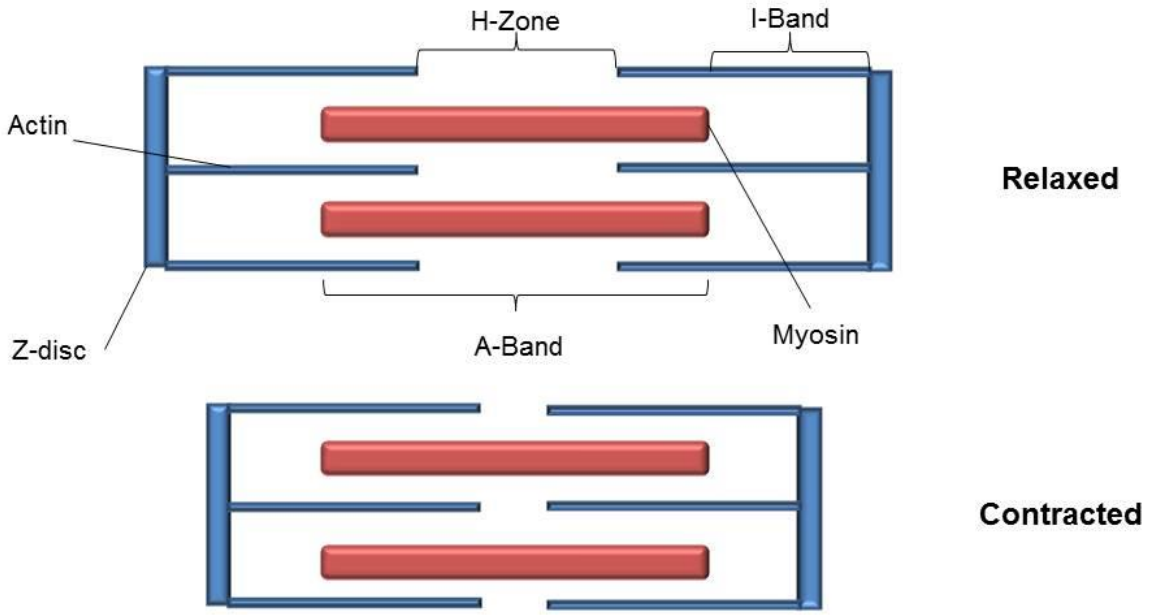

Figure 2.4 Schematic of muscle contraction. During contraction, myosin interacts with actin, shortening the length of the sarcomere by decreasing both the H-zone and I-band.

Calcium binds to troponin C (TnC) on the actin thin filament of the sarcomere. TnC associates with inhibitory troponin I (TnI) and tropomyosin-binding troponin (TnT), and together they bind tropomyosin. Collectively, these proteins form the troponin-tropomyosin complex. Tropomyosin blocks the myosin binding site on the actin filament in the absence of calcium. Calcium binding to TnC induces a conformational change in TnI, and tropomyosin moves to reveal the myosin binding site [28].

Myosin bound with ATP causes a weak binding state between actin and myosin. ATP hydrolyzed into ADP and P_i results in a strong binding state between myosin and actin. The energy released by ATP hydrolysis, drives the myosin power stroke which

pulls actin towards the center of the sarcomere; this action results in both force production and sarcomere shortening. At the end of the power stroke, ATP again binds to myosin to cycle back to the weak binding state. The change from weak binding to strong binding to the power stoke to the weak binding state is the cross-bridge cycle. Repeated cycles result in actin moving past myosin in a sliding motion; hence the sliding filament theory of contraction [3]. During contraction, numerous cross-bridge cycles occur in multiple sarcomeres of many fibers, that yield contraction of the activated motor unit, and many motor units activated simultaneously, produces contraction by the whole muscle. As long as calcium and ATP are available, contraction will continue.

Relaxation occurs when calcium is released from TnC. Myosin is in a weak binding state with actin because ATP is bound; however, in the absence of calcium, the binding sites for myosin on actin are covered by tropomyosin. The cytosolic free calcium is pumped back into the SR, and in the case of fast twitch fibers (discussed in Section A.4.2), removal of calcium is facilitated by parvalbumin (PARV), a myoplasmic calcium binding protein [41]. Calcium is sequestered by the SR by the calcium ATPase pump, SERCA (sarco-endoplasmic reticulum calcium ATPase). Two isoforms of SERCA exist, SERCA1 is found in fast twitch fibers, and SERCA2 is found in slow twitch fibers [42]. Binding of calcium to SERCA initiates ATP binding, followed by ATP hydrolysis, which provides energy for the conformational change in SERCA so that two calcium molecules are pumped into the SR per ATP hydrolyzed. SERCA 1 activity is greater than that of SERCA 2 which yields faster recovery of calcium and faster relaxation, attributes common of fast twitch fibers (discussed below). Once in the SR, some calcium binds to calsequestrin (CSQ) for storage, while some calcium remains free in the SR until the next AP induces release of calcium for contraction [43].

A.4.2- Fiber Types

Fiber type is determined by the type of myosin ATPase present and the predominant ATP-generating metabolic pathway in the fiber (Table 2.1). The fiber types are determined by the type of myosin heavy chain and its rate of ATP hydrolysis. Muscle fibers in small mammals such as mice, rats, and rabbits can be categorized as slow

(type I) or fast (types IIa and IIb) [44], corresponding to slow, intermediate and fast rates of ATP hydrolysis, respectively. In human muscle, the fast fiber is IIx instead of type IIb [28]. Skeletal muscles are comprised of both fast and slow twitch fibers, yet muscle can be preferential for certain fiber types.

A.4.2.1- Type I Fibers

Type I fibers are characterized by their slow twitch contraction and relaxation times, lower force production compared to fast fibers, and red color due to increased oxidation of hemaglobin. These fibers contain a large content of mitochondria, which provide ATP generation through oxidative phosphorylation, are more fatigue resistant, and are referred to as slow oxidative (SO). Fatigue is defined as the reversible inability to sustain a desired force output [45]. Myosin ATPase in these fibers hydrolyzes ATP more slowly, and therefore the fiber has a slower contraction velocity. These fiber types are found in large numbers in postural muscles where they are continually activated [28]. Primarily fast-twitch muscles, such as the extensor digitorum longus (EDL), also contain small numbers of type I fibers.

A.4.2.2- Type IIa Fibers

Type IIa fibers have faster contraction and relaxation twitch times compared to type I fibers, and also produce more force. These fibers are more susceptible to fatigue than type I fibers, yet are still considered fatigue resistant. The type IIa myosin ATPAse splits ATP faster, producing quicker fiber contraction velocities. Type IIa fibers are high in both oxidative and glycolytic enzymes, and have been defined histochemically as fast oxidative-glycolytic (FOG) fibers [44]. When a stronger contraction is required both type I and IIa fibers will be activated. Motor units will be activated based on the force required, with slower, less fatigable motor units being activated first, followed by faster motor units. This order of activation is referred to as Henneman's size principle [46].

A.4.2.3- Type IIb/x fibers

The third group of fibers, IIx in humans and IIb in small mammals, are also the fastest fiber types. These fibers have low mitochondrial content, and appear almost

white in color. The type IIb/x myosin ATPAse splits ATP faster, producing the quickest fiber contraction velocities. Type IIb/x fibers also generate the most force of the three fiber types, but are unable to maintain this force production due increased lactic acid build up as a result of anaerobic metabolism. IIb/x fibers rely on glycolysis and quickly fatigue, only allowing activation for a short period time. These fibers are also known as fast glycolytic (FF) fibers and will be activated in need for a quick response, such as sprinting [44].

Table 2.1. Fiber type classifications [26, 47]

	Type I	Type IIa	Type IIb/x
Color	Red	White	White
ATPase activity/ [Concentration]	Slow/Low	Fast/High	Fast/High
Metabolic Activity	SO	FOG	FG/FOG
Z-line width	Wide	Intermediate	Narrow/Intermediate
Contractile Speed	Slow	Fast	Fast
Endurance	High	Moderate	Low
SR Calcium Pump	SERCAII	SERCAI	Mixed

SO- Slow oxidative, FOG- Fast oxidative glycolytic, FG- Fast glycolytic, SERCA- Sarcoplasmic/Endoplasmic reticulum calcium ATPase

A.5- Skeletal Muscle Contractile Properties

To investigate the role that sphingolipids may play in the modulation of the inflammatory response in dystrophic mice, it will be important to determine if sphingolipids can rescue function in dystrophic muscle. To assess this possibility, several skeletal muscle functional relationships will be investigated. This section explains fundamental functional properties of skeletal muscle, including: length-tension, force-frequency, force-velocity, fatigue, and fatigue recovery.

A.5.1- Length-Tension Relationship

The maximum force a muscle can produce depends on the sarcomere length and overlap of thick and thin filaments. At resting tension *in vivo*, a muscle exists at an

optimal length (L_0) to generate the most force when stimulated (active force) [48]. At L_0, the sarcomere is characterized by optimal overlap of thick and thin filaments; myosin heads can bind to actin easily at numerous binding sites, essentially providing the most potential interactions between the two filaments. Myosin filaments are 1.65 µm long, and the actin filaments are 2.0 µm, with resting sarcomere length existing at a total sarcomere length of 2.0-2.2 µm [28]. As the sarcomere is stretched and total sarcomere length increases, active force decreases until total sarcomere length is 3.65 µm or greater [28]. At this point, there is no overlap of filaments and force cannot be generated. As sarcomere length shortens from 2.2 µm to 1.87 µm, actin filaments begin to overlap with each other reducing the total number of myosin-actin interactions [28]. Again, active forces will decrease in accordance with sarcomere shortening.

These interactions are referred to as the length-tension relationship (Fig 2.5), and are important for determining optimal sarcomere length for muscle isometric (constant length) contraction. Plotting these interactions gives rise to the ascending limb (sarcomere shortening), plateau (L_0), and descending limb (sarcomere lengthening) [49]. While this relationship is best described in single sarcomeres, it can be extrapolated as a percentage of the whole muscle length [49]. Investigating single sarcomeres is difficult, but can be performed with specialized single fiber equipment. However, the same principle applies to whole muscle, i.e., there is an optimal length of muscle at which force is maximal; this length is considered to represent the optimal overlap of actin and myosin within the sarcomeres of the fibers that make up the

muscle.

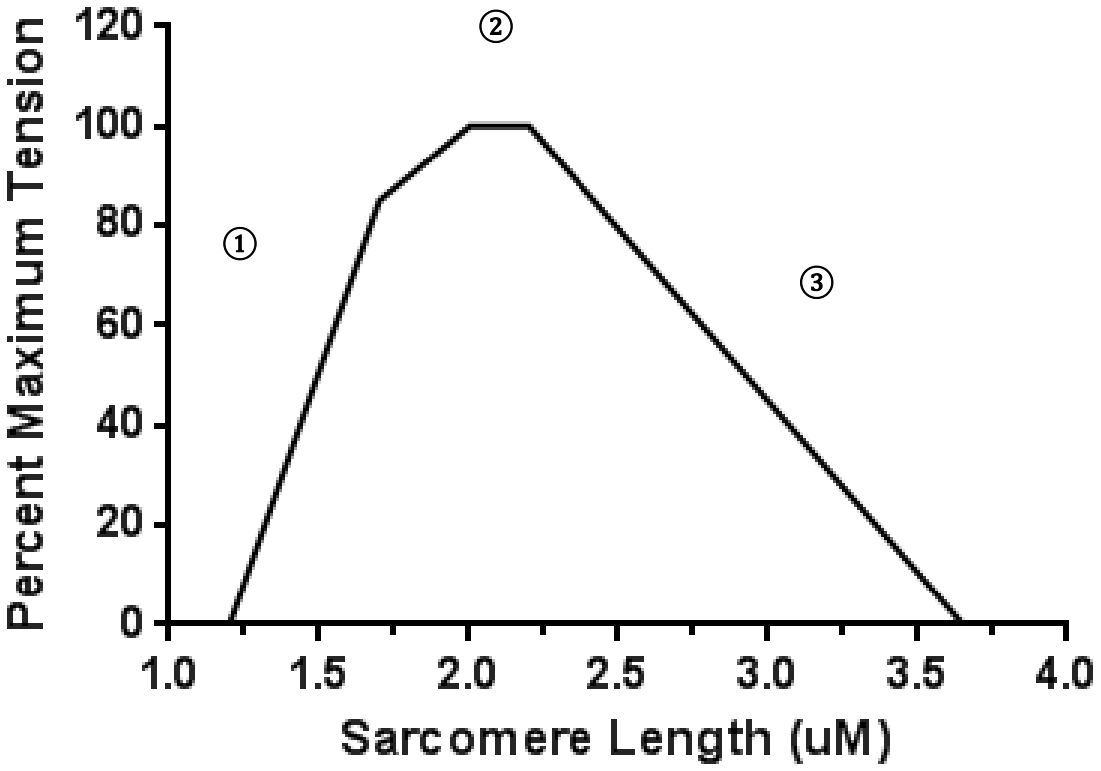

Figure 2.5. Length-tension relationship. 1. Ascending limb- myosin overlaps reducing the number of potential cross-bridge formations. 2. Plateau- optimal sarcomere length for overlap of thick and thin filaments needed for strongest contraction. 3. Descending limb- sarcomere is stretched reducing the number of actin-myosin cross bridges reducing overall tension. However, as the muscle is stretched, passive tension will increase (not shown).

A.5.2- Twitch, Tetanus, and Force Frequency

The twitch is the fundamental contractile response of an intact fiber, motor unit or muscle to a single action potential. Experiments to obtain these responses can be performed *in vitro* with the muscle removed from an anesthetized animal, or performed inside the organism, *in vivo*, The twitch response shows the force production in response to a single (electrical) stimulation, and also gives insights into other twitch parameters such as time to peak force (TPF), half relaxation time (HRT), and peak force (PF), or maximal force. Active maximal force is defined as the maximal force produced subtracted from the resting (baseline) force of the muscle. Resting force is the force generated by a non-activated muscle at $L_{0.}$ TPF is how long it takes the muscle to reach maximal force starting from baseline. HRT is how long it takes the muscle to relax to

half of the active maximal force. These basic contractile properties can help define a muscle as slow or fast twitch, as well as provide insight about the rate of calcium release from and reuptake by the SR. Modified twitch responses from a muscle can provide insight into potential mechanisms associated with a disease [50].

After a single stimulation, the muscle will increase force and return to resting baseline. However, if another stimulation arrives before the muscle can completely relax, the force response of the second stimulation will be added to the first. This effect is known as temporal summation [49]. The specific functional response will depend on the number of pulses and the time between them. The consequence is multiple pulses at a high stimulation frequency will result in a higher force production than a single pulse. When the pulses become close enough, a saturation point is reached, where

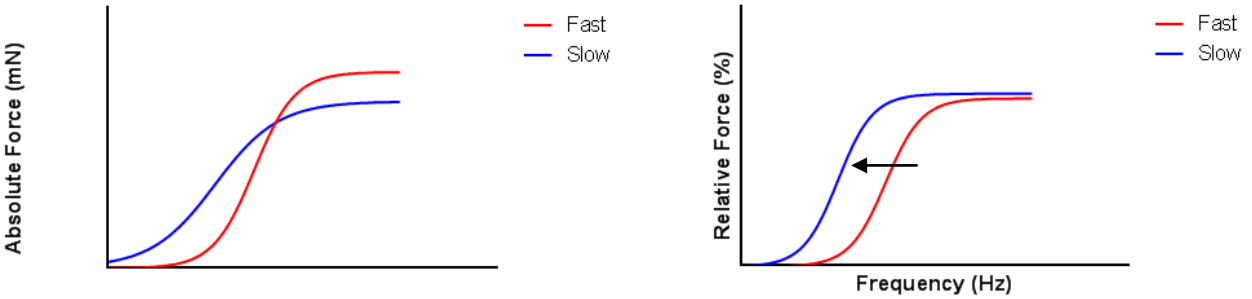

Figure 2.6. Force-frequency relationship. A. Force frequency expressed as absolute force. Fast twitch muscles reach higher forces at higher frequencies compared to slow twitch. B. Force frequency expressed as relative force. Slow twitch muscles reach maximum force at lower frequencies. This effect is demonstrated by the left shift of the relative force frequency curve for the slow compared to the fast muscle (arrow).

calcium is released much faster than it can be recovered by the SR, and individual twitches are indistinguishable. The outcome is known as a fused tetanus and is indicative of the maximal force a muscle can produce. The force-frequency relationship describes the peak contraction force as a function of stimulation frequency. To achieve a fused tetanus in a mouse EDL for example, stimulation frequency is slowly increased from a twitch activation (e.g., 1 Hz) to a tetanic activation (e.g., 150 Hz). As the frequency is increased, temporal summation results in higher force production. This relationship is shown in figure 2.6 which illustrates the different force-frequency profiles for fast and slow twitch muscles. For the purposes of this thesis, force-frequency relationships were observed *in vivo* to determine functional changes during the treatment period, and *in vitro* to determine the functional outcomes at the end of

treatment. We hypothesize that sphingolipid treatment would rescue mdx skeletal muscle so these relationships would be similar to the wild type mouse.

A.5.3- Force-Velocity

While the length-tension relationship describes a muscle's force production at a constant length (an isometric or static contraction), it is more practical to assess dynamic muscle contractions, because muscle force production and length change are necessary for movement. The force-velocity relationship describes the velocity generated by a muscle under isotonic (i.e., constant load) conditions as a function of force. An explanation of the relationship was provided by A.V. Hill in his classic equation [49]:

$$(P + a)v = b(P_0 - P)$$

Where *P* refers to muscle force, P_0 is the maximum tetanic tension, *v* is muscle velocity, and *a* and *b* are experimentally derived constants in units of force and velocity, respectively. This equation can be used to determine the force that is generated as the muscle is shortening at a given velocity. Alternatively, rearrangement of this equation leads to the theoretical value of V_{max} (maximum shortening velocity under no load) [28]:

$$V_{max} = \frac{bP_0}{a}$$

Measuring V_{max} is difficult, as a muscle at a true zero load is difficult to achieve experimentally. Instead, V_{max} is extrapolated using the Hill equation and the relation between submaximal velocity and load responses. As with the length-tension relationship, the force-velocity relationship is represented conceptually as a curve summarizing many individual experiments (Fig 2.7). Where the curve intersects the y-axis represents V_{max}. Slow twitch fibers demonstrate a slower V_{max}, and a more pronounced curve compared to fast twitch fibers. Some diseased muscles demonstrates lower V_{max} values compared to healthy muscle, and may result from impaired calcium release or altered myofilament interactions [51, 52]. Force-velocity is

relatively unchanged in mdx EDL muscles compared to wild type [53], although sphingolipid treatment may affect this response.

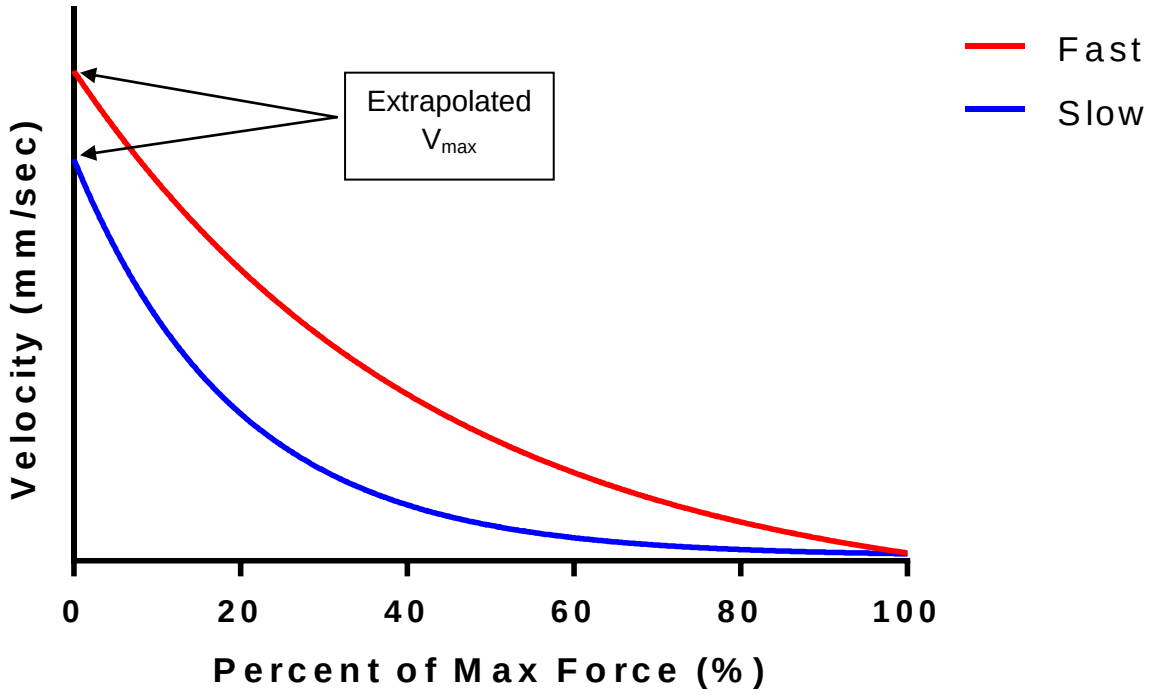

Figure 2.7. Force-velocity relationship. Fast twitch fibers demonstrate a higher V_{max} and a more gradual decline in velocity when compared to slow twitch fibers.

A.5.5- Fatigue and Fatigue Recovery

As a muscle is subjected to repeated stimulations, its ability to contract diminishes. Muscle fatigue is defined as a decline in the ability of a muscle to produce or sustain a given force [54]. At the motor nerve, it is likely that with repeated contractions there is an accumulation of potassium and depletion of sodium, resulting in a decreased ability to produce or propagate an AP, since sodium and potassium levels are unbalanced. Metabolic fatigue is also a common cause for muscle fatigue. Metabolic fatigue may arise from losses of ATP, phosphorylated creatine, or glycogen, although glycogen loss is most likely. Initial ATP is provided by phosphorylated creatine, then glycolysis, followed by other sources (i.e. cellular respiration). Once glycogen reaches depletion, fatigue is initiated to allow proper glycogen recovery [28]. Given time, muscle can recover from fatigue. How a muscle fatigues and recovers are good

indicators of the function of the muscle. Fatigue can be induced by multiple muscle contractions over time (e.g., many minutes). Recovery can then be assessed as a single contraction evoked at various time intervals after the fatiguing contractions. The recovery data can be used to determine how long it takes for the muscle to achieve either full or partial recovery of force output. Mdx mice demonstrate less resistance to fatigue (greater force loss) and slower recovery of force [55]; we hypothesize sphingolipid treatment may increase resistance to fatigue and increase the rate of force recovery

A.6- Summary

This chapter addressed basic skeletal muscle anatomy, physiology, and contractile properties. Sarcomeres are the fundamental contractile unit of muscle and are composed of myosin thick filaments and actin thin filaments, along with other proteins. Sarcomeres are arranged in series forming myofibrils. Myofibrils form muscle fibers that are grouped in fascicles, and many fascicles make up a muscle. The ability of myosin and actin to interact in the presence of calcium with energy from the hydrolysis of ATP forms the basis for muscle contraction.

The motor unit is a motor neuron and all the fibers that it innervates, and generates the initial AP. As an AP propagates down a motor neuron, the AP reaches a synapse where it diffuses across, and subsequently propogates along, the sarcolemma of the muscle. As the AP propagates into the t-tubules, DHPR and RyR are activated releasing calcium from the SR into the cytosol. TnC binds calcium to allow myosin to bind with actin and engage the cross-bridge cycle. Contraction of the muscle then occurs.

Skeletal muscle contractions are characterized by several key relationships: length-tension, force-frequency, force-velocity, fatigue, and fatigue recovery. These relationships define the capability of the muscle to produce force and shorten. These characteristics of muscle contraction are important to consider when investigating muscle disease, and prospective treatments and their effects.

Section B: Duchenne Muscular Dystrophy

B.1-Introduction

Duchenne muscular dystrophy (DMD) is an X-linked degenerative and fatal muscle disease that affects 1 in 3500 boys. An X-linked disease is caused by a mutation on the X-chromosome. Males have single X and Y chromosomes, while females have two X-chromosomes. Therefore, if a gene (e.g., dystrophin) is mutated on the X chromosome, males will be affected, while females have a second copy of the gene on their 2nd X chromosome that can compensate for the mutated gene. Hence, females are considered carriers of DMD as they can pass one copy of the X chromosome that carries the mutated gene to male offspring. As such, DMD normally affects only boys, while DMD affected females are rare [56]. Boys affected with DMD have progressive generalized deterioration in muscle function who become wheel-chair bound by age 14 and often die by their early twenties due to cardiac or respiratory failure [7]. DMD is caused by one or more mutations in the gene that encodes dystrophin, an integral protein that is part of the dystrophin-glycoprotein complex (DGC), a complex considered important to fiber membrane integrity and signaling. In the absence of dystrophin, the other DGC proteins are also absent. One consequence of this absence is a clear inflammatory response. Characterizing the inflammatory response could provide potential sites of intervention to ameliorate the disease. Sphingolipids are present in many common foods (e.g., milk and soy) and have emerged as critical secondary messengers for a variety of cellular process including cell growth, death, differentiation, and motility. Sphingolipids can reduce inflammation in some cancer cell lines (e.g., breast or colon, see Section D). Sphingolipids, therefore, may be effective in slowing as a treatment to slow the pathophysiology of DMD.

B.2- Clinical Presentation

Although DMD was first described by Italian scientists Giovanni Semmola (1834) and Gaetano Conte (1836), DMD was named after the French neurologist Guillaume Duchenne for his extensive investigation of the disease (1861) [57, 58]. Duchenne's work was critical in establishing the clinical presentation, as well as providing the first illustrations for the disease [58].

DMD is observed in boys as early as age 3 [7]. It is characterized by severe muscle wasting and fibrosis, inflammation, decreased muscle function, and muscle metabolic defects [59]. Calf muscles demonstrate pseudohypertrophy due to increased deposition of fatty and connective tissues [60]. Affected boys rely on the Gower's maneuver to get up off the floor: the boy reaches a standing position by "walking up" the legs with his hands. As the disease progresses, the child will develop a waddling gait, and increased walking on the toes [61]. Serum creatine kinase (CK) is elevated, indicative of muscle damage. Eventually, muscle degeneration leads to loss of stability, and a change in posture characterized by a protruding stomach and increased curvatures of the spine [62, 63]. Patients with DMD commonly present with a more severe kyphosis and other irregular spinal curvatures. With disease progression, stability will be completely lost and patients will be confined to a wheelchair by age 12 [64]. DMD also affects both the cardiac and respiratory muscles ultimately leading to muscle degradation and patient death by their mid-twenties [65, 66]. The underlying cause of muscle degradation begins with mutations in the gene associated with dystrophin.

B.3- Dystrophin

The gene that encodes dystrophin is located on the X chromosome at locus p21 and is composed of 79 exons with over 2.5 million base pairs[11]. However, only 14,000 bp are used for translation into protein [67]. The gene is composed of at least seven promoter regions, which can drive transcription of three different isoforms of the protein [1]. The isoforms can be located in a variety of tissues in the body including skeletal, cardiac, and brain. Due to its large size, the gene has high mutation rates. These mutations provide the basis for two muscular dystrophies: Becker's (BMD) and DMD[11]. BMD is defined by partial deletions in the dystrophin gene that yield expression of a shortened but partially functional protein, while DMD has deletions and frame shift mutations resulting in the complete absence of the skeletal muscle isoform [11].

The skeletal muscle isoform of dystrophin is 427kD and contains 3,685 amino

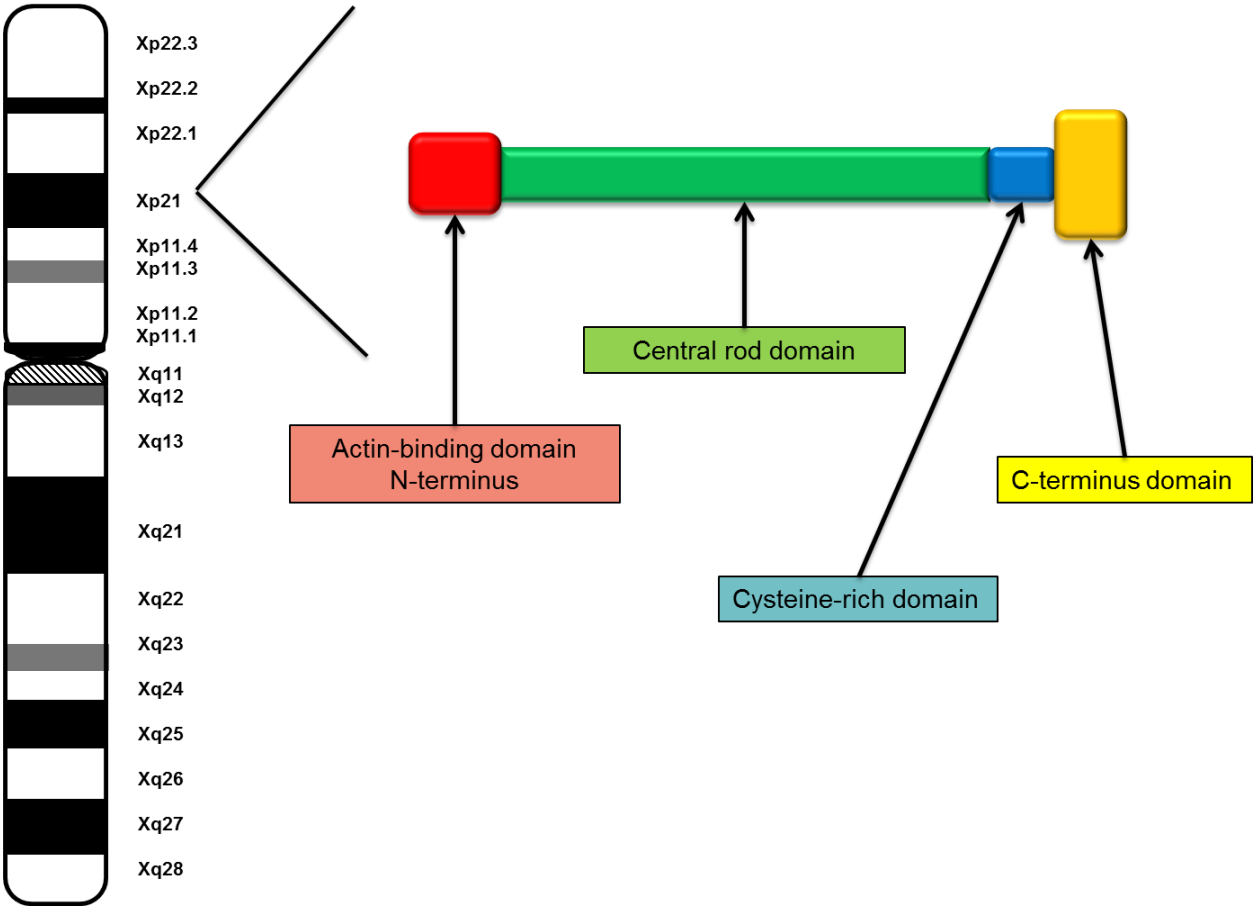

Figure 1.8. Dystrophin gene location and protein structure. Several promoter regions drive transcription of different isoforms of the protein [1]. The skeletal isoform of the protein contains 4 domains: 1. The N-terminus binds to cytoskeletal F-actin. 2. The central domain contains 24-109 amino acid spectrin-like repeats. 3. A cysteine rich domain. 4. The C-terminus domain that associates with the syntrophins, dystrobrevin, β-dystroglycan, and nNOS (neuronal nitric oxide synthase) [4].

acids[65]. Localized in the cytoskeletal membrane, dystrophin links the membrane to the extracellular matrix. Dystrophin is a member of the spectrin superfamily of proteins[68] and has four distinct regions: (a) The amino-terminal actin-binding domain, (b) a central domain, (c) a cysteine-rich domain, and (d) a carboxyl-terminal that interacts with the syntrophin family of proteins [4] (Fig 2.8). Dystrophin binds to several proteins at the membrane that form the dystrophin-glycoprotein complex (DGC) [69].

B.4- Dystrophin-Glycoprotein Complex

The DGC is a group of integral and peripheral proteins located along the sarcolemma that link the cytoskeleton to the extracellular matrix. The primary

components of the DGC are the dystroglycans, which bind to dystrophin through β-dystroglycan and the basal lamina through α-dystroglycan [2]. α-dystroglycan binds to agrin and laminin to provide the link to the extracellular matrix. In addition to the dystroglycans, the core of the DGC contains four sarcoglycans (α,β,γ and δ) and sarcospan, which are believed to assist with the stabilization of the complex within the sarcolemma [70]. Binding to the C-terminus of dystrophin are the syntrophins (α, β, γ and δ) [71]. These widely expressed cytoplasmic adaptor proteins can associate with voltage-gated ion channels and neuronal nitric oxide synthase (nNOS) through PDZ domains [72]. Figure 2.9 shows the structure of the DGC. The linkage of the DGC and dystrophin between the extracellular matrix and the cytoskeletal surface may provide signaling functions as well as provide structural stability, but these functions are not well defined [70, 73]. Patients with DMD present with absences of both dystrophin and associated DGC proteins, which contribute to the overall pathophysiology of DMD [74].

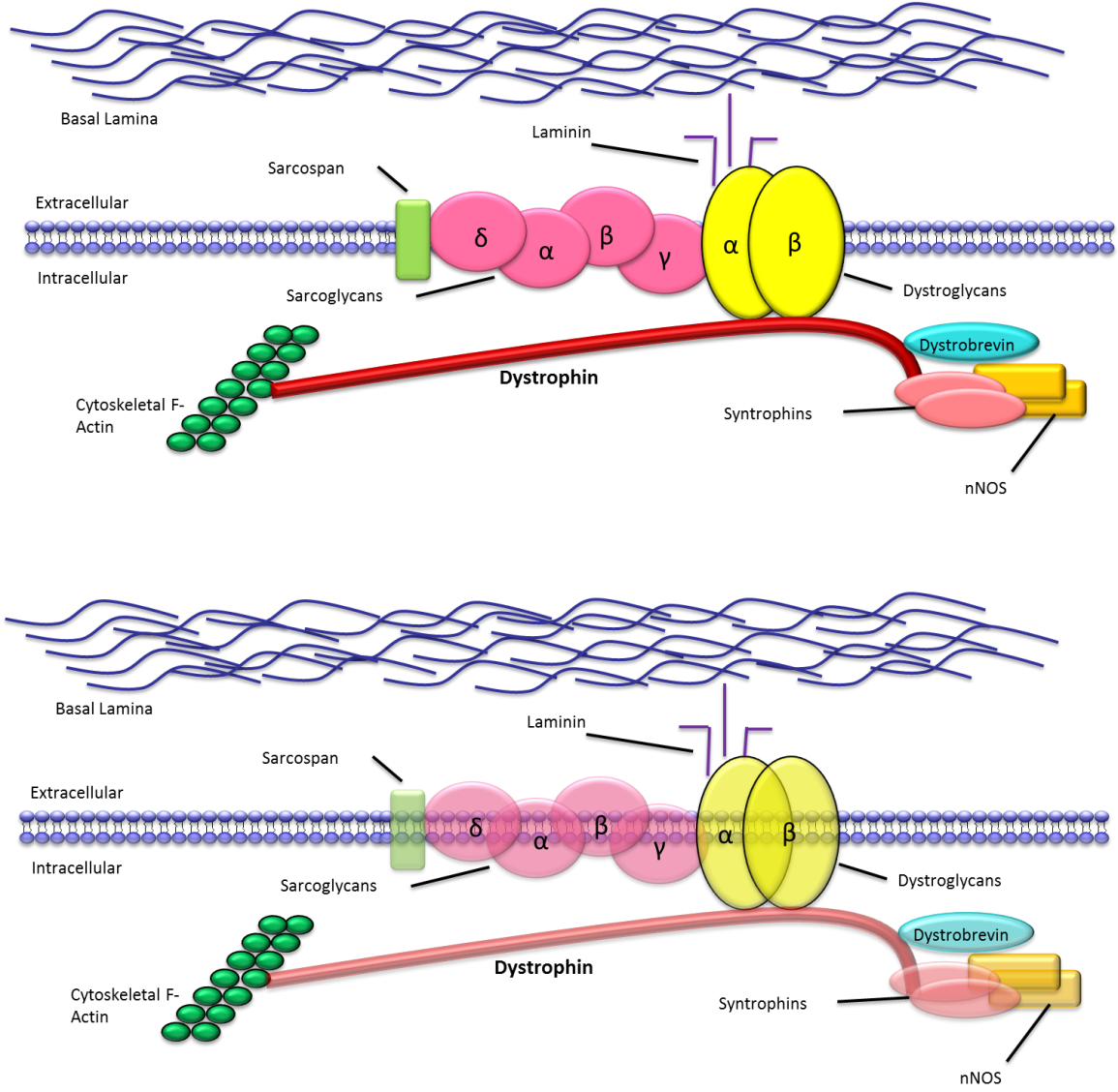

Figure 2.9. The DGC in healthy (top) and DMD (bottom) muscle. The DGC is composed of distinct integral membrane proteins that link the extracellular matrix to the cytoskeleton of the muscle cell. These proteins include the dystroglycans (α, β) the sarcoglycans (α, β, δ, γ), and sarcospan [2]. Association of the DGC to the extracellular matrix is accomplished through binding of laminin to α-dystroglycan [2]. Dystrophin associates with the DGC through its C-terminal domain interaction with β-dystroglycan. The N-terminal of dystrophin associates with F-actin of the cytoskeleton [2]. Patients with DMD do not express dystrophin, thus portions of the DGC are absent (shown as transparent in the bottom figure). Figure adapted from Allen et al. (2010) [5].

B.5- Pathophysiology of DMD

Loss of dystrophin and the associated DGC proteins causes aberrant physiological responses. Alterations to the structural stability of the sarcolemma permit mechanically-induced tears and the unregulated exchange of ions [75]. By either mechanical damage or disrupted signaling, the pathophysiological responses result in a perpetual cycle of muscle fiber degeneration and regeneration. Eventually, satellite cells integral to the repair process are exhausted and damaged tissue is replaced with connective or fatty tissues. To study this disease, various animal models are used.

B.6- Animal models of DMD

A variety of animals express similar mutations to that of DMD including mice, cats, dogs, zebrafish, the worm *C. Elegans*, and primates [76]. Of these, canines represent the best model for DMD, with golden retriever muscular dystrophy (GRMD) being the most studied among canines [77]. GRMD is characterized by skeletal muscle weakness, atrophy, and cardiac failure. A point mutation at the intron 6 splice acceptor site of the canine DMD gene causes skipping of exon 7 and a premature stop codon in exon 8 resulting in the lack of dystrophin [77]. As with human DMD, loss of dystrophin in GRMD causes skeletal deformities, muscle hypertrophy, cycles of muscle degeneration and regeneration, and fibrosis [76, 77]. The skeletal and cardiac similarities of GRMD make it similar to DMD, with the genetic background and the body size of the golden retriever more similar to the human than other models [77]. However, the cost required to raise and house GRMD dogs make performing studies difficult, with many researchers opting to study the mdx mouse.

The X-linked muscular dystrophy mouse (mdx) was found to randomly occur in the C57BL/10 strain, with a nonsense mutation at exon 23 of the DMD gene [78]. As with DMD, this mutation causes a lack of dystrophin expression. Mdx muscle demonstrates infiltration of neutrophils or macrophages at age 2 weeks with muscle degeneration occurring at age ~1 month [78]. The cycles of degeneration and regeneration peaks around 3 to 4 weeks, and this developmental period is thought to model the cycle in DMD most closely [76]. However, while some muscles are affected (i.e., lower limb muscles), other muscles seem to be unaffected (i.e., masseter muscle) [79]. While deposits of fatty and connective tissue in DMD renders muscle nonfunctional, muscles in the mdx mouse continue to function, and the animals live a normal lifespan. This recovery may be attributed to increased expression of the dystrophin homolog protein, utrophin.

Utrophin is a protein that shares structural and functional motifs with dystrophin, and can associate with the DGC [80]. Named for its ubiquitous nature, utrophin is found in skeletal muscle tissues, nerves, blood vessels, and a variety of organs [81]. In adult normal skeletal muscle, utrophin is expressed at the neuromuscular junction [82] and is

closely associated with acetylcholine receptors [83]. Utrophin expression exists in two isoforms (A- and B- utrophin), with A-utrophin being the dominant form in skeletal muscle fibers [83]. Utrophin expression will occur before dystrophin expression in developing and regenerating muscle, where it is found along the sarcolemma [84]. However, in patients with DMD and in the mdx mouse, utrophin expression is increased in skeletal muscle [85, 86]. In the mdx mouse, increased expression of utrophin results in a less severe disease state and survival of the animal [86]. Studies showed that with increased utrophin expression, the defective linkage between actin filaments and the sarcolemma is rescued [86-88]. Researchers have tested utrophin as a potential treatment in mdx mice with success [89, 90]. Utrophin is one potential treatment for DMD.

B.7- Hypotheses of DMD Pathophysiology

The mechanisms responsible for DMD are complex and not well understood. Numerous studies have focused on characterizing the pathophysiology in patients and in animals models; however, onset mechanisms still remain undefined. Currently, it is hypothesized that dystrophin provides a structural link between cytoskeletal actin fibers and the DGC, and gives stability to the sarcolemma [69, 91]. Two major dystrophic mechanisms have been proposed: the mechanical hypothesis and the impaired calcium hypothesis. In addition, hypotheses related to gene regulation, vascular regulation, and inflammation have also been investigated [6]. Critical to this thesis, inflammation, will be discussed in section C.

B.7.1- The Mechanical Hypothesis

The mechanical hypothesis suggests that the lack of dystrophin compromises muscle membrane integrity such that tears result, especially after sustained contractions [6]. In addition to its distribution along the sarcolemma, dystrophin is thought to contribute to force transduction at the myotendinous junction [92]. The DGC and associated proteins normally associate with costameres, rib-like lattices on the cytoplasmic face of the sarcolemma which link the sarcolemma to the extracellular matrix [6, 93]. Costameres act to distribute mechanical forces generated by the sarcomere through the sarcolemma to the basal lamina to maintain sarcomere length

along the fiber [94]. Lack of dystrophin leads to subsequent loss of the DGC and the structural integrity of the costamere, contributing to sarcolemmal fragility [95]. Therefore, continued muscle contractions may lead to increased damage of the fiber. With DMD, the dystrophic process may begin with small tears in the sarcolemma followed by degradation of the muscle fiber. Progression of the disease leads to further damage of the sarcolemma [96]. To explore this hypothesis, evaluation of serum CK, membrane permeable dyes such as Evans blue dye (EBD) and procion orange (PO), and changes in ion concentrations have been used [97-100] to demonstrate leakiness of the membrane.

B.7.3- Calcium Hypothesis

In the calcium hypothesis, dystrophin-deficient fibers cannot properly regulate intracellular calcium, where calcium leak channels, thought to be part of the transient receptor potential channel (TRPC) family of receptors [101], are more likely to remain open, causing higher levels of intracellular calcium compared to normal muscle [52]. This influx of calcium to the cytosol hinders the muscle cell's ability to maintain physiologically low calcium levels, activating calcium-dependent proteases (calpains) [100]. These activated calpains lead to protein degradation and subsequent necrosis [102]. Investigations show that while calcium does enter the myoplasm, it is not yet well defined when these activations begin, and how they contribute to the overall pathophysiology of DMD [6].

B.7.4- Additional Hypotheses

In the gene regulation hypothesis, the DGC is thought to play a role in signaling of gene transcription. A disrupted DGC leads to selective regulation of a variety of genes [103], which contribute to the pathophysiology by interfering with normal cell signaling and repair [104]. It is not presently known how these changes impact the onset or progression of DMD [6]. In the vascular hypothesis, nitric oxide (NO), a vasodilator, is produced by neuronal nitric oxide synthase (nNOS) that is normally bound to the DGC by dystrobrevin and the syntrophins. In dystrophin-deficient muscle, nNOS becomes delocalized into the cytosol, becoming unavailable [105]. During exercise, oxygen need is increased, and muscle ischemia may occur without NO-

induced vasodilation [105]. Current studies report that nNOS knockout mice do not present with muscle weakness, yet a dystrophin/nNOS double knockout mouse has a more severe dystrophic phenotype [106]. These results suggest that nNOS may not play a direct role in DMD, but it could contribute to dystrophic pathophysiology.

Muscle damage that results from any of the mechanisms described above requires repair, which in part is a function of the inflammatory response. An aggressive inflammatory response in DMD contributes to the pathophysiology. The contributions of the inflammatory response will be discussed in section C.

B.8- Summary

Dystrophin is an important protein that links the cellular cytoskeleton to the extracellular matrix in skeletal muscle. Absence of dystrophin causes DMD [6]. DMD is characterized by severe muscle wasting that eventually results in death of affected boys. The precise role(s) of dystrophin in the normal muscle cell is (are) not well understood, nor are the mechanisms that contribute to DMD pathophysiology in its absence. Dystrophin is thought to provide mechanical stability to the sarcolemma and the DGC. Loss of this stability may lead to tears along the sarcolemma surface causing damage, unregulated exchange of ions (e.g., Ca^{2+}), and loss of muscle force [6, 107]. Repair of this damage is regulated in part by the inflammatory response. Inflammation can be both beneficial and detrimental.

Section C: Inflammatory Response

C.1- Introduction

Inflammation is part of the immune response. The immune response is the major line of defense for the body against antigens. Antigens stimulate the immune system to produce antibodies. Many antigens are foreign, including viruses, bacteria, and toxins, or may be created in the organism through normal cells as a result of normal metabolism or due to infection by viruses or bacteria. Antibodies help remove the unwanted antigens. The inflammatory response is a reaction to tissue infection, cell injury, or toxin exposure and involves the migration of proteins and immune cells to the site of injury. Inflammation initiated without an infection is referred as sterile

inflammation, or inflammation that occurs in a sterile environment [108]. While inflammation can serve a protective function, it may also exacerbate tissue damage and disease. This chapter seeks to explain both positive and negative influences of the inflammatory response in DMD.

C.2- Basics of Inflammation

The inflammatory response fights infections, cancers, and heals wounds. Inflammation is manifested in all cells (not just immune cells) and is an essential surveillance and defense mechanism used to sense physical, chemical, and biological stress. Inflammation helps to regulate a variety of physiological responses including dilation of blood vessels, movement of specific cells to site of infection or injury, and increased body temperature. These responses all contribute to the primary inflammatory characteristics including swelling, redness, and warmness [109]. Inflammation can be acute or chronic, depending on the severity and persistence [109]. Acute inflammation is defined by a rapid response lasting minutes, hours, or days [109]. Chronic inflammation is defined by responses that last years and is characterized by infiltration of mononuclear cells such as macrophages and lymphocytes into affected tissue [110]. Inflammation has two main components: cellular and exudative. The exudative component, and more specifically chemokine signaling will be the focus of this thesis.

C.2.1- Cellular Component

The cellular component is comprised of white blood cells, or leukocytes, and their initiation and maintenance of the inflammatory response. Leukocytes are normally found in the blood, and must be directed to the site of inflammation through a variety of mechanisms. This process of relocation is known as leukocyte extravasation, and requires secondary messengers (discussed below) [111]. Leukocytes can be divided into groups based on their function. Some leukocytes will act as phagocytes, ingesting foreign pathogens and destroying them. Granulocytes release enzymatic granules to damage foreign pathogens. Finally, B and T cells are responsible for secretion of antibodies.

C.2.2- Exudative Component

The exudative component refers to the movement of plasma fluid and the transport of a variety of proteins to the site of inflammation. Movement is achieved through dilation of blood vessels and subsequent loss of plasma fluid to tissues causing edema. Vascular changes associated with the exudative component include vasodilation, redness and heat due to increased blood flow, and a process called stasis, where cells remain in high concentrations in blood vessels. Other signaling processes and cascades associated with the exudative component will be discussed below.

C.2.2.1- Cytokines and Chemokines

To initiate an inflammatory response, signaling between critical cells is important. Signaling is achieved through many mechanisms, most notably by small proteins known as cytokines. Cytokines are small protein molecules (usually between 8 and 30kDa) used in cell signaling [112]. Cytokines are secreted by a variety of cell types and can be classified as a protein, glycoprotein, or peptide. The term cytokine encompasses a diverse and large family of molecules throughout the body [113]. Each cytokine is specific for a cell surface receptor, which in turn initiates a signaling cascade which alters cell function [112]. These effects can be wide-ranging from up or down regulation of genes or transcription factors, production of other cytokines, regulation of surface receptors, and suppression of their own effects through feedback inhibition [112]. The effect initiated by any cytokine is dependent on the type, abundance, and availability of receptors on cells.

Cytokines include a large family of molecules, and can be divided into smaller subsets. One subset of cytokines are chemokines, named for their chemotaxic effects on other cells [114]. Chemokines are smaller than most cytokines ranging in size from 8-10kDa, and are involved primarily in the inflammatory response [115]. Twenty to fifty percent of chemokines share gene and amino acid sequence homology [114]. Conserved amino acids in each chemokine contribute to the tertiary structure of chemokines [114]. The major functions of chemokines are to act as a chemo-attractant guide for the migration of cells. Migration will follow the concentration of the chemokine and can lead to a number of functions including roles in cellular development and inflammation. Inflammatory chemokines (such as interleukin 8) function primarily as

chemoattractants for leukocytes, recruiting other inflammatory cells to the site of infection or injury [114]. Chemokines can be further classified by the spacing found in the first two cysteine residues of the polypeptide chain. Nomenclature for these classes are L (for ligand) or R (for receptor), i.e., CCL1: CC chemokine ligand 1 and CXCR3: CXC receptor 3. Chemokine classification and receptors are discussed below (Table 2.2).

C.2.2.1.1- CC Chemokines

CC chemokines are distinguished by two adjacent cysteine residues near the N-terminus. Over 27 chemokines belong to this classification and contain chemokines CCL1, CCL15, CCL21, and CCL23 [116]. CC chemokines cause migration of monocytes, NK cells, dendritic cells, T cells, and B cells [116]. For example, CCL2 is responsible for inducing monocytes to leave the bloodstream and enter surrounding tissue to become macrophages [116].

C.2.2.1.2- CXC Chemokines

In CXC chemokines, the two N-terminal cysteine residues are separated by a single amino acid (designated by the “X”) [114]. Seventeen CXC chemokines have been described in mammals [116]. Most CXC chemokines perform one of two functions: induce migration of neutrophils, or act as a chemoattractant for lymphocytes [116]. For example, interleukin-8 (IL-8) causes neutrophils to leave the bloodstream and enter the surrounding tissue, and CXCL13 acts as a chemoattractant for lymphocytes [116]. Interleukins (IL) are a class of cytokines that contribute to propagation of the immune response. It is important to note that IL-8 is the only one also classified as a chemokine.

C.2.2.1.3- C Chemokines

C Chemokines only contain two total cysteines, one at the N-terminal, and one somewhere further along the polypeptide chain. This group contains only two chemokines in mammals and is primarily involved with attracting T cell precursors to the thymus where they can mature [116].

C.2.2.1.4- CX_3C Chemokines

These chemokines contain three amino acids between the two N-terminal cysteines. There is only one currently known: fractalkine (CX_3CL1) [116]. It is secreted and attached to the same cell that secretes it, serving as both an adhesion molecule and a chemoattractant [114].

Table 2.2 Chemokine classifications

Chemokine type	CC	CXC	C	CX_3C
Alternative Name	β-Chemokine	α-Chemokine	γ-Chemokine	δ-Chemokine
Cysteine Spacing	N'-…-C-C-…	N'-…-C-X-C-…	N'-…-C-…	N'-…-C-X-X-X-C-…-
Examples	CCL2, CCL3	CXCL1, CXCL2	XCL1, XCL2	Fractalkine

C.2.2.1.5- Chemokine Receptors

The receptors that bind chemokines are known as G-protein coupled receptors (GPCRs) that contain seven transmembrane domains and are found on the surface of a variety of cell types [114]. Nineteen different chemokine receptors have been discovered, which are divided into four groups depending on the type of chemokine that binds [114]. The N-terminus of these receptors reside on the outside of the cell membrane and bind the specific chemokine, while the intracellular C-terminus is important for receptor regulation [114]. Some receptors can bind multiple different chemokines to initiate the same signal transduction pathway.

Signal transduction is activation of proteins in sequence to initiate some cellular response. In chemokine signaling, a chemokine binds to its respective receptor, causing a conformational change and activation of associated G-proteins [114]. These activated G-proteins start a signaling cascade and results in some change in the cell, resulting in chemotaxic attraction of inflammatory cells [114].

C.3- Role of Inflammation in the Pathophysiology of DMD

Four to eight week old mdx mice and 6-9 year old DMD patients show infiltration of a variety of immune cells including: B-cells, macrophages, T-lymphocytes, and

dendritic cells [13, 117, 118]. These studies suggest that there is a persistent inflammatory response of dystrophin-deficient muscles. Unfortunately, it is unclear if this inflammatory response is involved during disease onset. Inflammation associated with DMD is not the result of infection, and the inflammatory response is sterile, likely initiated by the damaged muscle tissue. Dysregulated signaling of the inflammatory response likely plays a role [119]; gene expression studies have helped to describe some potential mechanisms for this inflammatory response. Microarray studies investigating human dystrophic muscle have demonstrated that the inflammatory process is a primary component of early disease onset. Complement components, chemokines, and human leukocyte antigens (HLAs) all demonstrate increased expression during both pre-symptomatic and symptomatic stages of the disease. Similarly, mdx mice also show many inflammatory genes that are up-regulated compared to normal mice. Microarray studies have also demonstrated a clear inflammatory response in mdx mice.

Porter et al. (2002) examined the gene signature in mdx mice using microarray analysis. Gastrocnemius and soleus muscles were dissected from 8 week old C57BL10 and mdx mice, with muscles from 10 mice pooled for each of five replicates for each mouse strain. RNA from the mice was extracted and placed on an Affymetrix murine MG-U74A array. Pairwise comparisons were made between replicates and strains, with fold changes relative to control greater than 1.5 deemed significant.

In general, the microarray revealed that gene class expression changes were consistent with the documented pattern of regeneration and degeneration of mdx mice, exhibiting gene expression associated with inflammation, muscle regeneration, proteolysis, and others. Mdx hind limb muscles exhibited a chronic, persistent inflammatory response. Cytokines responsible for inflammation initiation (e.g., IL-4, IL-6, TNFα) did not demonstrate altered expression; however, the TNFα receptor was up-regulated. Interestingly, a variety of chemokines (CXC, CC) and receptors (CC) were shown to be up-regulated in mdx tissue. This change in expression suggests a major chemotaxis response for lymphocytes and macrophages. Finally, complement components (e.g., C1qa, C1qb, C3) were also differentially expressed in mdx muscle,

and suggest an additive effect to the inflammatory response. In summary, mdx mice show a clear inflammatory response during muscle fiber degeneration/regeneration phases [13].

Similar inflammatory changes were found in human DMD patients on the basis of microarray studies. Chen et al, (2000), studied the genetic profile of patients with muscular dystrophy to document potential signaling events. In DMD muscle, several genetic markers associated with the immune response were found up-regulated, including complement and chemokine components. Immunostaining showed increased infiltration of macrophages and dendritic cells into the muscle [117]. Evans et al. (2009), suggests that the initiation of the inflammatory response could be the result of this overexpression of signaling molecules before disease onset. Consequently, infiltration of macrophages, lymphocytes and neutrophils can facilitate muscle wasting by continued cellular injury [119]. The inflammatory signaling components (i.e., chemokines) are expressed due the activity of a variety of transcription factors including NF-κB, NFAT, and AP-1 [119]. Activation of these transcription factors rely on specific signaling cascades, which in turn may depend on the presence of the DGC, the absence of which may cause dysregulated signaling [119].

C.3.1- Akt/NF-κB

NF-κB is a widely studied transcription factor known to play a role in inflammation initiation and perpetuation. NF-κB is a heterogeneous dimer, binding to DNA to initiate transcription [120]. NF-κB is held in the cytoplasm by IκB inhibition proteins, until IκB is phosphorylated by IκB kinase (IKK) where it is then subject to ubiquitin-dependent degradation [119]. Once IκB is degraded, NF-κB is free to localize to the nucleus where it then binds to DNA to initiate transcription of cytokines, chemokines, and a variety of other inflammatory proteins [121]. NF-κB activity is greatest during initial DMD onset, decreases with the age of the patient, but is evident during disease progression [122]. These characteristics suggest NF-κB plays an important role in the pathophysiology of DMD.

NF-κB can be activated by the PI3k/Akt signal cascade. PI3k/Akt are kinases involved in a variety of cellular responses including cell survival, metabolism, and

proliferation[123]. PI3k/Akt have been implicated in muscle hypertrophy and NF-κB activation [119, 124, 125]. While activation of PI3k/Akt through the DGC remains unclear, theories suggests activation in a laminin-dependent manner [126, 127]. Increased PI3k/Akt has been seen in mdx mice in early stages of the disease [124], and supports the notion of PI3k/Akt plays an important role in the propagation of the inflammatory response. As a consequence of NF-κB activation, chemokine receptors can also be produced and presented at the membrane, although this process is poorly understood [128]. Further activation of these chemokine receptors can also result in additional NF-κB activity, creating a positive feedback loop, until the inflammation is no longer required [129]. Inflammation contributes to muscle repair, and therefore is important to both muscle degeneration and regeneration.

C.3.2- Degeneration and Regeneration

The influence of the inflammatory response on the pathophysiology of DMD cannot be overstated, as inflammation is important for removing damaged tissue. Damaged or necrotic muscle fibers need to be removed or repaired, and is accomplished through the use of the inflammatory response. As cytokines and chemokines are produced, immune cells migrate toward the site of damage and remove the damaged tissue. However, the injury site must be repaired, and this is accomplished by satellite cells. Satellite cells are located between the muscle basal lamina and muscle fibers, and remain quiescent in uninjured muscle [130]. In injured muscle, satellite cells are activated by a number of mitotic stimuli (MyoD family of transcription factors, miRNA, and others) [130] and begin to proliferate. As they proliferate, satellite cells migrate to the site of injury and align themselves with the basal lamina and begin to fuse into myotubes, the precursors of muscle fibers [28]. As proliferation and regeneration continues, the myotubes begin to mature and continue to differentiate, synthesizing new fiber proteins. A hallmark of regeneration is centralized nuclei in the fiber. As the fiber matures, more fiber proteins are deposited and the nuclei are pushed to the periphery, resulting in the appearance of a mature fiber [28].

Specifically, the satellite cells are self-renewing. At quiescence, satellite cells express Pax7, and once activated by injury, express MyoD regulators. Pax7 is a paired

box transcription factor expressed in quiescent satellite cells [131], while MyoD regulators include MyoD, myf5, myogenin and Mrf4, and are transcription factors responsible for myogenic differentiation [132]. After satellite cells proliferate as Pax7 and MyoD positive cells, Pax7 is down regulated, MyoD expression is maintained, and differentiation occurs [133]. Other cells however, down regulate MyoD and maintain Pax7 expression, returning to quiescence [133] (Fig 2.10). This self-renewal is thought to ensure a constant pool of satellite cells for regeneration.

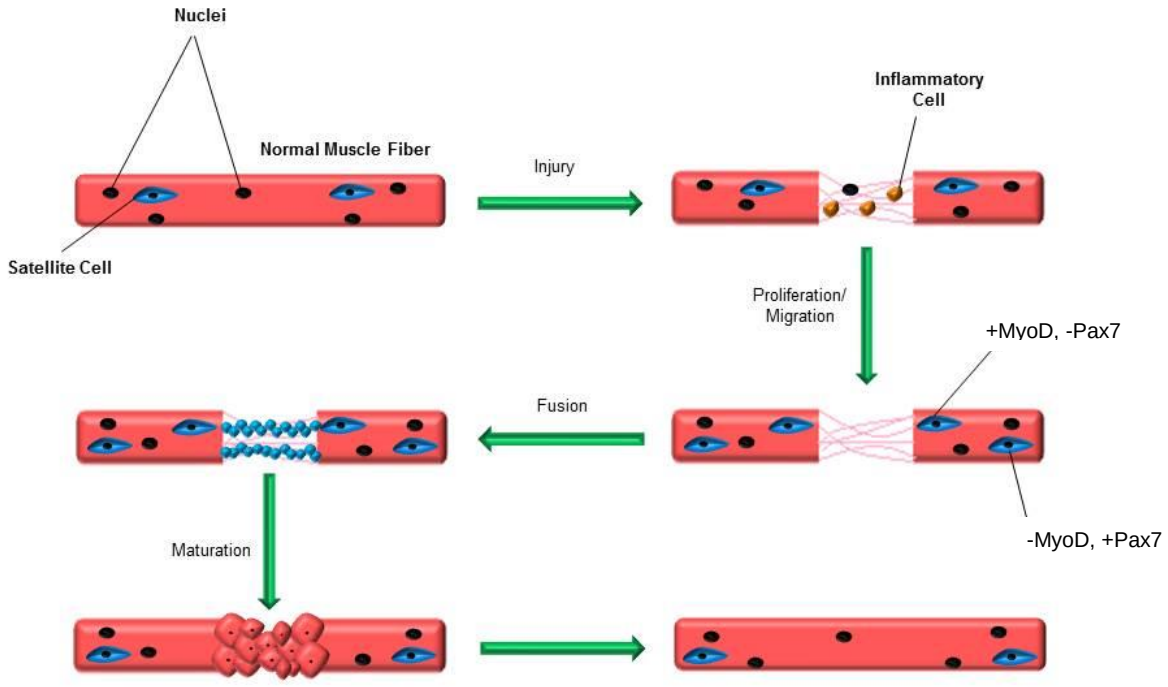

Figure 2.10. Muscle regeneration. After injury, inflammatory cells are mobilized to remove damaged tissue. Satellite cells activate MyoD leading to proliferation and fusion of satellite cells into myotubes. Myotubes mature and replace damaged tissue. Satellite cells that express Pax7 remain quiescent leading to satellite cell self-renewal.

In DMD, lack of dystrophin and mechanical stress incurred by repeated contractions results in higher rates of muscle degeneration. In turn, satellite cells are activated to repair the damaged tissue. However, dystrophin deficiency is not addressed by the cell, and muscle fibers enter into prolonged cycles of degeneration and regeneration. Eventually, satellite cells and self-renewal are unable to keep up with degeneration and are exhausted [134]; damaged muscle is then progressively replaced with either fatty or connective tissue [135], and muscle function is lost.

C.4- Summary

As part of the immune response, inflammation is a process conserved in all cell types. It is primarily responsible for the migration of immune cells, increased body temperature, and dilation of blood vessels. Inflammation contains two branches: the cellular and exudative components. The cellular side of inflammation concerns leukocytes and other immune cells and their various functions. The exudative side refers to plasma and the movement of a variety of proteins including cytokines and chemokines. These proteins can have a number of functions, but chemokines generally signal chemotactic properties in immune cells. There are a variety of chemokines, each with their own structure and function, but unfortunately not all of these functions are well understood. Chemokines must bind to a respective receptor to produce a specific function.

In DMD, patients present with a chronic inflammatory response that persists for the duration of the disease. While the inflammatory process is important by contributing to muscle repair, it may also be detrimental as it continues to exhaust the associated satellite cells responsible for muscle regeneration. Therefore, modulation of this inflammatory response could be beneficial to the overall DMD pathology. DMD and mdx tissue both demonstrate up-regulation of a variety of inflammatory genes. Targeting some of these markers could result in amelioration of the disease. Targeting Akt and NF-κB may be promising. Activation of Akt can lead to propagation of the NF-κB signaling pathway in DMD. NF-κB expression could be regulated through treatment to reduce, but not negate the inflammatory response. A promising family of molecules that could modulate the inflammatory response are the sphingolipids.

Section D: Sphingolipids

D.1- Introduction

As a potential modulator of the inflammatory response in DMD, sphingolipids represent a subset of lipid molecules found in the body. J.L.W. Thudichum named these molecules in 1884 because of their enigmatic nature and similarity to the riddle of the sphinx (what walks on 4 legs in the morning, 2 legs at noon, and 3 legs in the evening) [136]. While previously thought to play structural roles, sphingolipids also have signaling properties [19]. These signaling properties include positive modulation of the inflammatory response in a variety of cancers and other disease states. Because a similar inflammatory signature is evident between that of these cancers and DMD, sphingolipids may present a good treatment option for DMD.

D.2- Basic Properties

Sphingolipids are a class of lipids primarily involved in membrane structure [137]. Sphingolipids are not a single molecule, but rather a group of specific lipids each with their own specific functions [137]. These different sphingolipids are the result of various metabolic pathways that are discussed below. The structures of sphingolipids are based on building blocks known as sphingoid bases [138]. In mammals, the main sphingoid bases include sphingosine and dihydrosphingosine [138, 139]. Sphingosine is a long acyl chain with a head group containing two hydroxyl groups and one amino group at the end of the chain [139]. With the addition of a fatty acid chain to the amino group of sphingosine, ceramide is generated [139]. Ceramide is the simplest sphingolipid structure, and can give rise to a variety of more complex sphingolipids through metabolic pathways, altering the structure of the head group [140]. By adding a phosphocholine group to one of the terminal hydroxyl groups, sphingomyelin (SM) is generated [141]. Addition of a sugar to the head group will lead to the production of glycosphingolipid (GSL) [141]. Phosphorylation of the head group leads to sphingosine-1-phosphate (S-1-P) [141]. Production of these compounds is achieved by a complex metabolic pathway. These compounds are produced depending on the initial source, endogenously or exogenously. Exogenous sphingolipids refer to obtaining sphingolipids from outside the body, usually obtained through the diet. On a normal western diet,

adult humans ingest approximately 0.3-0.4g of sphingolipids per day, through sources such as meat, milk, and eggs. The major form of sphingolipid received through these sources is SM [142]. Digestion of the dietary SM is discussed below. Endogenous sphingolipids refer to sphingolipids that are synthesized with in the body through a complex series of reactions. These reactions are discussed in the next section.

D.3- Synthesis (*De Novo*) of Endogenous Sphingolipids

The formation of sphingolipids within the body occurs through a process known as *de novo* synthesis, this process occurs through a variety of reactions within the outer leaflet of the endoplasmic reticulum [141]. Synthesis of sphingolipids in the body begins with a condensation reaction of serine and palymitoyl-CoA to form 3-ketodihydrosphingosine, through the use of the enzyme serine palymitoyl transferase (SPT) [141]. 3-ketodihydrosphingosine is reduced through the enzyme 3-ketodihydrosphingosine reductase to sphinganine. Sphinganine is further acetylated by one of six dihydroceramide synthases to produce dihydroceramide [141]. Each dihydroceramide synthase has a preference for acetylation based on the fatty acid chain length [141]. Dihydroceramide is in turn, desaturated through the use of dihydroceramide desaturase, which introduces a double bond at the 4 position of the sphingoid base, producing ceramide [141]. Ceramide is at the core of sphingolipid metabolism, and once produced, is transferred to the Golgi apparatus by ceramide transfer protein (CERT) where the formation of more complex sphingolipids occurs [138, 141]. Movement of ceramide to the Golgi apparatus also signifies the end of *de novo* synthesis.

Once ceramide is produced, more complex sphingolipids can be produced in the Golgi through the use of a variety of separate enzymes. Formation of the most common complex sphingolipid, SM, occurs through the use of sphingomyelin synthase [141]. Sphingomyelin synthase adds a phosphocholine group to the head group of ceramide resulting in SM and diacylglycerol [141]. Ceramide may be also glycosylated through glucosyl- or galactosylceramide synthase to form glycosphingolipids or gangliosides. Ceramidase degrades ceramide into sphingosine, which can be further modified into sphingosine-1-phosphate (S-1-P) by sphingosine kinase [141]. As shown in figure 2.11,

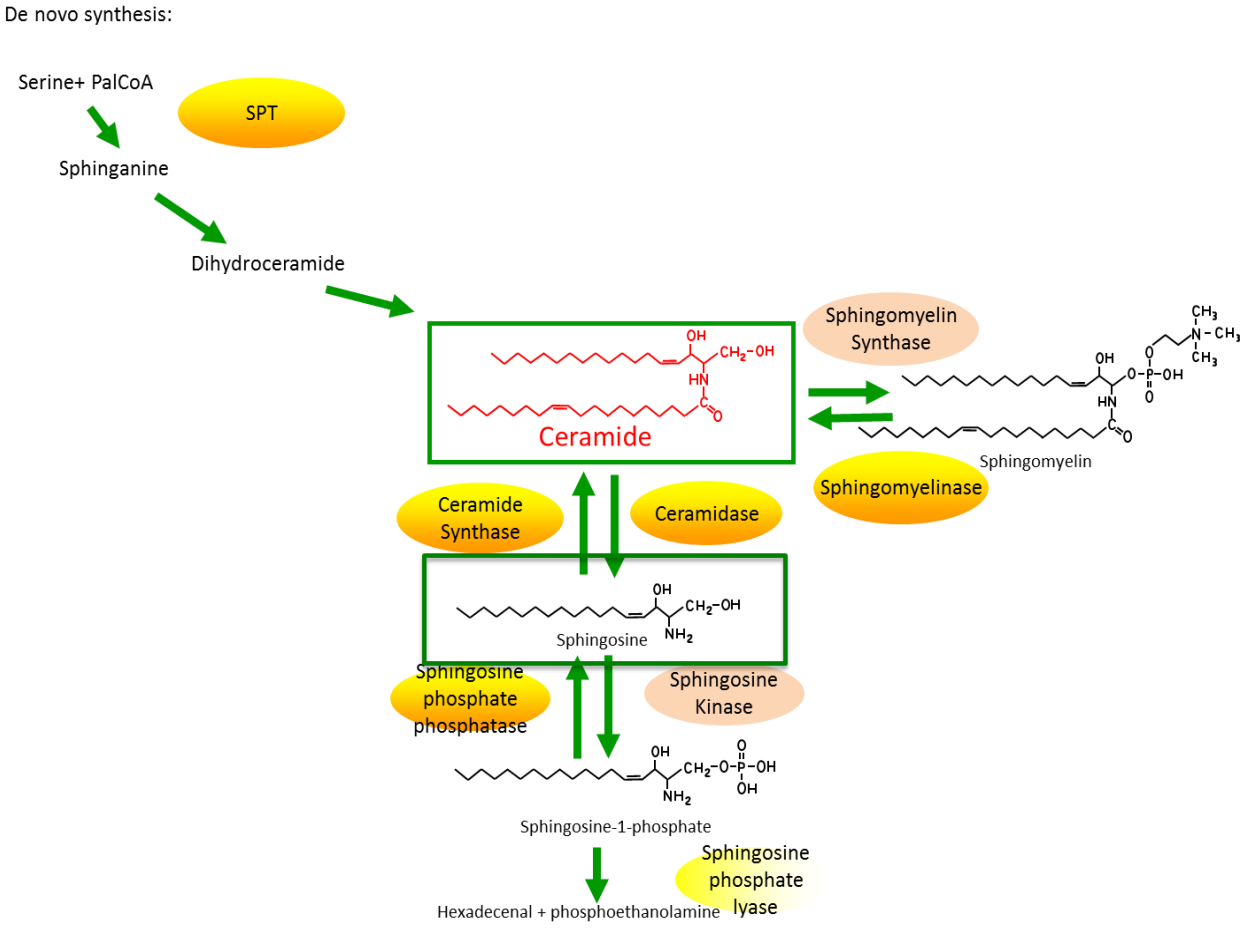

Figure 2.11. Sphingolipid structures and metabolism. De Novo Synthesis begins with Serine+ Palmitoyl CoA, and ends with the formation of ceramide, the central hub of sphingolipid metabolism. Once formed, ceramide can be converted to other metabolite forms based on the cell's needs.

most of these reactions are reversible, which allow the cell to control the concentrations of each metabolite as needed. Similarly, dietary sphingolipids, once absorbed in the cell, can be altered through these pathways. However, digestion of sphingolipids also presents a complex pathway.

D.4- Digestion of Exogenous Sphingolipids

In a normal diet, an adult human will ingest 0.3-0.4g sphingolipids per day, and constitute approximately 0.01% of the daily diet [142]. Foods such as eggs, meats, milk, and fish provide a good source of sphingolipids [142]. Most animal-based dietary sphingolipids are in the form of SM [142, 143]. Absorption of dietary SM occurs in the intestine where SM must first be broken down by Alk-SMase and ceramidase into sphingosine; it can then be absorbed by the intestinal lumen [144]. Once incorporated into the mucosal cells of the lumen, sphingosine is converted back to ceramide and fatty acids [144]. Some of this ceramide is converted into more complex sphingolipids (through the processes above), and may be incorporated into the membrane of the cell

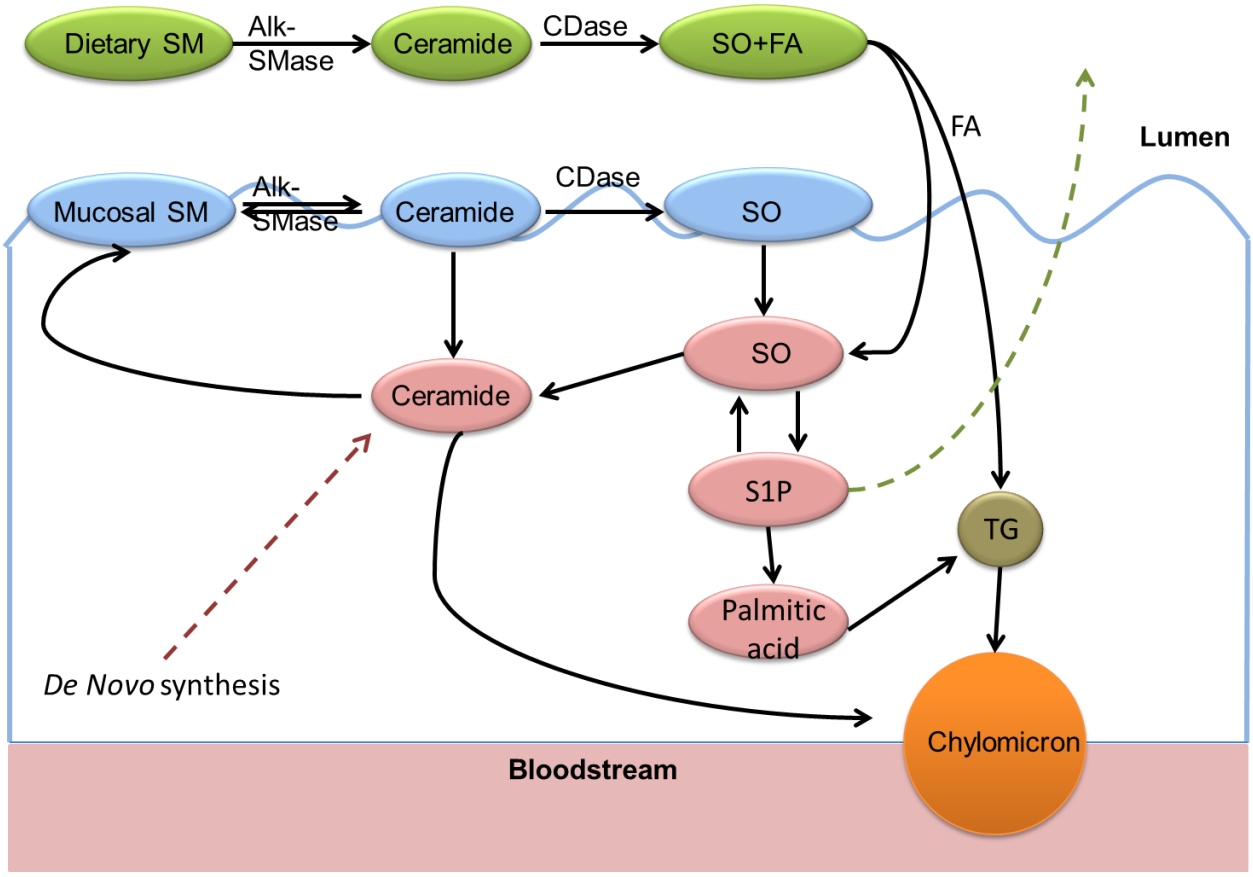

Figure 2.12. Digestion of sphingolipids. SM (sphingomyelin) either from food sources or found in the membrane can be broken down to SO (sphingosine); SO diffuses into the cell. Additional reactions convert SO to ceramide or S1P (Sphingosine-1-phosphate). Conversely, *de novo* synthesis can also contribute to ceramide production. Ceramide and triglycerides are incorporated into chylomicrons where they enter the lymph system and subsequently enter the bloodstream (not shown). Adapted from Duan and Nilsson (2009).

[144]. Alternatively, some ceramide/SM will be incorporated into chylomicrons, which can then enter the lymph and subsequently the bloodstream for transport to other parts of the body (Fig 2.12).

Once the chylomicron is formed and enters the bloodstream, lipoprotein lipase present on the surface of cells, breaks it down so ceramide can be taken into the cell [144]. The chylomicron remnants will circulate to the liver, where they are converted to other lipoproteins (very low density- VLDL, high density- HDL, low density- LDL), which are redistributed through the body, and where ceramide may be further incorporated into cells [142]. Ceramide concentration is greatest in LDL, followed by VLDL and HDL [143]. The ceramide incorporated into cells can be interconverted to other metabolite forms depending on the concentration of sphingolipid enzymes in the target cell [145]. At present in skeletal muscle the concentrations of sphingolipids and related enzymes have not been well-defined. However, concentrations of ceramide, SM, and S1P have been observed [146]. The actions of sphingolipids in cells can vary depending on the metabolite, and exist in a highly balanced state.

D.5- Functions of Sphingolipids (Sphingolipid Rheostat)

The various sphingolipid metabolites generated from synthesis and digestion have a variety of functions, unfortunately, many are not well-defined. However, these metabolites play an important role in a variety of signaling pathways in the cell. In general, ceramide, and to a lesser extent, sphingosine are both associated with arrest of cell growth and apoptosis [20]. While the exact mechanism of how these metabolites work is not well understood, ceramide inhibits Akt, acting in direct opposition to the functions of Akt [147]. Ceramide accomplishes this by promoting dephosphorylation of Akt through protein phosphatase 2A and by preventing Akt translocation by inhibiting PKCζ [20]. Ceramide signaling pathways are activated during times of stress leading to eventual apoptosis of the cell, and inhibit inflammatory pathways [144, 148]. Alternatively, S1P is implicated in cell survival and pro-inflammatory properties during signaling [21, 144]. S1P binds to 5 specific GPCRs on the cell membrane to initiate downstream activation of survival signals including NF-κB, Akt, and others [21, 149]. In skeletal muscle, 3 S1P receptors have been identified, named $S1P_{1-3}$ [149]. After S1P

binds to the receptor, G proteins are activated initiating a number of downstream events, including activation of Akt and ERK, and inhibition of JNK and other pathways [21]. S1P may also act as a secondary messenger; however the mechanism of action is undefined (Fig 2.13) [21].

In summary, ceramide and sphingosine demonstrate death signaling properties, while S1P demonstrates cell survival properties. This distinct difference in action

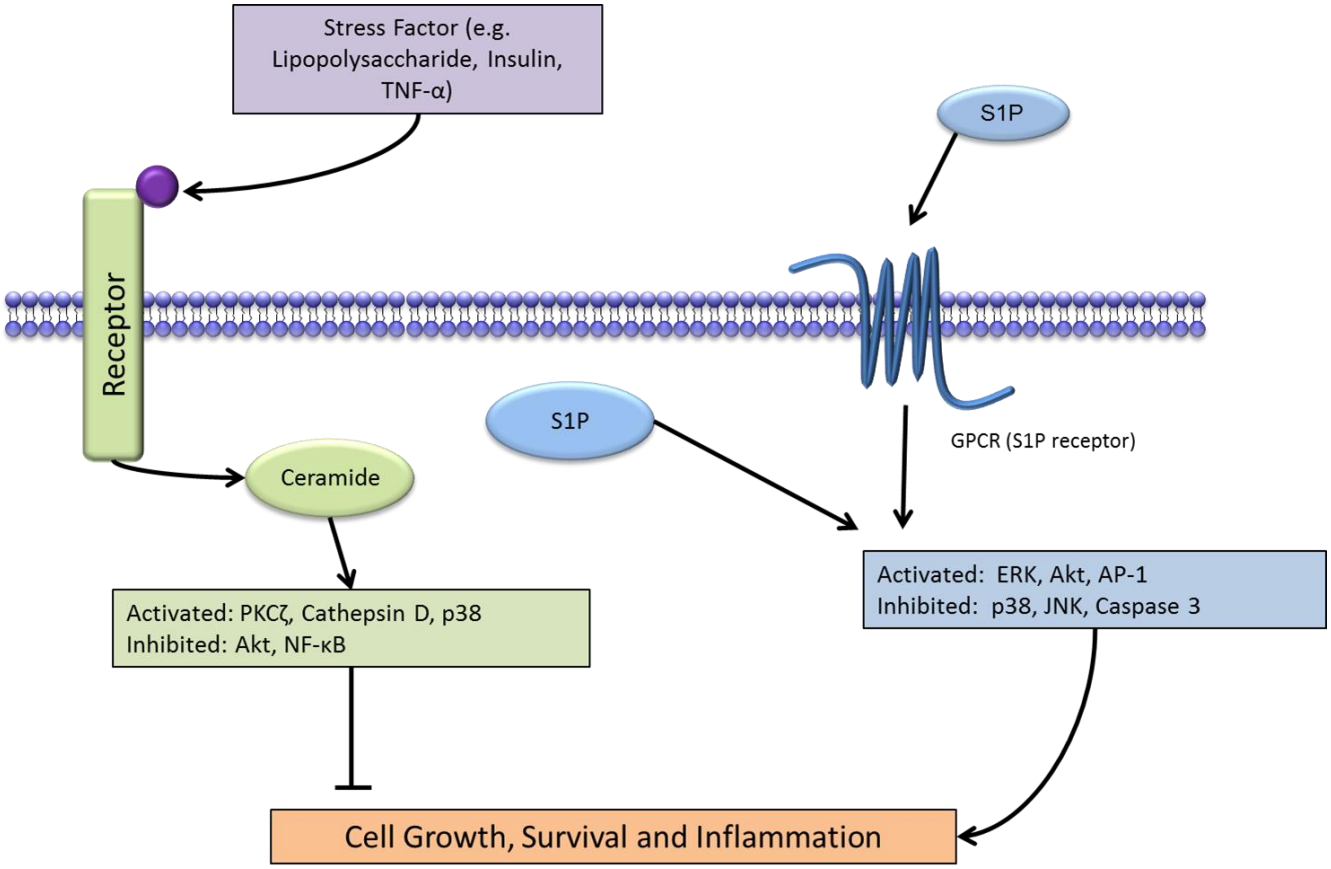

Figure 2.13. Signaling with sphingolipid metabolites in cells. Ceramide acts primarily as an inhibitor of cell growth and inflammation, while S1P promotes growth and inflammation. Conversely, S1P can bind to S1P receptors, or act as a secondary messenger. Other sphingolipid metabolites also have signaling properties, but are not well defined. In skeletal muscle, the enzymes responsible for sphingolipid conversion are observed, but their concentrations are not presently known

suggest a balancing act between the differing metabolite states. During stress, *de novo* synthesis is activated producing ceramide and subsequently sphingosine to signal cell death [22]. Meanwhile, many other stimuli such as growth and survival factors result in the production of S1P, which subsequently inhibits ceramide-induced apoptosis [22].

Thus, the interplay of these opposing functions are important to whether a cell will live or die [22, 136]. This sphingolipid rheostat concept has many clinical implications.

D.6- Clinical Applications of Dietary Sphingolipids

The sphingolipid rheostat can be manipulated to produce more of a given sphingolipid metabolite [22]. For instance, production of more ceramide rather than S1P results in a stronger anti-inflammatory/apoptotic response, whereas if there is more S1P, further growth and inflammatory signals are produced [22]. Manipulation of the sphingolipid rheostat can be accomplished by targeting specific enzymes in the sphingolipid metabolic pathway such as the ceramidases or sphingosine kinases, to alter production of sphingolipid metabolites [23, 137]. Alternatively, targeting downstream signaling molecules such as Akt, NF-κB, ERK and others, can influence genetic expression of inflammatory markers that could otherwise be influenced by sphingolipids. A common and convenient method to alter sphingolipid metabolites is through the diet. Ingested sphingolipids usually enter the digestive tract as SM, where they are converted and transported as ceramide (seen above). An increase in ceramide concentration can increase anti-inflammatory signaling, which is effective in the treatment of certain diseases.

Simon et al. (2010) studied the effects of dietary SM on breast cancer growth and suppression. Pre-malignant human breast epithelial cells, MCF10AT1, were injected into 8-week old NCR nude female mice, where the cells were left to produce lesions. Once produced, 0.1% by weight SM diet (AIN 76A) was provided to half the mice. Mice treated with the dietary SM demonstrated several beneficial effects. Cell proliferation decreased, and apoptosis was not increased. Cells stained for Ki-67, a marker for proliferation and growth, showed decreased positive nuclei in the dietary SM-treated compared to the untreated mice. Cells stained for capsase-3, an apoptotic marker, showed negatively in both the treated and untreated groups. Vascular endothelial growth factor (VEGF) expression was decreased in the SM-treated mice, reducing overall angiogenesis, thereby depriving the cancer of a key need: oxygen. Proteins associated with cancer cell growth were decreased in the SM-treated group. Finally, enzymes responsible for conversion of SO to S1P decreased, while enzymes

responsible for ceramide (SMase, Ceramidase, etc.) conversions were relatively unchanged. This study demonstrated several beneficial effects of dietary SM to slow growth of breast cancer [23]. Dietary SM also have beneficial effects on the inflammatory response associated with cancer.

Mazzei et al. (2011) examined the effects of dietary SM on inflammation associated with colon cancer in mice. Decreased expression of nuclear peroxisome proliferator-activated receptor (PPAR) γ was examined specifically as a potential cause for increased susceptibility to colonic inflammation. Mice were split into groups of PPAR γ positive or negative groups and were given either a normal AIN 76A diet, or AIN 76A diet supplemented with 0.1% by weight SM (10 mice per group).

Again, several beneficial effects of dietary SM were observed. The body masses of the mice between treatment groups were unchanged, and the disease activity index (DAI) was only different in the untreated PPARγ-/- mice. Tumor formation in $PPAR\gamma^{-/-}$ mice treated with dietary SM was significantly less from untreated mice, while tumor growth in $PPAR\gamma^{+/+}$ mice was unchanged. Using qRT-PCR, the potential influences of dietary SM on genetic expression of inflammatory markers was examined. SM increased many chemokines and cytokines by more than two-fold, but $PPAR\gamma^{+/+}$ mice showed decreased expression of many markers. Inflammatory intermediates such as Myd88, DOCK2, and transcriptional factors NF-κB and Stat3 expression were depressed in SM-treated mice, favoring an anti-inflammatory environment. This study found that dietary SM decreased inflammation associated with colon cancer, and again, slowed the progression of the disease [24]. Many other studies showed the beneficial effects of dietary SM to attenuate disease progression and inflammatory response [150-153], although current research on DMD and sphingolipids are limited.

D.7- Summary

Sphingolipids are a class of molecules known as “bioactive lipids” that demonstrate signaling properties, among their traditional role as components of the cellular membrane [137]. Sphingolipids are not one molecule, but rather a group of molecules (metabolites) that share a common structure. Alterations in the head group change the structure and function. The various sphingolipid metabolites are produced

by different reactions. *De novo* synthesis of ceramide requires serine and palmitoyl-CoA and intermediates [138]. Alternatively, sphingolipids can be obtained through the diet, usually in the form of SM [144]. SM is broken down into ceramide and absorbed into the mucosal cells of the digestive tract where it may be incorporated into chylomicrons for transport to various tissues via the blood [144, 154]. Once produced, ceramide in response to various reactions, can form complex sphingolipids such as S1P, SO, and SM [144, 155].

Each sphingolipid metabolite has different signaling properties that can influence cell functions [156]. Ceramide and SO both have apoptotic/ anti-inflammatory properties by inhibiting the action of signaling intermediates such as Akt and PKC, and inhibiting cell survival and inflammation [21]. S1P has cell growth/pro-inflammatory properties by promoting the activities of Akt, ERK, and MAPK, resulting in infiltration of macrophages, propagation of the inflammatory response, and promoting the expression of growth factors [21, 140]. These opposite actions of the sphingolipid metabolites are constantly rebalanced, an idea referred to as the sphingolipid rheostat [22]. Depending on the tissue, the expression of any given metabolite will vary, resulting in a specific cell state. The rheostat is an important concept behind the potential of sphingolipids as treatment for a variety of diseases.

Sphingolipids and their effects have been examined most closely in a variety of cancers. These studies showed that not only do sphingolipids reduce the inflammation associated with some cancer lines, but also inhibits growth of cancer cells and propagation of the disease, with no visible side effects [23, 24, 151]. It is probable then, that the sphingolipid properties could carry over to other diseases such as DMD. Unfortunately, the effect of sphingolipids has not been thoroughly assessed in muscle tissue. However because of similarities between the inflammatory signatures of cancer and DMD, sphingolipids could present a viable option in the modulation of the inflammatory response associated with DMD. The motivation for this study, therefore, was to address the potential roles of sphingolipids to modulate the skeletal muscle inflammatory response and to improve skeletal muscle function in mdx mice, a model of DMD.

Chapter 3: Methods

Animals and Study Design

Male C57BL/10ScSnJ and mdx mice aged 4 weeks (n=40) were purchased from Jackson Laboratories (Bar Harbor, Maine). Mice were single housed on a 12:12-h light:dark cycle and provided food and water ad libitum. After 1 week of acclimation, mice were randomly assigned to receive either a standard AIN 76A diet, or AIN 76A diet with 0.1% sphingomyelin for 7 weeks. Mice were given approximately 40 g of the assigned diet every week, and body masses and food consumption were monitored weekly. During the 7 week diet treatment period, mice were assessed for hind limb torque *in vivo*. After 7 weeks, mice were sacrificed under ketamine/xylazine anesthesia IP (20mg ketamine, 2 mg xylazine per 100g body mass). All procedures were approved by the Institutional Animal Care and Use Committee at Virginia Tech (Fig 3.1).

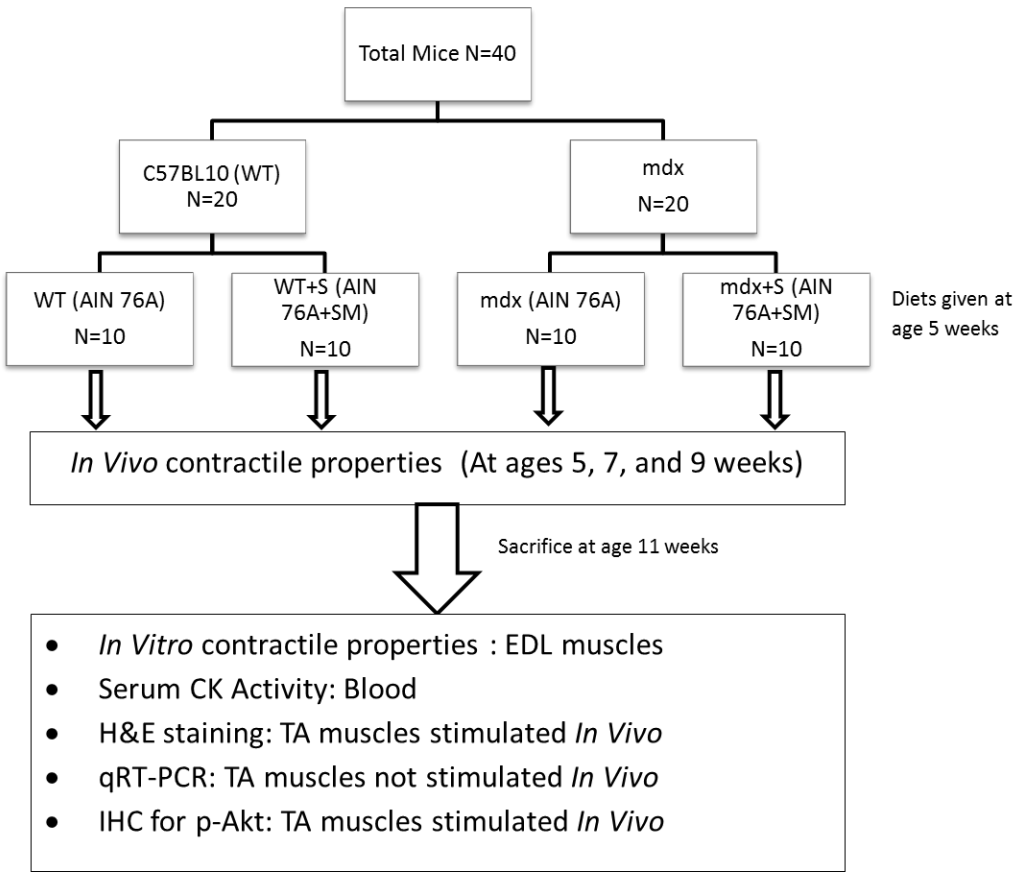

Figure 3.1. Study Design

In Vivo Torque Measurements

Mice were anesthetized using isoflurane gas (2.5%) mixed with 100% oxygen (1L/min) in a vaporizer delivered to an induction box (Model Impac5, VetEquip, Pleasanton, CA). After the mouse was anesthetized, the mouse was transferred to the preparation area with supplemental anesthesia delivered via nose cone. Hair on the right hind limb was shaved with a Wahl trimmer (Sterling, IL) and further removed with depilatory cream (Nair). Nair was left on the limb for 30 seconds and then removed with 2x2 gauze soaked in clean water. Finally, iodine and betadine were applied to clean and disinfect the skin with 2x2 gauze. The mouse was positioned on its dorsal side on a folded paper towel to provide insulation from the unheated metal plate of the torque apparatus (Model 300C-LR FP, Aurora Scientific, Ontario, CA). The right foot of the mouse was taped with surgical tape to a metal foot plate, which was connected to the shaft of the servomotor (Model 300C-LR FP, Aurora Scientific). The malleolus of the ankle was considered the center of rotation and so was aligned with the servomotor axle. The foot was positioned at a 90 degree angle to the tibia and the tibia at a 90 degree angle to the femur. To maintain the mouse in position, a 7/64" allen wrench was wrapped in gauze (to reduce heat loss) and placed to brace the mouse's side. The mouse was then taped from one side of the platform to the other across the ventral surface. The anesthetic nose cone was also secured to the platform with tape.

Two sterilized platinum subdermal needle electrodes (model E2-12, Grass Technologies, West Warwick, RI) were inserted through the skin on either side of the left common peroneal nerve. One electrode was placed just distal to the fibular head, while the other electrode was placed ~4mm distal to the first electrode. Stimulation was delivered using a stimulator (Models 701C, Aurora Scientific) to induce contraction primarily of the anterior crural muscles (tibialis anterior, extensor digitorum longus, and extensor hallucis longus muscles) [157]. The parameters on the stimulator were a 200-ms contraction duration consisting of a single 0.5 ms square wave pulse to produce maximal isometric twitch torque at the ankle. The voltage on the stimulator was initially set at 3.0V and was adjusted between 1.0 and 7.0 V until twitch torque no longer increased. Peak values were determined every 2 weeks, at 5, 7, and 9 weeks of age.

The investigator collected data at weeks 5 and 9 for all mice and at week 7 for 20 mice, while Dr. Robert Grange collected data for week 7 for the remaining 20 mice.

The force-frequency protocol consisted of two twitch measurements at optimal voltage 30 seconds apart, followed by a tetanus consisting of 0.5-ms square wave pulses at 150hz. The mouse rested 5 minutes and then contractile responses were obtained at 1, 10, 30, 50, 80, 100, 150, 200, and 250hz, delivered 30-60 seconds apart. After the final stimulation, body mass was determined on a Sartorius portable scale (Model PT1200, Bohemia, NY). In addition, heel to toe length, and ankle to toe lengths were measured by positioning the foot against the wooden stem of a cotton swab, marking the stem as appropriate with a fine-tipped marker, followed by measurements with a ruler. To revive the mouse, it was placed in an oxygenated (1 L/min) plexiglass recovery box until the animal was awake and began to move around the box. Isometric data are presented as torque per gram of body mass (mN-m/g).

In Vitro Contractile Properties

At age 11 weeks, mice were deeply anesthetized (20mg ketamine, 2 mg xylazine per 100g body mass IP injection), and the fast-twitch EDL muscles were excised. Non-absorbable braided silk suture (4-0) was tied to the proximal and distal tendons at the myotendinous junctions. EDL muscles were placed in an incubated 30^0C oxygenated (95% O_2, 5% CO_2) physiological salt solution (PSS) containing (in mM): 120.5 NaCl, 4.8 KCl, 1.2 $MgSO_4$, 20.4 $NaHCO_3$, 1.6 $CaCl_2$, 1.2 NaH_2PO_4, 10 dextrose, and 1.0 pyruvate. EDL muscles were then fixed between an arm of a dual-mode servomotor system (300B, Aurora Scientific) and a clamp positioned at the bottom of the muscle bath. Muscles were set to an initial resting tension of 1.0g, which was maintained by a stepper motor; The force and position inputs of the servomotor arm and the stepper motor were controlled by Dynamic Muscle Control software (DMC Version 4.1.6, Aurora Scientific). In response to stimulation, the software collected both position and force output data from the servomotor during muscle contraction. Stress values were determined by converting the output force values (g) to millinetwons (mN) by multiplying by the acceleration of gravity (9.81 m/s^2), then by dividing by the cross sectional area (CSA) of the muscle. CSA was calculated by dividing the mass of the muscle (mg) by

the product of the muscle length (mm) and skeletal muscle density (1.06 mg/mm^3). Finally, power curves were generated from the force-velocity relation for each muscle by multiplying load (in g) by its associated velocity (mm/s) and converting to milliwatts (mW).

After EDL dissection and mounting to the contractile apparatus, additional samples from each mouse were obtained. Blood was first collected by cardiac puncture (1mL insulin syringe) and transferred to heparinized tubes (Becton Dickson), and refrigerated for 30 minutes to clot blood. The tubes were centrifuged (5415 D, Eppendorf, Hauppange, NY) at 4600 rpm for 10 min at 4^{0}C to separate serum. Serum was stored at -80^{0}C until analyzed for serum CK concentration. Tibialis Anterior (TA) muscles were harvested, with the muscle from the *in vivo* stimulated leg cut transversely at midbelly. The distal half was frozen in liquid nitrogen and stored at -80^{0}C, and the proximal half preserved in immunomount (Sakura Finetek, Torrance, CA) in a tissue biopsy mold (Sakura Finetek) and stored at -80^{0}C. The TA muscle from the non-stimulated leg was preserved in RNAlater for 48 hours. After this period, the RNAlater was decanted and the TA stored at -80^{0}C until qRT-PCR analysis. The heart and liver were excised and frozen in liquid nitrogen, and stored at -80^{0}C. Lungs were removed and stored in RNAlater for 48 hours, where RNAlater was decanted and the lungs then stored at -80^{0}C for later analysis. Other hind limb muscles including the quadriceps, soleus, gastrocnemius, and adductor magnus muscles were excised, frozen in liquid nitrogen and stored at -80^{0}C until further analysis.

The stimulated muscle protocol consisted of 5 steps: 1) pre-twitch and tetanus; 2) force-frequency; 3) force-velocity; 4) fatigue; and 5) fatigue recovery. In step 1, the stimulated muscle was subjected to 2 isometric twitches and a single tetanus (150 hz) each separated by 1 minute. In step 2, the muscle was subjected to a force frequency protocol as described above. The muscle was then quiescent at L_0 for 5 minutes, and then subjected to a force-velocity protocol. The muscle was stimulated 6 times at various percentage loads relative to the maximum tetanic force (force value at 150 hz obtained from the force-frequency protocol). The loads included 5, 10, 25, 50, 75, and 90%, each separated by 1 minute. In step 4, the muscle was stimulated at 60hz once

every 5 seconds for 5 minutes to induce fatigue. Finally in step 5, 60 hz tetany were evoked at 5, 10, 15, and 30 minutes after step 4 to determine the recovery from fatigue. Data are reported as normalized stress (mN/g)

Serum CK Analysis

Blood was collected via cardiac puncture (1mL syringe) into heparinized tubes (Becton Dickson) and stored at 4^0C for at least 30 minutes. Tubes were centrifuged (5415D, Eppendorf) at 4600 RPM for 10 minutes, and serum for each sample was removed by pipette and stored in a separate microcentrifuge tube (Eppendorf) at -80^0C until analysis. Serum CK was determined with the MaxDiscovery Creatine Kinase Enzymatic Assay kit (Bioo Scientific, Austin, TX) following the manufacturer's instructions. Briefly, serum samples were thawed on ice and a 5µl of each sample placed into a separate well of the 96 plate provided by the manufacturer, in duplicate (i.e., two wells per sample). 250µl of provided reagent was added to each well, and samples were immediately analyzed using a Synergy 2 multi-mode microplate reader (Biotek, Winooski, VT) at 340nm, and again after 5 minutes. Calculations to determine CK activity were performed per the manufacturer's instructions.

mRNA Extraction and qRT-PCR

mRNA was extracted from non-stimulated *in vivo* TA samples using trizol (MRC, Cincinnati, OH), and Qiagen RNeasy minikit (Qiagen, Valencia, CA), following the manufacturer's instructions. Five hundred ng of RNA were reverse-transcribed to cDNA using the ImProm-II Reverse Transcription system (Promega, Madison, WI), with random hexamer and oligo-dT primers added according to the manufacturer's directions. Quantitative real-time polymerase chain reaction (qRT-PCR) was performed on 5ng of cDNA using gene-specific primers (designed with Beacon Design software; Palo Alto, CA) and SensiMix plus Sybr mastermix (Quantace, Taunton, MA) in a 15µL reaction. The reaction mixture was pre-incubated for 10 minutes at 95ºC, and the qRT-PCR was performed for 42 cycles at 95^0C for 15 seconds, 54-58^0C for 30 seconds, and 72^0C for 15 seconds on a 364 well plate. The plate was analyzed using the ABI 7900HT Fast Real-Time PCR system (Applied Biosystems, Foster City, CA), and dissociation

curves were produced to insure purity of the PCR product. The ΔΔCt method was used to determine fold change [158].

Sectioning and H&E Staining

Harvested TA muscles from the *in vivo* stimulated leg were cut transversely at mid-belly. The largest portion was mounted in OCT (Sakura Finetek) to present the largest CSA for sectioning. Eight µm serial sections were obtained with a Microm HM 550 cryostat at -20^{0}C. Sections were collected on frosted slides (Fisherbrand, Atlanta, GA), and allowed to air dry at room temperature for 1 hour. After drying, slides were stored at -80^{0}C until stained.

TA sections were stained using hematoxylin and eosin (H&E). Slides were placed in hematoxylin (Fisherbrand) for 30 seconds and then washed in fresh tap water for 1 minute, followed by 30 seconds in eosin (Fisherbrand), and washed in fresh tap water for 1 minute. Slides were allowed to air dry at room temperature, mounted with Permount (Fisherbrand), and were coverslipped. Slides were imaged using a Nikon Eclipse 80*i* epifluorescence microscope, equipped with NIS elements. Images were enhanced with Adobe Photoshop.

A quantitative analysis of the muscle histopathogy included identification of regenerating, degenerating, and necrotic fibers, as well as inflammatory cell infiltrate. Regenerating fibers were identified by a smaller diameter and centralized nuclei. At 20x magnification, regenerating fibers were counted per total number of fibers per section. Degenerating fibers were identified by eosinophilic, hyalinized, and pyknotic fibers. Necrotic fibers were identified as fibers with distrupted fibers with invaded inflammatory cells. At 40x magnification, a grid was superimposed over each selected image and the numbers of intersections over pathological markers were counted and reported as a percent of the total intersections [16].

Immunohistochemistry

Frozen TA sections were warmed at room temperature for 30 minutes, and then fixed in cold acetone for 5 minutes. Sections were allowed to dry for 30 minutes. Sections were rinsed in PBS 2 times for 2 minutes each, followed by incubation with

peroxidase quenching solution (Invitrogen, Carlsbad, CA) for 45 seconds and rinsed in PBS briefly. Sections were then blocked with 2% chicken serum for one hour at room temperature. After blocking, sections were incubated with primary antibodies specific for p-Akt (Invitrogen) at 1:10 2% chicken serum dilution and placed at 4ºC overnight without rocking. Sections were rinsed in PBS 3 times for 2 minutes each. *SuperPicTure* Polymer Detection Kit (Invitrogen) was used for secondary antibodies, following the manufacturer's instructions. Briefly, 100 µL of horseradish peroxidase (HRP) polymer conjugate was applied to each section and incubated at room temperature for 10 minutes. Sections were rinsed with PBS 3 times for 2 minutes each. Meanwhile, reagents B1 (1 drop- 20x buffer/substrate), B2 (2 drops- 20x DAB chromogen), and B3 (1 drop- 20x 0.6% H_2O_2) was mixed with 1 mL of deionized water and vortexed to form the total DAB chromogen. One hundred µL of DAB chromogen was added to each section and incubated at room temperature for 5 minutes. Sections were rinsed in deionized water 3 times for 2 minutes each. Finally, sections were counterstained with hematoxylin (Fisherbrand) for 45 seconds and rinsed with deionized water until water ran clear; then sections were permanently mounted with Permount (Fisherbrand). Images were digitally captured on a Nikon Eclipse 80*i* epifluorescence microscope, equipped NIS elements. Images were edited with Adobe Photoshop. Images were evaluated by visual inspection and analysis software (NIS elements).

Statistics

For *in vivo* measurements, two-way analysis of variance (ANOVA) with repeated measures was used. Age was the repeated measure, and diet (genotype ± sphingolipid; WT, WT+S, mdx, mdx+S) used as the between factor. For in vitro measurements, a two-way ANOVA with repeated measures was used for force-frequency, force-velocity, fatigue, and fatigue recovery protocols, with frequency, percent load, and time as the repeated measure, respectively. One way ANOVA was used to ascertain differences in body mass, foot length, food consumed, twitch and tetanic responses between the treatment groups, serum CK concentration, and percent centralized nuclei. When significant interactions were evident post hoc analysis was performed. Post hoc analysis included Tukey's multiple comparison to compare specific sets of means. All data is

represented as mean ± standard error of the mean (SEM). Significance was set at $\alpha=0.05$.

Chapter 4: Results

Body Mass and Diet Consumption

Body mass increased for all treatment groups over the 6 week study period (P<0.0001). There were no interactions between age and diet (P=0.0950). Food consumption was not different between groups at any age (P=0.6220). For all groups, food consumption increased between 6 and 11 weeks of age (P<0.0001, Fig 4.1).

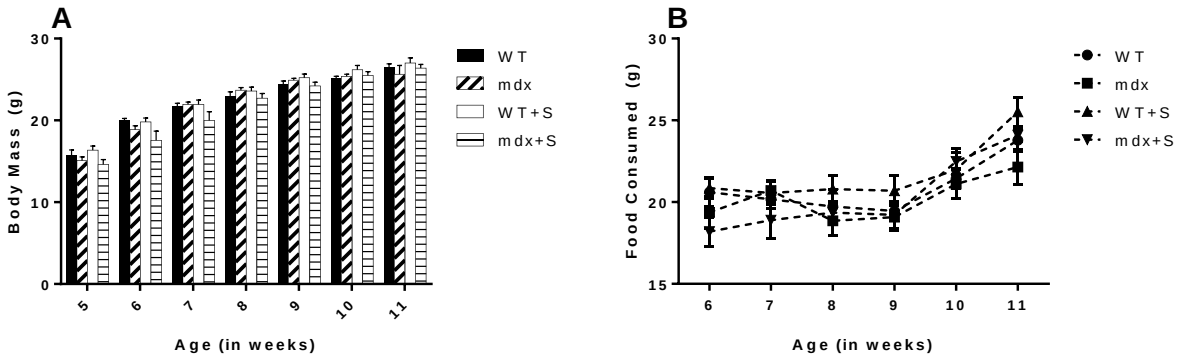

Figure 4.1. Body mass and food consumed during in vivo time-course. A: Body mass increased over time. B: Amount of food consumed increased with age. Values are mean ± SEM. n=10 per treatment group

In Vivo Muscle Strength

Torque generation of the anterior muscles of the hind limb (EDL, TA) were unchanged at age 5 and 7 weeks (P=0.3278, P=0.9561, respectively) across increasing stimulation frequencies and treatment groups. At age 9 weeks, the interaction between stimulation frequency and treatment group was significant (P=0.0012), but only at stimulation frequencies greater than 50 hz (Fig 4.2). At age 9 weeks, Mdx+S demonstrated greater normalized torque production than mdx or WT(in N*mm/kg: 68.8 ± 5.3 (Mdx+S) vs. 52.4 ± 5.1 (Mdx, P=0.0070) vs. 44.4 ± 5.2 (WT, P<0.0001)) at 150 hz. WT was also significantly different from WT+S (44.4 ± 5.2 vs. 63.4 ± 4.3 N*mm/kg, respectively; P=0.0011). Across age, there were no differences in maximum torque between treatment groups (P=0.0550).

The temporal properties of both the twitch and maximum tetanus are shown in Table 4.2. The ability of the muscles to generate force quickly and relax (Time to peak

torque and half-relaxation time, respectively) were unchanged at 5 and 7 weeks of age. However, at 9 weeks of age WT time to peak (TPT) was different from mdx+S (28.5 ± 2.79 vs. 24.0 ± 0.40 ms, respectively; P=0.004). The maximum and minimum rates of torque production (Max and Min dT/dt, respectively), and torque time integral (TTI) were not different among groups at ages 5 and 7weeks.

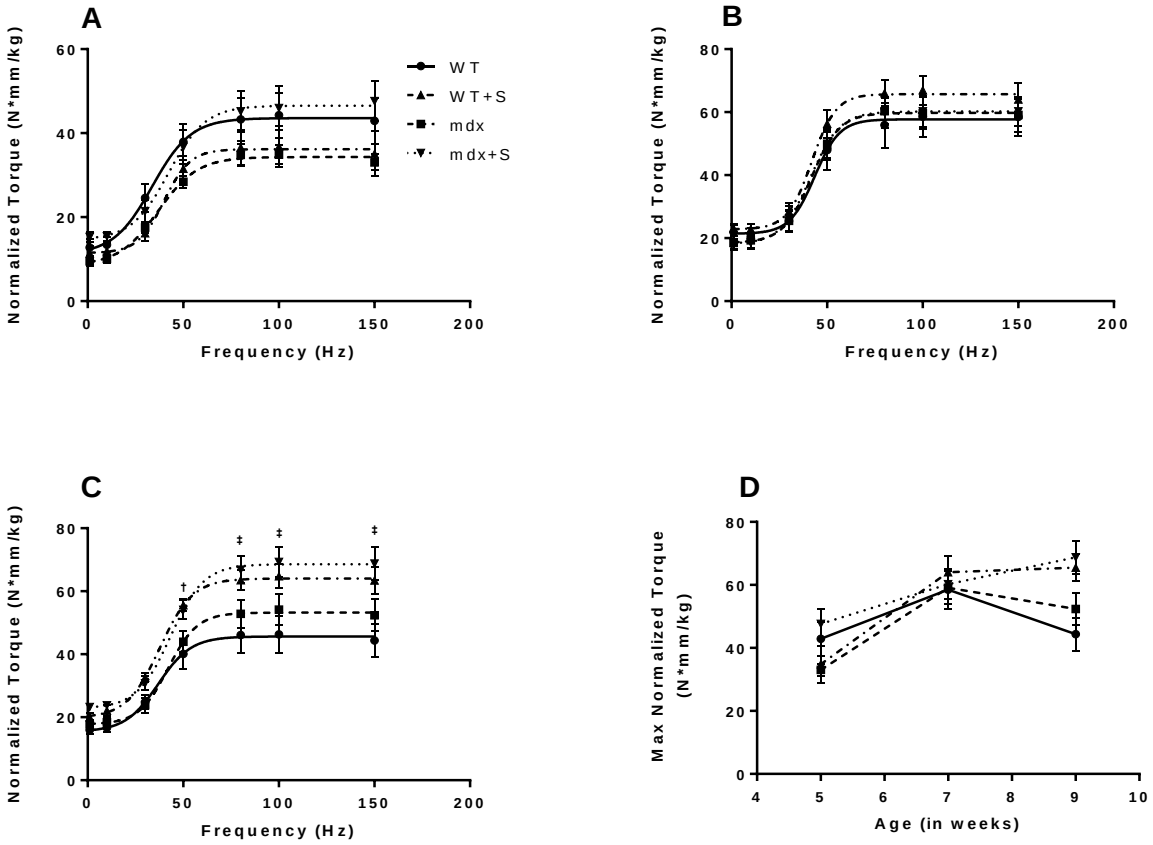

Figure 4.2. Torque-frequency relations. Age 5 weeks (A), 7 weeks (B), 9 weeks (C), Across time (D).Values are ± SEM, and normalized to body mass. †WT different from WT+S and mdx+S (P<0.05). ‡mdx+S greater than mdx and WT, and WT different from WT+S (P<0.05). n=10 per treatment group

Table 4.1. Body masses, twitch and tetanic properties from mdx and C57BL10 mice fed an AIN 76A diet with or without 0.1% sphingomyelin at age 5, 7, and 9 weeks.

	C57BL10		mdx	
	Control	0.1% SM	Control	0.1% SM
	5 Weeks of Age			
Body Mass (g)*	15.71 ± 0.67	16.36 ± 0.51	15.09 ± 0.45	14.62 ± 0.60
TPT (ms)	27.31 ± 0.91	26.09 ± 0.66	26.11 ± 0.65	27.81 ± 1.86
HRT (ms)*	17.44 ± 0.89	17.37 ± 0.75	20.09 ± 1.58	17.17 ± 1.19
Max dT/dt (g/s)*	52.88 ± 6.80	51.99 ± 7.60	42.94 ± 3.63	67.91 ± 8.20
Min dT/dt (-g/s)*	31.51 ± 4.36	30.69 ± 7.27	23.37 ± 3.44	38.63 ± 8.12
TTI (g*s)*	0.85 ± 0.12	0.67 ± 0.13	0.60 ± 0.04	0.91 ± 0.12
	7 Weeks of Age			
Body Mass (g)*	21.71 ± 0.39	21.95 ± 0.53	21.95 ± 0.29	19.98 ± 1.08
TPT (ms)	25.00 ± 0.63	25.15 ± 0.57	25.53 ± 0.56	26.32 ± 1.44
HRT (ms)*	15.71 ± 0.47	15.42 ± 0.37	15.64 ± 0.66	15.53 ± 0.57
Max dT/dt (g/s)*	106.0 ± 5.39	102.0 ± 5.02	101.0 ± 10.67	101.0± 14.6
Min dT/dt (-g/s)*	71.51 ± 7.86	66.34 ± 5.97	71.10 ± 8.20	77.67 ± 11.8
TTI (g*s)*	1.69 ± 0.13	1.57 ± 0.12	1.48 ± 0.15	1.50 ± 0.13
	9 Weeks of Age			
Body Mass (g)*	24.34 ± 0.46	25.22 ± 0.45	24.92 ± 0.21	24.22 ± 0.44
TPT (ms)	28.45 ± 2.79^{a}	27.08 ± 0.70	25.75 ± 0.55	24.03 ± 0.40^{a}
HRT (ms)*	16.76 ± 0.97	16.84 ± 0.74	15.23 ± 0.43	15.01 ± 0.54
Max dT/dt (g/s)*	104.0 ± 8.67^{a,b}	136.0 ± 10.7^{a}	124.0 ± 7.99^{c}	157.0 ± 8.39^{b,c}
Min dT/dt (-g/s)*	65.34 ± 9.87^{a,b}	97.33 ± 8.37^{a}	85.68 ± 10.3^{c}	116.10 ± 8.99^{b,c}
TTI (g*s)*	1.60 ± 0.20^{a,b}	2.40 ± 0.17^{a,c}	1.81 ± 0.19^{c,d}	2.54 ± 0.18^{b,d}

Values are means ± SEM. TPT, time to peak tension; HRT, half relaxation time; Max dT/dt, maximum rate of torque development; Min dT/dt, minimum rate of torque development; TTI, tension-time integral. TPT, HRT taken from twitch values; Max and Min dT/dt and TTI taken from 150Hz tetany.*Indicates a significant effect of time (P<0.05); values with same letter are different (P<0.05). n=10 per treatment group

In Vitro Muscle Strength

In vivo data were reported as torque, but *in vitro* data are reported as stress (force (mN)/cross sectional area(mm^2)),. The *in vitro* stress-frequency curves are reported in figure 4.3. Because the responses from muscles of the *in vivo* stimulated leg and unstimulated legs were not different (P>0.05), data were collapsed for additional analysis. There were main effects for treatment, stimulation frequency, and an

interaction (all, P<0.0001). In contrast to the *in vivo* results, WT+S demonstrated the greatest stress production at maximal stimulation, and was stronger than mdx, WT, and mdx+S (in mN/mm^2: 382.4 ± 11.4 (WT+S) vs. 240.4 ± 13.7 (Mdx, P<0.0001) vs. 306.8 ± 24.4 (WT, P=0.0015), vs. 273.0 ± 12.8 (Mdx+S, P<0.0001)). WT was also significantly different from mdx (306.8 ± 24.44 vs. 240.4 ± 13.74 mN/mm^2, respectively; P=0.0086; Figure 4.3A). When percent maximal stress is plotted, a left shift of the stress frequency curve is evident for the mdx+S group, which demonstrated differences from all other groups at 30 and 50hz (P<0.05), and from WT and WT+S at 80 hz (P<0.05).

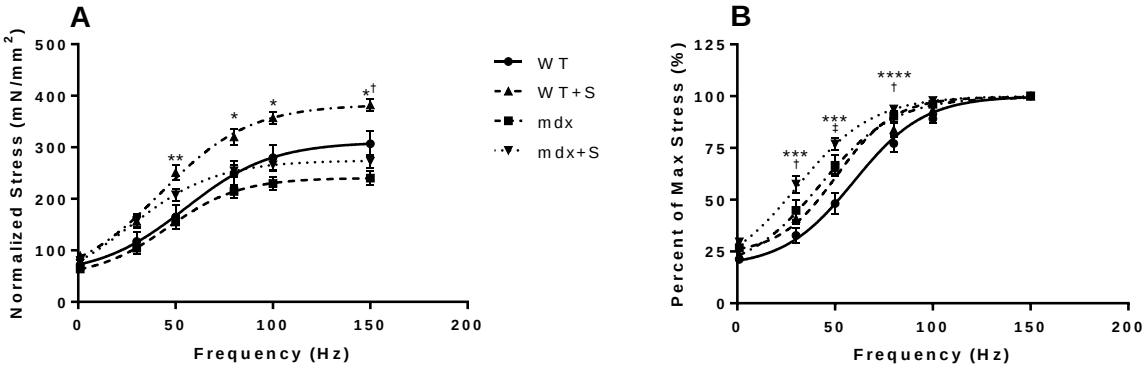

Figure 4.3. Stress-frequency *in vitro*. A: Absolute stress frequency. B: Relative stress-frequency. Values are ± SEM. *WT+S different from all other groups; **WT+S different from WT and mdx; ***mdx+S different from all other groups; ****mdx+S different from WT+S and WT; †WT different from mdx; ‡WT different from mdx and WT+S. n (mice)=8-10 per treatment group, n (muscles)= 15-19 per treatment group

The temporal properties from the stress-frequency data are reported in table 4.2. Dissection errors reduced sample size during in vitro experiments and are reflected in the n values reported in the table. EDL CSA across treatment groups was different (P<0.05). TPS (time to peak stress) was unchanged across treatment groups, while HRT increased due to the sphingolipid diet (from 19.0 to 21.8 ms in WT and 20.0 to 27.4 ms in mdx). Other temporal property changes were similar between groups.

Table 4.2. Cross-sectional area , twitch and tetany properties from mdx and C57BL10 mice fed an AIN 76A diet with or without 0.1% sphingomyelin during *in vitro* experiments at 11 weeks of age.

	C57BL10		mdx	
	Control	0.1% SM	Control	0.1% SM
n (mice)	8	9	8	10
n (muscles)	16	18	15	19
CSA (mm^2)	0.85 ± 0.02^{a}	$0.80 \pm 0.02^{b,c}$	$0.95 \pm 0.02^{a,b}$	0.92 ± 0.23^{c}
TPS (ms)	23.83 ± 0.64	26.72 ± 1.19	24.39 ± 0.41	26.39 ± 0.50
HRT (ms)	19.05 ± 1.72^{a}	21.77 ± 0.89	20.00 ± 1.06^{b}	$27.39 \pm 2.14^{a,b}$
Max dS/dt (g/s)	652.0 ± 60.5	700.0 ± 26.9	705.0 ± 35.2	688.0 ± 28.6
Min dS/dt (-g/s)	1077 ± 121	1233 ± 39.3	1106 ± 74.4	1018 ± 71.0
STI (g*s)	24.26 ± 2.56	28.68 ± 0.73	26.27 ± 1.31	25.52 ± 1.28

Values are mean ± SEM. CSA, cross sectional area; TPS, time to peak stress; HRT, half relaxation time; Max dS/dt, maximum rate of stress development; Min dS/dt, minimum rate of stress development; STI, stress-time integral. TPS, HRT taken from twitch values; Max and Min dS/dt and STI taken from 150Hz tetany. Values with same letter are different ($P<0.05$).

Decreased muscle stress generation during prolonged stimulation is referred to as fatigue (Fig 4). During *in vitro* experiments, WT+S demonstrated a higher initial stress, but rapidly decreased to meet stress values of the other treatments after approximately 100 seconds of prolonged stimulation. WT+S's initial values were significant from other treatment groups ($P<0.05$). The muscle's ability to recover from fatigue remained unchanged ($P=0.4472$). Velocity across treatment and percent load also remained unchanged ($P=0.9790$), and is represented as a velocity relative to percent of the max load (i.e. force) imposed on the muscle. Calculated V_{max} was also similar among groups (Fig. 4). Power curves were generated from the force-velocity relation for each muscle by multiplying load (in g) by its associated velocity (mm/s) and converting to milliwatts (mW; multiply by .00981). All treatment groups reached maximum power at approximately 40% of the maximum force (g). Interactions between treatment groups and percent of maximum force were significant ($P=0.0073$), with WT+S exhibiting a higher power at 40%. At 50% of max force, WT+S was significantly different from mdx (2.299 ± 0.083 vs. 1.511 ± 0.144 mW, respectively) and mdx+S

(2.299 ± 0.083 vs. 1.545 ± 0.134 mW, respectively), and WT was different from mdx (1.969 ± 0.201 vs. 1.511 ± 0.144 mW, respectively), with P<0.05 for all cases.

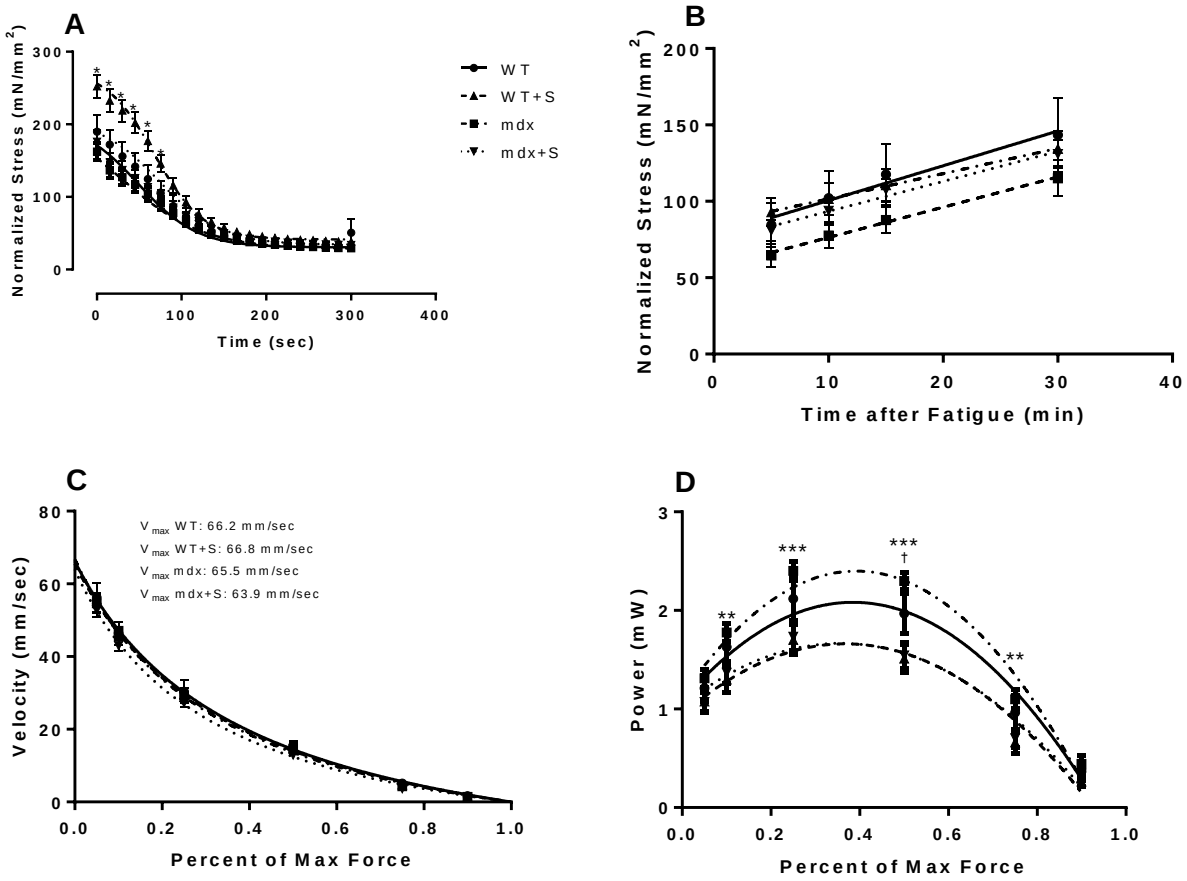

Figure 4.4. Fatigue, fatigue recovery, force velocity, and power curves *in vitro*. A: Fatigue, B: Fatigue recovery, C: Force velocity, D: Power. Values are mean ± SEM. *WT+S different from all groups; **WT+S different from mdx; ***WT+S different from mdx and mdx+S; †WT different from mdx. n (mice)=8-10 per treatment group, n (muscles)= 15-19 per treatment group

Serum Creatine Kinase Activity

Creatine kinase (CK) in the serum is a measure of skeletal muscle membrane injury. There was no difference in serum CK activity between 11-week-old WT and WT+S mice (Figure 4.5, P=0.9944), nor between mdx and mdx+S mice (P=0.9825). However, there was a difference between mdx mice (both treated and untreated) and WT mice (P<0.0001). Samples that were lysed (because of contribution from lysed RBCs) during

handling (n=14) that resulted in unusually high CK values, were removed from the data set. Properly handled samples (n= 26) are reflected in the figure.

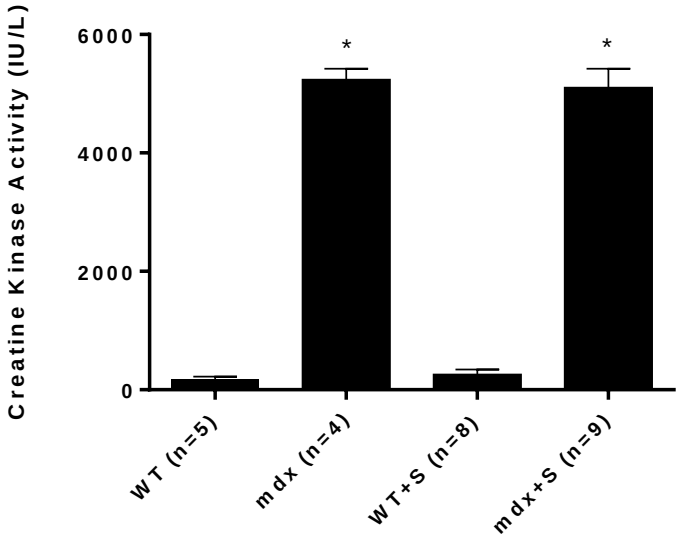

Figure 4.5. Serum CK activity. Values are mean ± SEM. *Different from WT and WT+S (P<0.05).

H&E Staining

Hematoxylin and Eosin (H&E) staining was performed on sections of TA to determine centralized nuclei as a measure of muscle regeneration in fibers. There was no difference between WT and WT+S mice (Figure 6, P=0.9999), nor between mdx and mdx+S mice (P=0.9768). There was a main effect of genotype between mdx mice to WT mice (P<0.0001). Mdx mice (both treated and untreated) also exhibited irregular cellular shape and increased immune cell infiltrate when compared to WT mice (Fig 4.6). Errors in freezing some samples resulted in unreadable slides, thus reducing sample numbers. These numbers are reflected in the figure.

Quantitative analysis of sections (Fig 4.7) revealed there was no difference in percent area of degenerating fibers between treatment groups. Percent area of necrotic fibers demonstrated that mdx was different from WT and WT+S, and mdx+S was different from WT+S (P<0.05). Immune cell infiltrate was different in mdx compared to WT and WT+S (P<0.05). Sample sizes are the same as those in Fig 4.6.

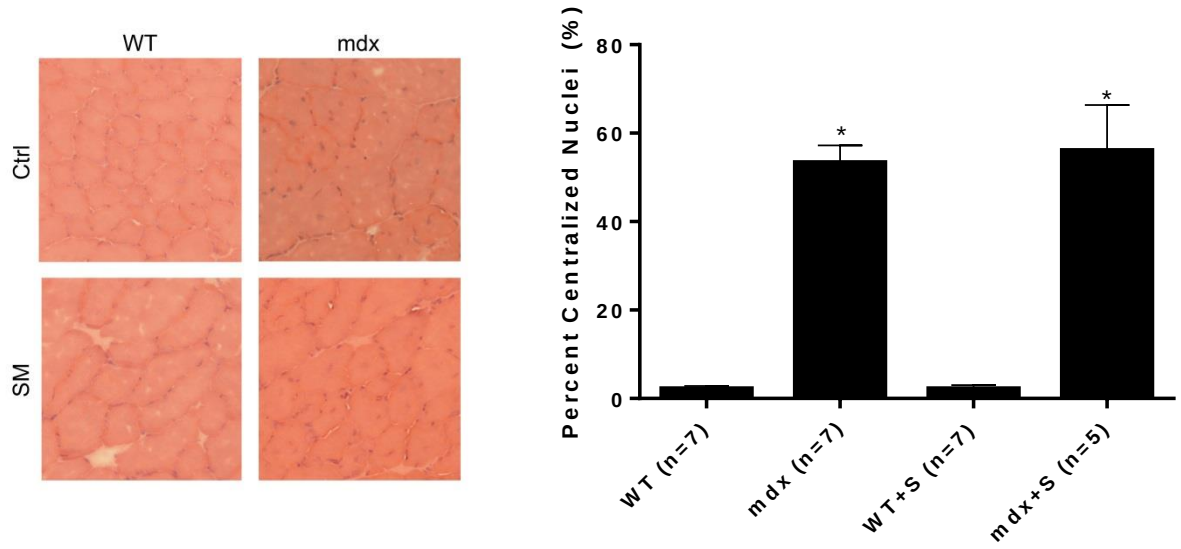

Figure 4.6. H&E results of centralized nuclei. Values are ± SEM *Different from WT and WT+S (P<0.05).

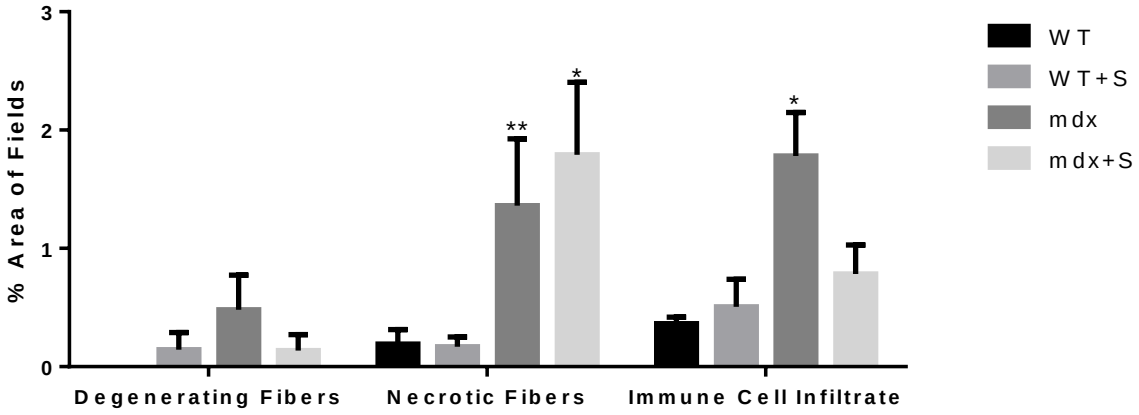

Figure 4.7. H&E quantitative analysis. There were no degenerating fibers in WT. Values are ± SEM. *different from WT and WT+S (P<0.05), **different from WT+S (P<0.05). n= 5-7 per treatment group.

qRT-PCR

Quantitative real-time polymerase chain reaction (qRT-PCR) was performed on mRNA isolated from the TA muscles that were not stimulated *in vivo*. Fourteen genetic markers identified from a preliminary study (Appendix A) were investigated. Of these, 7 were up-regulated: C1qa, Ccl8, Cd59a, Fcer1g, Ly86, Serpina3n, and Thbs1. C1qa, Ccl8, Fcer1g, Ly86, Serpina3n, and Thbs1 were increased in mdx+S compared to WT

(P<0.05); Cd59a was increased in WT+S compared to mdx (P<0.05); Serpina3n was also increased in mdx compared to WT (P<0.05, Fig 4.7).

Table 4.3. ΔCt values of selected genes in C57BL10 and mdx mice fed an AIN76A diet with or without 0.1% sphingomyelin.

	C57BL10		mdx	
	Control	0.1% SM	Control	0.1% SM
ACP5	10.48±1.09	7.88±0.69	7.75±0.88	6.58±1.43
ALOX5AP	9.19±1.09	6.11±0.68	7.70±1.35	5.41±1.20
C1QA	6.54±0.87[a]	4.12±0.55	4.20±0.73	2.17±0.79[a]
C1QC	6.69±1.22	5.18±0.60	5.48±0.94	3.31±0.57
CCL8	13.46±1.20[a]	10.78±0.64	10.27±1.11	8.04±1.13[a]
CCR5	10.60±1.47	6.36±0.59	9.48±1.42	7.06±1.43
CD59A	8.25±1.01	5.54±0.78[a]	9.55±0.82[a]	7.07±0.62
CFD	7.32±1.04	3.91±0.54	7.56±1.34	4.80±1.13
CFP	11.39±1.70	8.03±1.70	9.14±1.28	8.20±1.81
FCER1G	8.27±1.21[a]	5.56±0.65	5.41±1.30	3.47±1.01[a]
FN1	6.55±2.00	4.14±1.01	5.85±2.20	3.67±1.94
LY86	10.47±1.08[a]	7.75±0.84	8.01±0.84	5.95±1.02[a]
SERPINA3N	14.15±2.63[a,b]	9.43±1.13	6.71±1.40[a]	5.59±1.22[b]
THBS1	9.52±1.15[a]	4.98±1.08	6.13±1.37	3.97±1.75[a]

Values are mean ± SEM. Values with same letter are different (P<0.05). n=9-10 per treatment group.

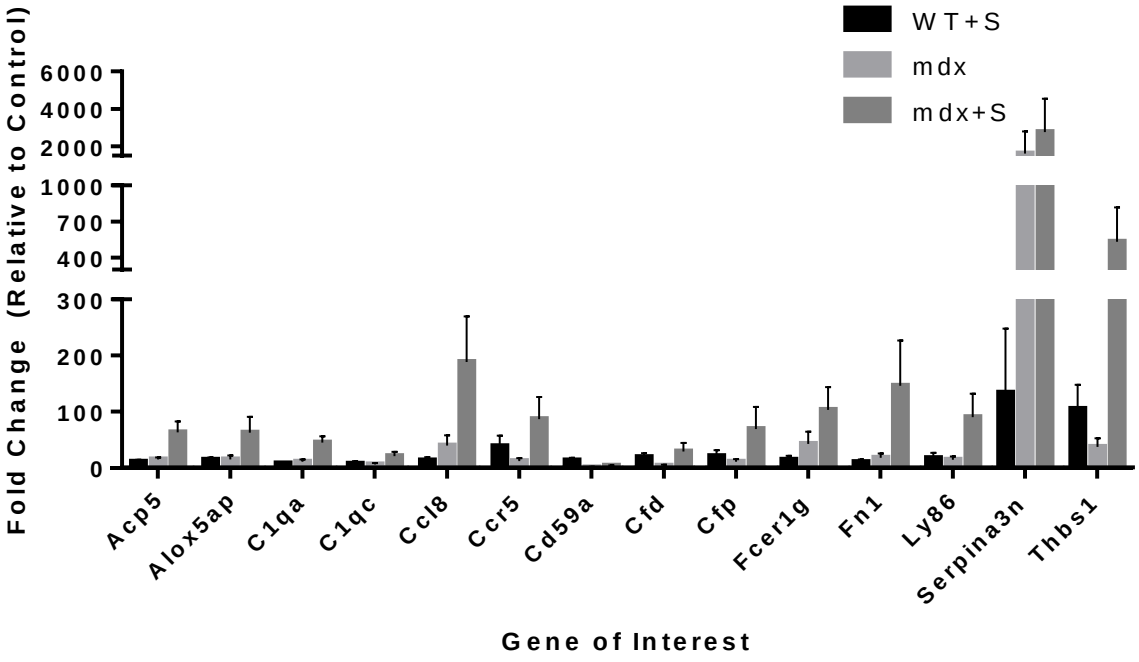

Figure 4.8. qRT-PCR of selected inflammatory markers. Values are mean ± SEM, and relative to WT (set at x-axis). n=9-10 per treatment group.

Immunohistochemistry

To investigate one potential inflammatory signaling pathway in muscle, immunohistochemistry (IHC) was performed to identify p-Akt. Activation of Akt is important in a variety of signaling pathways and was expected to be increased in mdx tissue as a result of an increased inflammatory response. In both WT and WT+S sections, there was weak to no expression of p-Akt. In both mdx and mdx+S groups, there was also weak to no expression of p-Akt. P-Akt may be short lived in the cell, and therefore difficult to discern differences between treatment groups via IHC.

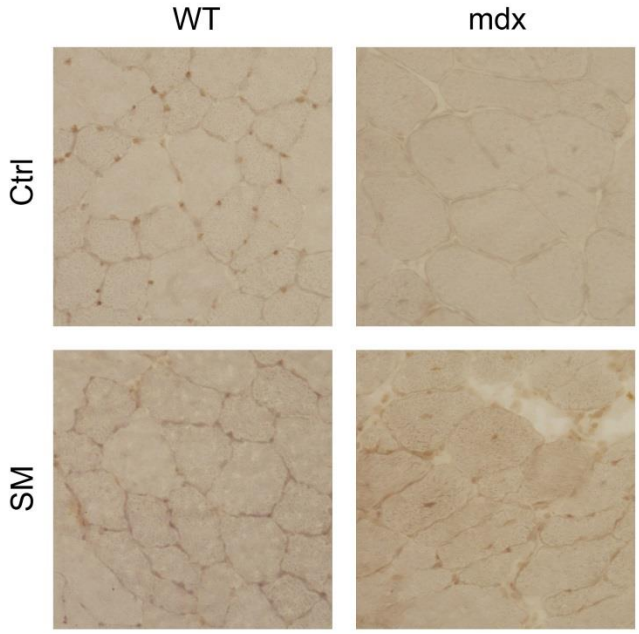

Figure 4.9. IHC of TA sections. Mdx and mdx+S demonstrate little p-Akt content, and are indistinguishable from control mice. n= 5-7 per treatment group.

Chapter 5: Discussion

Motivation for Study

DMD is a severe and fatal muscle wasting disease. Muscle function is decreased in both DMD boys and mdx mice, a model of DMD. An increased inflammatory response occurs in dystrophic muscle throughout disease progression. Prolonged inflammatory processes can lead to further cycles of degeneration and repair in affected muscle, leading to a decreased functional response. Dietary sphingolipids decrease the inflammatory response in a variety of other diseases such as cancer (in mice), and for this reason they were considered a potential intervention for mdx mice. The purpose of this study was to determine if 0.1% dietary sphingolipids added to a standard AIN76A diet would modulate the inflammatory response in mdx muscle, as well as improve muscle function.

Major Findings

The major findings of this study were: (1) hind limb torque production in WT+S and mdx+S at 9 weeks of age were increased *in vivo;* (2) power and resistance to fatigue were increased in WT+S mice at 11 weeks *in vitro*; (3) a left shift in the relative stress-frequency relationship was evident for mdx+S mice at submaximal stimulation frequencies at 11 weeks *in vitro*; and, (4) the inflammatory gene profile in mdx+S mice at 11 weeks was modulated. Each of these findings will be discussed below in order.

Muscle Function in WT+S

As a reminder, in this study S refers to dietary sphingolipids, which is comprised only of sphingomyelin.

In vivo. WT+S mice demonstrated increased torque production compared to WT at age 9 weeks (5 weeks of treatment). WT+S also had increased max and min dT/dt (rates of maximum and minimum torque development) and TTI (torque–time integral) compared to WT at 9 weeks. All of these changes suggest sphingolipids modified one or more aspects of E-C coupling. Sabbadini et al. (1992) tested the hypothesis that sphingosine (SO) could inhibit release of calcium from the sarcoplasmic reticulum of isolated rabbit psoas skinned fiber bundles by binding to ryanodine receptors (RyR). However, what

their data revealed was that SO could either inhibit or enhance RyR calcium release, i.e., low concentrations inhibited (<3μM), whereas high concentrations (>3μM) enhanced release. They hypothesized that this dichotomy may be the result of SO's ability to induce two states (closed or open) of the RyR [159]. Alternatively, neutral SMase (sphingomyelinase), responsible for converting sphingomyelin (SM) to SO is localized to T-tubule membranes [160]. On the basis of these results, it would be reasonable to speculate that dietary sphingolipids were converted to SO, which then diffused across the t-tubular membrane to bind and activate the RyR. The subsequent increase in the release of calcium was then responsible for increased force production in the contractile apparatus of WT+S muscles. Also, the increased max and min dT/dt in WT+S, which suggests enhanced contractile and relaxation phases, might also be explained by increased SR calcium release, and increased rate of SERCA activity. These responses suggest that SO may have effects on SERCA, troponin C, or other aspects of the contractile apparatus. Since TTI was also increased, and the testing duration was unchanged, this outcome also confirms a greater torque response in the WT+S muscle (TTI is the area under of the curve), therefore if the test duration is the same, the only way to increase area is to increase torque).

In Vitro. At age 11 weeks*, in vitro* data of EDL muscles were obtained in place of the in vivo assessments. The assumption was that if increased EDL force was observed, that increased torque would have also been evident *in vivo*. WT+S EDL muscles demonstrated increased force production at a given activation frequency, increased power generation, and an increased resistance to fatigue compared to other treatment groups. Power is calculated by multiplying a given absolute load (mN) by the peak velocity of the muscle at that load. Because absolute force was greater at any given velocity for the WT+S muscles compared to those of the other treatment groups, power was increased. This outcome supports the idea that SO influences muscle force production (described above), but not speed of shortening (i.e., velocity).

WT+S EDL muscles demonstrated increased resistance to fatigue. Danieli-Betto et al. (2005) tested the effects of SO and sphingosine-1-phosphate (S1P) on muscle fatigue. Danieli-Betto et al. (2005) incubated isolated EDL muscles from 3 month old

CD1 mice for 15 minutes, in a PSS solution. After incubation, fatigue protocols were performed using different concentrations of SO, S1P, and other lipids added to the incubation solution. With respect to the SO and S1P treatments, the authors reported that both SO and S1P reduced the rate of fatigue. The effect was due to SO being converted in S1P. They also reported S1P did not affect intracellular calcium levels; they instead hypothesized that S1P initiated an undefined signal pathway by binding to receptors on the extracellular face of the sarcolemma [161]. These data suggest that similar but as yet undefined mechanisms may have contributed to the resistance to fatigue demonstrated by the WT+S mice in our study.

Differences between in vivo and in vitro responses. Although similar changes in force production (torque or stress) were seen in WT+S both *in vivo* and *in vitro,* the two experimental preparations may provide insight into the mechanism of SO on SR function. The *in vivo* preparation retains NMJ function as the electrical pulse stimulates the nerve thereby inducing an AP down the nerve and through the NMJ, while the *in vitro* preparation does not include the nerve and therefore stimulation is achieved via field stimulation over the sarcolemma bypassing the NMJ. Also, both of the proposed hypotheses above suggest an internal (SO enhancing calcium release) and external (t-tubule/S1P binding to surface receptors acting via an undefined pathway) effect of dietary sphingolipids. The external effect may be lost or reduced *in vitro* due to the muscle fiber being exposed to the outside environment thereby releasing S1P from its receptor on the sarcolemma (Fig 5.1).

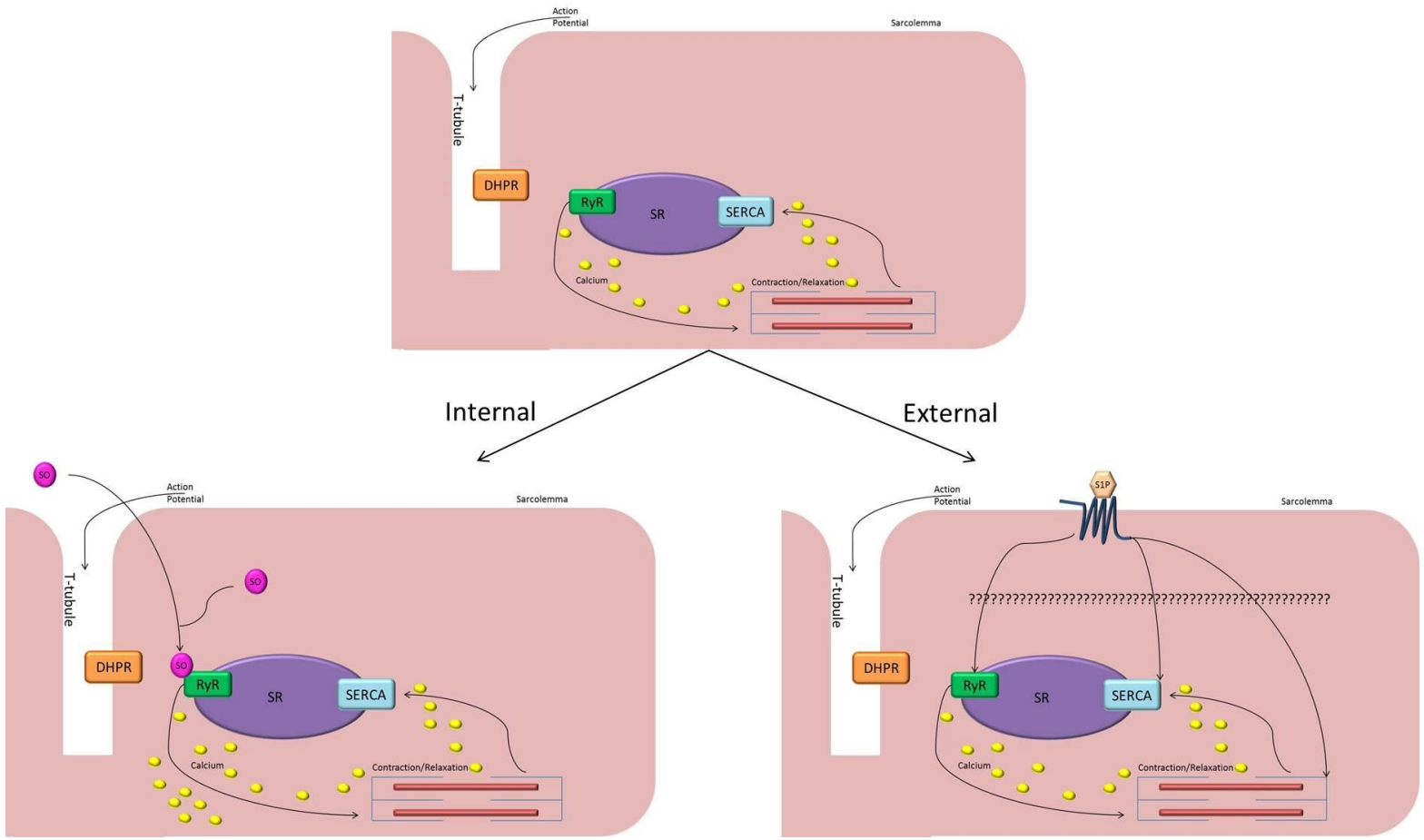

Figure 5.1. Hypothesized methods of action of sphingolipid metabolites. During normal muscle contraction an AP is propagated along the sarcolemma and down t-tubules to initiate release of calcium and induce contraction (see chapter 2). Our data suggest two hypotheses about sphingolipid metabolite methods of action: internal and external. The internal hypothesis suggests SO is taken into the muscle fiber, binds in high concentrations to the RyR, inducing a more open state releasing more calcium enhancing muscle contraction. The external hypothesis suggests that S1P binds to a surface receptor causing an undefined signaling pathway resulting in enhanced muscle function.

Muscle Function in mdx+S

In vivo. Mdx+S demonstrated greater torques than mdx and WT mice at age 9 weeks. Mdx+S also had increased max and min dT/dt and TTI compared to WT and mdx, and increased time to peak torque (TPT) compared to WT at 9 weeks. These changes suggest mechanisms to enhance calcium release via the RyR were similar to those described for WT+S, but because these values were less ($P<0.05$) for mdx+S, the mechanisms were blunted. This may be due to decreased ability of the SR in mdx tissue to properly handle calcium. The SR of mdx muscle has been described as having RyR that leaks calcium [162], and a decreased uptake of calcium by SERCA [163], both leading to reduced force production in the muscle. The proposed mechanisms may therefore be blunted by an already inhibited ability of the muscle to contract.

In vitro. In contrast to the increased stress of the WT+S EDL *in vitro*, which implied increased torque *in vivo*, mdx +S EDL stress at a given activation frequency was not increased. This result implies that *in vivo* torque was not increased at age 11 weeks. Interestingly, if *in vitro* stress values were expressed relative to maximum stress for each muscle and plotted, a left shift of the stress-frequency curve in mdx+S was evident at submaximal frequencies. This outcome is potentially important because human muscle, during normal exertion (i.e., walking, posture), is activated at submaximal frequencies (10-20 Hz relative to a max of 100 Hz) [164, 165]. Since there was an observed change at submaximal frequencies in the mdx+S mice, it may be possible that a sphingolipid supplement could produce the same result in DMD boys. This improved muscle force output could potentially improve mobility and quality of life and delay the need for a wheelchair. However, power between mdx and mdx+S was not different, and both had the lowest power compared to other treatment groups. These results suggest that sphingolipid treatment increased relative stress output, but it did not increase power *in vitro*. From the perspective of DMD muscle, it is unclear howe these specific effects would influence function. Additional studies are warranted.

Differences between in vitro and in vivo. While *in vivo* the mdx+S exhibited a stronger torque response at age 9 weeks, the absolute stress produced *in vitro* was not different from mdx at age 11 weeks. The most likely explanation is the *in vitro* vs. *in vivo* muscle preparation. The lack of increased stress *in vitro* may be due to loss of sphingolipid metabolites present in the extracellular space available to bind a receptor on the sarcolemma (i.e., S1P). Should this be the case, then it is possible that the external mechanism described above (i.e., S1P-external receptor interaction) may dominate over the internal mechanism (i.e., SO-RyR interaction) *in vivo*, the lack of which reduces mdx stress *in vitro*.

Explanation of Differences in Muscle Function Between mdx and WT

One major morphological difference between mdx and WT mice independent of dietary sphingolipids, was that EDL cross-sectional area was greater. Increased hypertrophy of muscle is a common hallmark associated with DMD [166]. However, while the muscle may have increased mass, this does not imply increased function. Hypertrophic muscles in boys with DMD are the result of an increase deposition of fatty and connective tissues [6]; however, in the mdx mouse, while hypertrophy is evident, muscles retain their functional ability, albeit in a reduced capacity [167]. Mdx muscle has a small number of necrotic fibers, which may explain the reduced function of the muscle. WT+S demonstrated stronger torque and stress responses both *in vivo* and *in vitro*, while mdx+S was only stronger *in vivo*, suggesting more necrotic or damaged fibers in the muscle. However, H&E results showed no difference in the percent of total necrotic fibers from mdx to mdx+S, or mdx+S to WT. Therefore, it is unlikely that the differences seen were due to necrotic fibers. These differences seen between WT+S and mdx+S may be explained in the potential differences in the proposed mechanisms of sphingolipid action, where in WT+S these mechanisms are more prominent than in mdx+S, yet this has yet to be determined.

Inflammatory Response: WT

Expression of mRNA for selected inflammatory markers was minimal and not different between WT and WT+S muscles. In addition, there were minimal and no differences in the numbers of degenerating, regenerating, or necrotic fibers, immune cell infiltrate (H&E analysis), or p-Akt content (IHC). Taken together, these results suggest that

WT±S mice exhibited minimal inflammation and muscle damage (i.e., serum CK levels were low) in agreement with previous studies [16, 119].

Inflammatory Response: mdx

In contrast to WT±S values, serum CK values were dramatically increased for mdx and mdx+S. qRT-PCR revealed increases in several genetic inflammatory markers in mdx+S compared to WT(note: all fold changes were expressed relative to WT values), although values were not different from mdx or WT+S. Significant changes were evident for *C1QA, CCL8, FCER1G, LY86, THBS1* (mdx+S vs. WT); *CD59A* (WT+S vs. mdx); and *SERPINA3N* (mdx and mdx+S vs. WT)(Table 4.3). However, IHC for p-Akt was unchanged among all treatment groups. Surprisingly, increases in TNF-α and other typical inflammatory markers (IFNγ, IL-1) reported in the literature for mdx mice were not evident in our preliminary gene array study. The absence of these markers is discussed below.

The H&E data demonstrated there was no effect of dietary sphingolipids on the numbers of centralized nuclei, degenerating or necrotic fibers, or immune cell infiltration in mdx TA. However, at age 11 weeks, the cycles of fiber degeneration/regeneration are thought to be much less than evident between ages 4-10 weeks [16]. It appears that dietary sphingolipids did not exacerbate nor attenuate inflammation at age 11 weeks, suggesting these markers were neither anti- nor pro- inflammatory. However, what is not known is what the magnitude of these markers would have been during the 4-9 week critical period, nor whether they were pro or anti-inflammatory. The discussion below speculates on how these markers may have modulated inflammation during ages 4-9 weeks in mdx muscle.

Description of genes with altered expression. The *C1QA* gene encodes the C1QA protein, and plays a critical role in initiation of the complement system. The complement system is part of the immune response and assists (“complements”) removal of pathogens by antigens and phagocytic cells. The complement system has a number of functions including opsonization, chemotaxis, and cell lysis (through formation of the membrane attack complex or MAC). Complement can proceed through one of three

pathways: the classical, alternative, and lectin pathways. C1QA is part of the C1 complex responsible for initiation of the classical pathway. The classical pathway relies on activation of several sequential proteins to elicit a response, beginning with the formation and activation of the C1 complex. Complement is not well understood in the inflammatory response in mdx mice; however, it is thought to contribute to the pathophysiology [13]. Complement may assist in removing cellular debris during skeletal muscle remodeling after injury [168]. During ages 4-9 weeks, mdx muscles demonstrate increased necrotic and degenerating fibers [16]. This hypothesis may explain the overexpression of *C1QA* in mdx+S, such that increased C1QA may have activated cellular mechanisms to remove damaged tissue, which would be beneficial for to the muscle.

CCL8 is a chemokine responsible for cellular activation of immune cells and inflammatory mediator release (i.e., histamine) by basophils and eosinophils [169], and was up-regulated in mdx+S tissue compared to WT. Although not different compared to mdx muscle, the increased expression in mdx+S of *CCL8* suggests increased activation of inflammatory cells (i.e. monocytes). At 4-9 weeks, this increase would indicate increased activation of immune cells, and therefore enhanced necrotic fiber removal. This enhanced removal would allow for further muscle repair and could improve muscle function.

SERPINA3N was also increased in both mdx and mdx+S tissue. SERPINA3N (serine protease inhibitor a3n) is a member of the serpin superfamily of proteins which is divided into nine groups (A-I) [170]. SERPINA3 is thought to be an inhibitor of cathepsin G (although there may be other targets), which is released by neutrophils at the site of inflammation to remodel tissue and activate pro-inflammatory cytokines and chemokines [170]. SERPINA3N is a member of the SERPINA3 classification. Both mdx and mdx+S muscles demonstrated elevated levels of serpina3n, suggesting an increased need for inhibition of cathepsin G. Cathepsin G has not been fully explored in mdx muscles; however, cathepsin G mRNA was not increased on the basis of our microarray (data not shown). At 4-9 weeks, this may inhibit the action of cathepsin G, thereby reducing the ability to remodel tissue, which may be detrimental to the muscle.

FCER1G is an Fc receptor, a family of receptors responsible for binding immunoglobins (IGs). FCER1G belongs to the FcεRI subclass of Fc receptors, which specifically bind IgE, promoting release of proinflammatory cytokines and chemokines [171]. Activation of this receptor also leads to degranulation of basophils. Unfortunately, this receptor has not been thoroughly investigated in skeletal muscle. At 4-9 weeks, it is possible that up-regulation of this receptor in mdx+S may lead to increased cytokine release (assuming there is also a sufficient amount of IgE to activate these receptors). This may be beneficial to stimulate immune cell responses to help remove damaged tissue.

LY86 (Lymphocyte antigen 86) has not been thoroughly investigated, although it is suggested to play a role in lymphocyte activation. Therefore, it is likely that LY86 may propagate inflammation, although further exploration would be required.

Finally, THSB1 (Thrombospondin 1) is a multi-functional protein expressed by cells involved in would healing (i.e., platelets) and endothelial cells [172]. It also interacts with numerous adhesion molecules (i.e., laminin), as well as activating TGF-β, a protein responsible to proliferation and activation of immune cells [172]. THBS 1 has been implicated in a variety of diseases, primarily due to its activation of TGF-β release and subsequent association with fibrotic tissue [172]. THBS1 has been demonstrated to propagate the inflammatory response in skeletal muscle diseases [173], this effect would likely carry over into the mdx muscle. Mdx+S demonstrated elevated levels of THBS1, suggesting further support for an increased inflammatory response, which would likely be seen at 4-9 weeks.

Only one inflammatory gene was differentially expressed in WT+S: *CD59A*. CD59A protein inhibits MAC formation. Increased expression of this protein in WT+S would suggest inhibition of complement activation; this was likely because the muscles were not damaged.

Implications of altered gene expression. Genes overexpressed in mdx+S muscles suggest increased capacity for removal of damaged tissue and an increased inflammatory response. However, it is unclear if this capacity would be beneficial or detrimental to mdx pathophysiology. Although removal of damaged tissue is clearly

beneficial to the muscle, this response could require a quicker activation of satellite cells for regeneration, possibly increasing the overall degeneration/regeneration phase of the pathophysiology. This dichotomy should be further explored.

In summary, if these inflammatory markers were expressed at 4-9 weeks, there may have been an increased pro-inflammatory response. The pro-inflammatory response would enhance damaged fiber removal, a may result in skeletal muscle repair earlier. In turn, skeletal muscle function may then also be improved. Future studies should seek to explore this possibility.

Although these genes were up-regulated in mdx+S, results from H&E and serum CK analysis disagree with the qRT-PCR results. H&E results demonstrated that there was no difference in centralized nuclei, degenerating fibers, necrotic fibers, and immune cell infiltrate between mdx and mdx+S. If the genetic markers described above were up-regulated, it is expected that the outcomes of an increased inflammatory response would be observed in the other assays (i.e., increased immune cell infiltrate). This disagreement between the results of the assays may be due to the age of the mice.

Disagreement Between Assays

One likely explanation for the discrepancy between expressed genetic markers and the results of serum CK and H&E is the age of the mice. Mice were sacrificed at 11 weeks, and may have been in a more pronounced state of regeneration, where inflammatory processes would be the least active. Degeneration in the mdx muscle wanes at age 11-12 weeks, and regeneration peaks between 6 and 12 weeks of age [174]. If samples are collected at a younger age (4-6 weeks), when degeneration processes are at their peak, there may be a more defined inflammatory response, and there would be more immune cell infiltrate in H&E stains. Alternatively, another scenario may be that these markers were up-regulated at both age 11 and 9 weeks of age. If true, then this upregulation may explain the increased torque response seen *in vivo* of the mdx+S mice at age 9 weeks of age. The increased inflammatory response could have reduced degeneration processes. A reduced degeneration process may improve muscle function.

Another hypothesis that was not supported by the data was serum CK. Sphingolipids are a constituent of the lipid bilayer, making up 10-20% of the total membrane lipids [145]. Mdx tissue also presents with a leaky membrane. We hypothesized that dietary sphingolipids may supplement the membrane of skeletal muscle, although the serum CK results do not support this.

Another potential discrepancy between the present results and those of the literature is that common inflammatory markers TNF-α (Tumor necrosis factor alpha), IFNγ (Interferon gamma), and IL-1 (Interleukin 1), responsible for initiating and perpetuating the inflammatory response in mdx tissue (2-9 weeks of age) [119, 175, 176], were not observed in our preliminary gene array study (Appendix A), and therefore qt-PCR was not performed in the present study. A current collaboration with Dr. Zhiyong Cheng (Virginia Tech, Blacksburg, Virginia) revealed TNF-α was not expressed in soleus muscles from mdx or mdx+S mice at age 11 weeks. This result along with our own data suggest very little inflammation at 11 weeks of age in mdx or mdx+S mice, and this outcome is confirmed by the H&E data that showed very few inflammatory cells were evident. It is likely then, that while not expressed at 11 weeks of age, inflammation markers such as TNF-α were present at an earlier age [175].

Another potential discrepancy was the unchanged number of central nuclei in mdx+ S muscles despite a report that sphingolipids could activate satellite cells and improve regeneration. Loh et al. (2012) described S1P enhancement of satellite cell activation in mdx mice [177]. Their results show that S1P is deficient in mdx tissue due to over expression of sphingosine phosphate lyase (SPL), which is responsible for degradation of S1P [177]. By inhibiting the activity of SPL, Loh demonstrated an increased propensity for regeneration by satellite cells in mdx tissue [177]. The sphingolipid rheostat suggests that a tissue will have varying levels of sphingolipid metabolites based on the needs of that tissue. Additionally, tissues dominated by an inflammatory response (i.e., dystrophic muscle) have higher activation of SMases than healthy tissue [178]. This greater activity increases conversion of SM to ceramide, and leads to subsequent conversion to S1P. Based on these findings, we suggest that increasing the total sphingolipid content through the diet, could increase S1P (before

SPL could break it down) and increase satellite cell activation for improved regeneration. This was not supported by the number of centralized nuclei seen in mdx+S tissue.

Our data suggests that while inflammatory genetic expression may be increased in mdx+S, these changes to do not support an increased inflammatory response at 11 weeks. However, if an increased inflammatory response was present at 9 weeks of age (counter to the increased torque response in mdx+S observed at this age), then it is unlikely the mechanisms proposed above were present. If true that dietary sphingolipds instead blunts inflammation between age 4-9 weeks, a sphingolipid dietary supplement could be beneficial at early stages of the disease. This possibility should be confirmed.

Sources of Inconsistencies

A confounding result in our data were the *in vivo* torques. Our values for torque were ~20% lower than those reported in similar *in vivo* studies in mdx mice of similar ages [179, 180]. Lack of agreement may be due to the placement of electrodes during experiments. Stimulation of anterior crural muscles may not have been uniform at each time point, producing conflicting results to those in the literature. Alternatively, while the mice were placed on paper towels to reduce heat loss, a heating pad was not used. Loss of heat may also contribute to lower torque values [181].

While our study suggests that there were little to no effects of sphingolipids on inflammation, other studies in different disease models have suggested a more profound response to the inflammatory state, particularly in cancer models [24, 158]. One possibility for the discrepancy may be due to the amount of sphingolipids added to the diet. In our study, the modified diet contained 0.1% sphingolipid, which may be too low to affect muscle. Nevertheless, other studies have used 0.1% sphingolipid and suppressed the inflammatory response in non-muscle tissues (colon, breast)[24], thus it is unlikely that sphingolipid dose affected the results. However, sphingolipid uptake and or signaling may be less in muscle compared to other tissues; the sphingolipid was excreted before absorption; or it was used structurally in the membrane instead of being used to initiate signaling. These possibilities should be explored in future studies.

Future Directions

The experimental design for further investigation should be modified. Future studies should seek to repeat this experiment in mdx mice but at younger ages (in vivo at 4, 6 and 8 weeks, followed by sacrifice at 9 weeks) to assess changes in inflammation and muscle function. Also, the following hypotheses should be considered.

The results of the present study suggests two key hypotheses: 1) SO alters calcium release by RyR and initiates signaling critical in the development of fatigue, 2) S1P binds to surface receptors initiating an undefined signaling pathway that increases force output, possibly by increasing SR calcium release or directly at the contractile apparatus. To determine if these hypotheses can be accepted, it is most important to establish the levels of sphingolipid metabolites in mdx muscle when treated with SM. The sphingolipid rheostat suggests that there are likely different metabolites present in

dystrophic versus control muscle. Looking at RyR in mdx and WT treated/untreated muscle would also provide insight to how calcium release is affected. Alternatively, investigation of SERCA or other calcium handling machinery in the muscle (i.e., Troponin C), may give insight to other effects sphingolipids may have on calcium signaling and release.

Lack of necrotic fibers and immune infiltrate in H&E images suggest that mdx muscle (treated and untreated) were in a more pronounced state of regeneration. qRT-PCR showed minimal changes in inflammatory gene expression. Taken together, mdx mice may be past the point of peak inflammatory activation (mice sacrificed at 11 weeks). Degeneration in the mdx muscle wanes at age 11-12 weeks, and regeneration peaks between 6 and 12 weeks of age [174]. If samples are collected at a younger age (4-6 weeks), when degeneration processes are at their peak, there may be a more defined inflammatory response, where Akt activation may be more clearly seen, and there would be more necrotic fibers in H&E stains. Alternatively, a younger mouse would feasibly indicate stronger genetic expression of inflammatory genes. If these modifications are taken into account, more information about how sphingolipids contribute to clearing damaged tissue would be gleaned.

P-Akt content in sections of muscle tissue revealed no changes between treatment groups. IHC may not have captured the content of p-Akt in the muscle, and may be due to the short lived nature of p-Akt in muscle; other assays may be used. However, should p-Akt be short lived in the muscle, it may be more pertinent to investigate other parts of the signaling pathway. For instance, directly investigating NF-κB through IHC would indicate propagation of the inflammatory response and activation of Akt. We are also exploring the p-65 expression (a pre-cursor to NF-κB activation) with Dr. Greg Henderson (Rutgers University, New Brunswick, New Jersey). Alternatively, investigating other upstream targets (PI3K, etc.) may also indicate if Akt is being activated. Finally, since sphingolipids are shown to either inhibit or activate Akt [22], investigating GPCRs (G-protein coupled receptors) along the surface of muscle fibers, whether up- or down-regulated, would provide information of potential signaling sphingolipids (and specifically, S1P) could induce.

Main Hypotheses Conclusions

1.) Hypothesis: Sphingolipid treatment will reduce the inflammatory response by promoting expression of anti-inflammatory molecules, while reducing those that are pro-inflammatory. Conclusion: Our data only showed 7 genetic markers differentially expressed; however, based on H&E results, their expression did not affect the inflammatory response. Of these, 5 were significantly expressed in mdx+S. Sphingolipids appear to have a modulatory effect on inflammatory gene expression in mdx male mice at age 11 weeks, but the benefits of these changes are not presently clear.

2.) Hypothesis: Sphingolipid treatment will inhibit phosphorylation of Akt. Conclusion: p-Akt was not different between treatment groups. Sphingolipids have little to no effect on Akt activation in muscle.

3.) Hypothesis: Sphingolipid treatment will reduce the inflammatory response such that contractile/mechanical properties of the EDL muscles will improve over time, and serum CK levels and numbers of centralized nuclei will be reduced. Conclusion: For WT muscles treated with 0.1% sphingolipid, torque production, max and min dT/dt, and TTI were increased *in vivo at age 9 weeks*, and stress production, resistance to fatigue, and power were increased *in vitro at age 11 weeks*. For mdx muscles similarly treated, torque production, max and min dT/dt and TTI were increased *in vivo* at age 9 weeks, and relative stress production at submaximal activation frequencies was increased in vitro at age 11 weeks. Sphingolipids have a beneficial effect on the functional response in both mdx and WT mice.

References

1. Sadoulet-Puccio, H.M. and L.M. Kunkel, *Dystrophin and its isoforms.* Brain Pathol, 1996. **6**(1): p. 25-35.
2. Ervasti, J.M. and K.P. Campbell, *A Role for the Dystrophin-Glycoprotein Complex as a Transmembrane Linker between Laminin and Actin.* Journal of Cell Biology, 1993. **122**(4): p. 809-823.
3. Koubassova, N.A. and A.K. Tsaturyan, *Molecular mechanism of actin-myosin motor in muscle.* Biochemistry (Mosc), 2011. **76**(13): p. 1484-506.
4. Bogdanovich, S., et al., *Therapeutics for Duchenne muscular dystrophy: current approaches and future directions.* J Mol Med (Berl), 2004. **82**(2): p. 102-15.
5. Allen, D.G., et al., *Calcium and the damage pathways in muscular dystrophy.* Can J Physiol Pharmacol, 2010. **88**(2): p. 83-91.
6. Deconinck, N. and B. Dan, *Pathophysiology of duchenne muscular dystrophy: current hypotheses.* Pediatr Neurol, 2007. **36**(1): p. 1-7.
7. Blake, D.J., et al., *Function and genetics of dystrophin and dystrophin-related proteins in muscle.* Physiol Rev, 2002. **82**(2): p. 291-329.
8. Gehrig, S.M., et al., *Making Fast-Twitch Dystrophic Muscles Bigger Protects Them from Contraction Injury and Attenuates the Dystrophic Pathology.* American Journal of Pathology, 2010. **176**(1): p. 29-33.
9. Grange, R.W., et al., *Fast-twitch skeletal muscles of dystrophic mouse pups are resistant to injury from acute mechanical stress.* Am J Physiol Cell Physiol, 2002. **283**(4): p. C1090-101.
10. Tadayoni, R., et al., *Dystrophin Dp71: the smallest but multifunctional product of the Duchenne muscular dystrophy gene.* Mol Neurobiol, 2012. **45**(1): p. 43-60.
11. Koenig, M., et al., *Complete cloning of the Duchenne muscular dystrophy (DMD) cDNA and preliminary genomic organization of the DMD gene in normal and affected individuals.* Cell, 1987. **50**(3): p. 509-17.
12. Marden, F.A., et al., *Compositional analysis of muscle in boys with Duchenne muscular dystrophy using MR imaging.* Skeletal Radiology, 2005. **34**(3): p. 140-148.
13. Porter, J.D., et al., *A chronic inflammatory response dominates the skeletal muscle molecular signature in dystrophin-deficient mdx mice.* Hum Mol Genet, 2002. **11**(3): p. 263-72.
14. Kissel, J.T., et al., *Mononuclear cell analysis of muscle biopsies in prednisone- and azathioprine-treated Duchenne muscular dystrophy.* Neurology, 1993. **43**(3 Pt 1): p. 532-6.
15. Spencer, M.J., M.W. Marino, and W.M. Winckler, *Altered pathological progression of diaphragm and quadriceps muscle in TNF-deficient, dystrophin-deficient mice.* Neuromuscul Disord, 2000. **10**(8): p. 612-9.
16. Evans, N.P., et al., *Green tea extract decreases muscle pathology and NF-kappaB immunostaining in regenerating muscle fibers of mdx mice.* Clin Nutr, 2010. **29**(3): p. 391-8.
17. Knieke, K., et al., *Migration of Th1 Lymphocytes Is Regulated by CD152 (CTLA-4)-Mediated Signaling via PI3 Kinase-Dependent Akt Activation.* PLoS One, 2012. **7**(3).
18. Yahiaoui, L., et al., *CC family chemokines directly regulate myoblast responses to skeletal muscle injury.* J Physiol, 2008. **586**(16): p. 3991-4004.
19. Hannun, Y.A. and L.M. Obeid, *Principles of bioactive lipid signalling: lessons from sphingolipids.* Nat Rev Mol Cell Biol, 2008. **9**(2): p. 139-50.
20. Bikman, B.T. and S.A. Summers, *Ceramides as modulators of cellular and whole-body metabolism.* Journal of Clinical Investigation, 2011. **121**(11): p. 4222-4230.

21. Maceyka, M., et al., *Sphingosine kinase, sphingosine-1-phosphate, and apoptosis.* Biochim Biophys Acta, 2002. **1585**(2-3): p. 193-201.
22. Spiegel, S. and S. Milstien, *Sphingosine 1-phosphate, a key cell signaling molecule.* J Biol Chem, 2002. **277**(29): p. 25851-4.
23. Simon, K.W., et al., *Suppression of breast xenograft growth and progression in nude mice: implications for the use of orally administered sphingolipids as chemopreventive agents against breast cancer.* Food Funct, 2010. **1**(1): p. 90-8.
24. Mazzei, J.C., et al., *Suppression of intestinal inflammation and inflammation-driven colon cancer in mice by dietary sphingomyelin: importance of peroxisome proliferator-activated receptor gamma expression.* J Nutr Biochem, 2011. **22**(12): p. 1160-71.
25. Grounds, M.D. and T. Shavlakadze, *Growing muscle has different sarcolemmal properties from adult muscle: A proposal with scientific and clinical implications Reasons to reassess skeletal muscle molecular dynamics, cellular responses and suitability of experimental models of muscle disorders.* Bioessays, 2011. **33**(6): p. 458-468.
26. Scott, W., J. Stevens, and S.A. Binder-Macleod, *Human skeletal muscle fiber type classifications.* Phys Ther, 2001. **81**(11): p. 1810-6.
27. Millman, B.M., *The filament lattice of striated muscle.* Physiol Rev, 1998. **78**(2): p. 359-91.
28. Lieber, R.L., *Skeletal Muscle Structure, Function, and Plasticity*. 2010. p. 6-21.
29. Oda, T., et al., *The nature of the globular- to fibrous-actin transition.* Nature, 2009. **457**(7228): p. 441-5.
30. Itoh-Satoh, M., et al., *Titin mutations as the molecular basis for dilated cardiomyopathy.* Biochemical and Biophysical Research Communications, 2002. **291**(2): p. 385-393.
31. Udaka, J., et al., *Disuse-induced preferential loss of the giant protein titin depresses muscle performance via abnormal sarcomeric organization.* J Gen Physiol, 2008. **131**(1): p. 33-41.
32. Degens, H. and L. Larsson, *Application of skinned single muscle fibres to determine myofilament function in ageing and disease.* J Musculoskelet Neuronal Interact, 2007. **7**(1): p. 56-61.
33. Koubassova, N.A., et al., *Direct modeling of X-ray diffraction pattern from contracting skeletal muscle.* Biophys J, 2008. **95**(6): p. 2880-94.
34. Tamura, T., et al., *Dynamics of thin-filament activation in rabbit skeletal muscle fibers examined by time-resolved x-ray diffraction.* Biophys J, 2009. **96**(3): p. 1045-55.
35. Tanner, B.C., T.L. Daniel, and M. Regnier, *Filament compliance influences cooperative activation of thin filaments and the dynamics of force production in skeletal muscle.* PLoS Comput Biol, 2012. **8**(5): p. e1002506.
36. Agarkova, I. and J.C. Perriard, *The M-band: an elastic web that crosslinks thick filaments in the center of the sarcomere.* Trends in Cell Biology, 2005. **15**(9): p. 477-485.
37. Edman, K.A., *Contractile performance of striated muscle.* Adv Exp Med Biol, 2010. **682**: p. 7-40.
38. Huxley, A.F., *Muscle structure and theories of contraction.* Prog Biophys Biophys Chem, 1957. **7**: p. 255-318.
39. Huxley, H.E., *Fifty years of muscle and the sliding filament hypothesis.* Eur J Biochem, 2004. **271**(8): p. 1403-15.
40. Protasi, F., *Structural interaction between RYRs and DHPRs in calcium release units of cardiac and skeletal muscle cells.* Frontiers in Bioscience, 2002. **7**: p. D650-D658.
41. Call, J.A., et al., *Adaptive strength gains in dystrophic muscle exposed to repeated bouts of eccentric contraction.* Journal of Applied Physiology, 2011. **111**(6): p. 1768-1777.
42. Periasamy, M. and A. Kalyanasundaram, *SERCA pump isoforms: Their role in calcium transport and disease.* Muscle & Nerve, 2007. **35**(4): p. 430-442.

43. Kinnunen, S. and S. Manttari, *Specific effects of endurance and sprint training on protein expression of calsequestrin and SERCA in mouse skeletal muscle.* Journal of Muscle Research and Cell Motility, 2012. **33**(2): p. 123-130.
44. Schiaffino, S. and C. Reggiani, *Fiber Types in Mammalian Skeletal Muscles.* Physiological Reviews, 2011. **91**(4): p. 1447-1531.
45. Enoka, R.M. and J. Duchateau, *Muscle fatigue: what, why and how it influences muscle function.* J Physiol, 2008. **586**(1): p. 11-23.
46. Mendell, L.M., *The size principle: a rule describing the recruitment of motoneurons.* J Neurophysiol, 2005. **93**(6): p. 3024-6.
47. Peter, J.B., et al., *Metabolic profiles of three fiber types of skeletal muscle in guinea pigs and rabbits.* Biochemistry, 1972. **11**(14): p. 2627-33.
48. Mela, P., et al., *The optimal stimulation pattern for skeletal muscle is dependent on muscle length.* Ieee Transactions on Neural Systems and Rehabilitation Engineering, 2002. **10**(2): p. 85-93.
49. Lieber, R.L. and S.C. Bodine-Fowler, *Skeletal muscle mechanics: implications for rehabilitation.* Phys Ther, 1993. **73**(12): p. 844-56.
50. Harris, J.B. and P. Wilson, *Mechanical properties of dystrophic mouse muscle.* J Neurol Neurosurg Psychiatry, 1971. **34**(5): p. 512-20.
51. Dupont-Versteegden, E.E. and R.J. McCarter, *Differential expression of muscular dystrophy in diaphragm versus hindlimb muscles of mdx mice.* Muscle Nerve, 1992. **15**(10): p. 1105-10.
52. Gailly, P., *New aspects of calcium signaling in skeletal muscle cells: implications in Duchenne muscular dystrophy.* Biochim Biophys Acta, 2002. **1600**(1-2): p. 38-44.
53. Gillis, J.M., *Understanding dystrophinopathies: an inventory of the structural and functional consequences of the absence of dystrophin in muscles of the mdx mouse.* J Muscle Res Cell Motil, 1999. **20**(7): p. 605-25.
54. Enoka, R.M., *Muscle fatigue--from motor units to clinical symptoms.* J Biomech, 2012. **45**(3): p. 427-33.
55. Gregorevic, P., et al., *Improved contractile function of the mdx dystrophic mouse diaphragm muscle after insulin-like growth factor-I administration.* Am J Pathol, 2002. **161**(6): p. 2263-72.
56. Brioschi, S., et al., *Genetic characterization in symptomatic female DMD carriers: lack of relationship between X-inactivation, transcriptional DMD allele balancing and phenotype.* Bmc Medical Genetics, 2012. **13**.
57. Nigro, G., *One-hundred-seventy-five years of Neapolitan contributions to the fight against the muscular diseases.* Acta Myol, 2010. **29**(3): p. 369-91.
58. Clarac, F. and J.G. Barbara, *The emergence of the "motoneuron concept": From the early 19th C to the beginning of the 20th C.* Brain Research, 2011. **1409**: p. 23-41.
59. Tidball, J.G. and M. Wehling-Henricks, *The role of free radicals in the pathophysiology of muscular dystrophy.* J Appl Physiol, 2007. **102**(4): p. 1677-86.
60. Markert, C.D., et al., *Exercise and duchenne muscular dystrophy: Where we have been and where we need to go.* Muscle & Nerve, 2012. **45**(5): p. 746-751.
61. Darras, B.T., D.T. Miller, and D.K. Urion, *Dystrophinopathies.* 1993.
62. Wilkins, K.E. and D.A. Gibson, *The patterns of spinal deformity in Duchenne muscular dystrophy.* J Bone Joint Surg Am, 1976. **58**(1): p. 24-32.
63. Ganea, R., et al., *Gait assessment in children with duchenne muscular dystrophy during long-distance walking.* J Child Neurol, 2012. **27**(1): p. 30-8.
64. Kornegay, J.N., et al., *Canine models of Duchenne muscular dystrophy and their use in therapeutic strategies.* Mammalian Genome, 2012. **23**(1-2): p. 85-108.
65. Hoffman, E.P., R.H. Brown, Jr., and L.M. Kunkel, *Dystrophin: the protein product of the Duchenne muscular dystrophy locus.* Cell, 1987. **51**(6): p. 919-28.

66. Bendixen, R.M., et al., *Participation and quality of life in children with Duchenne muscular dystrophy using the international classification of functioning, disability, and health.* Health Qual Life Outcomes, 2012. **10**(1): p. 43.
67. Hoffman, E.P., et al., *Restoring Dystrophin Expression in Duchenne Muscular Dystrophy Muscle Progress in Exon Skipping and Stop Codon Read Through.* American Journal of Pathology, 2011. **179**(1): p. 12-22.
68. Koenig, M., A.P. Monaco, and L.M. Kunkel, *The complete sequence of dystrophin predicts a rod-shaped cytoskeletal protein.* Cell, 1988. **53**(2): p. 219-28.
69. Roberts, R.G., *Dystrophins and dystrobrevins.* Genome Biol, 2001. **2**(4): p. REVIEWS3006.
70. Gumerson, J.D. and D.E. Michele, *The dystrophin-glycoprotein complex in the prevention of muscle damage.* J Biomed Biotechnol, 2011. **2011**: p. 210797.
71. Sunada, Y. and K.P. Campbell, *Dystrophin-glycoprotein complex: molecular organization and critical roles in skeletal muscle.* Curr Opin Neurol, 1995. **8**(5): p. 379-84.
72. Kramarcy, N.a.S., R, *Syntrophin Isoforms at the Neuromuscular Junction: Developmental Time Course and Differential Localization.* Molecular and Cellular Neuroscience, 2000. **15**(3): p. 262-274.
73. Cirak, S., et al., *Restoration of the dystrophin-associated glycoprotein complex after exon skipping therapy in Duchenne muscular dystrophy.* Mol Ther, 2012. **20**(2): p. 462-7.
74. Chandrasekharan, K. and P.T. Martin, *Genetic defects in muscular dystrophy.* Methods Enzymol, 2010. **479**: p. 291-322.
75. Millay, D.P., et al., *Genetic and pharmacologic inhibition of mitochondrial-dependent necrosis attenuates muscular dystrophy.* Nat Med, 2008. **14**(4): p. 442-7.
76. Collins, C.A. and J.E. Morgan, *Duchenne's muscular dystrophy: animal models used to investigate pathogenesis and develop therapeutic strategies.* International Journal of Experimental Pathology, 2003. **84**(4): p. 165-172.
77. Nakamura, A. and S. Takeda, *Mammalian Models of Duchenne Muscular Dystrophy: Pathological Characteristics and Therapeutic Applications.* Journal of Biomedicine and Biotechnology, 2011.
78. Bulfield, G., et al., *X chromosome-linked muscular dystrophy (mdx) in the mouse.* Proc Natl Acad Sci U S A, 1984. **81**(4): p. 1189-92.
79. Muller, J., et al., *Comparative evolution of muscular dystrophy in diaphragm, gastrocnemius and masseter muscles from old male mdx mice.* J Muscle Res Cell Motil, 2001. **22**(2): p. 133-9.
80. Juretic, N., et al., *Electrical Stimulation Induces Calcium-dependent Up-regulation of Neuregulin-1beta in Dystrophic Skeletal Muscle Cell Lines.* Cell Physiol Biochem, 2012. **29**(5-6): p. 919-30.
81. Perronnet, C. and C. Vaillend, *Dystrophins, utrophins, and associated scaffolding complexes: role in mammalian brain and implications for therapeutic strategies.* J Biomed Biotechnol, 2010. **2010**: p. 849426.
82. Zhou, G.Q., et al., *Current understanding of dystrophin-related muscular dystrophy and therapeutic challenges ahead.* Chin Med J (Engl), 2006. **119**(16): p. 1381-91.
83. Haenggi, T. and J.M. Fritschy, *Role of dystrophin and utrophin for assembly and function of the dystrophin glycoprotein complex in non-muscle tissue.* Cell Mol Life Sci, 2006. **63**(14): p. 1614-31.
84. Tinsley, J.M. and K.E. Davies, *Utrophin: a potential replacement for dystrophin?* Neuromuscul Disord, 1993. **3**(5-6): p. 537-9.
85. Hirst, R.C., K.J. McCullagh, and K.E. Davies, *Utrophin upregulation in Duchenne muscular dystrophy.* Acta Myol, 2005. **24**(3): p. 209-16.
86. Perkins, K.J. and K.E. Davies, *The role of utrophin in the potential therapy of Duchenne muscular dystrophy.* Neuromuscul Disord, 2002. **12 Suppl 1**: p. S78-89.

87. Deconinck, N., et al., *Expression of truncated utrophin leads to major functional improvements in dystrophin-deficient muscles of mice.* Nat Med, 1997. **3**(11): p. 1216-21.
88. Tinsley, J., et al., *Expression of full-length utrophin prevents muscular dystrophy in mdx mice.* Nat Med, 1998. **4**(12): p. 1441-4.
89. Fairclough, R.J., M.J. Wood, and K.E. Davies, *Therapy for Duchenne muscular dystrophy: renewed optimism from genetic approaches.* Nat Rev Genet, 2013. **14**(6): p. 373-8.
90. Mattei, E., et al., *Utrophin up-regulation by an artificial transcription factor in transgenic mice.* PLoS One, 2007. **2**(8): p. e774.
91. Roberts, R.G., *Dystrophin, its gene, and the dystrophinopathies.* Adv Genet, 1995. **33**: p. 177-231.
92. Tidball, J.G. and D.J. Law, *Dystrophin Is Required for Normal Thin Filament Membrane Associations at Myotendinous Junctions.* American Journal of Pathology, 1991. **138**(1): p. 17-21.
93. Pardo, J.V., J.D. Siliciano, and S.W. Craig, *A Vinculin-Containing Cortical Lattice in Skeletal-Muscle - Transverse Lattice Elements (Costameres) Mark Sites of Attachment between Myofibrils and Sarcolemma.* Proceedings of the National Academy of Sciences of the United States of America-Biological Sciences, 1983. **80**(4): p. 1008-1012.
94. Danowski, B.A., et al., *Costameres are sites of force transmission to the substratum in adult rat cardiomyocytes.* J Cell Biol, 1992. **118**(6): p. 1411-20.
95. Rybakova, I.N., J.R. Patel, and J.M. Ervasti, *The dystrophin complex forms a mechanically strong link between the sarcolemma and costameric actin.* Journal of Cell Biology, 2000. **150**(5): p. 1209-1214.
96. Petrof, B.J., et al., *Adaptations in myosin heavy chain expression and contractile function in dystrophic mouse diaphragm.* Am J Physiol, 1993. **265**(3 Pt 1): p. C834-41.
97. Straub, V., et al., *Animal models for muscular dystrophy show different patterns of sarcolemmal disruption.* Journal of Cell Biology, 1997. **139**(2): p. 375-385.
98. Petrof, B.J., et al., *Dystrophin Protects the Sarcolemma from Stresses Developed during Muscle-Contraction.* Proceedings of the National Academy of Sciences of the United States of America, 1993. **90**(8): p. 3710-3714.
99. Matsuda, R., A. Nishikawa, and H. Tanaka, *Visualization of Dystrophic Muscle-Fibers in Mdx Mouse by Vital Staining with Evans Blue - Evidence of Apoptosis in Dystrophin-Deficient Muscle.* Journal of Biochemistry, 1995. **118**(5): p. 959-964.
100. Spencer, M.J. and R.L. Mellgren, *Overexpression of a calpastatin transgene in mdx muscle reduces dystrophic pathology.* Hum Mol Genet, 2002. **11**(21): p. 2645-55.
101. Vandebrouck, C., et al., *Involvement of TRPC in the abnormal calcium influx observed in dystrophic (mdx) mouse skeletal muscle fibers.* J Cell Biol, 2002. **158**(6): p. 1089-96.
102. Tidball, J.G. and M.J. Spencer, *Calpains and muscular dystrophies.* Int J Biochem Cell Biol, 2000. **32**(1): p. 1-5.
103. Goldspink, G., *Changes in muscle mass and phenotype and the expression of autocrine and systemic growth factors by muscle in response to stretch and overload.* J Anat, 1999. **194 (Pt 3)**: p. 323-34.
104. Nakamura, A., G.V. Harrod, and K.E. Davies, *Activation of calcineurin and stress activated protein kinase/p38-mitogen activated protein kinase in hearts of utrophin-dystrophin knockout mice.* Neuromuscul Disord, 2001. **11**(3): p. 251-9.
105. Sander, M., et al., *Functional muscle ischemia in neuronal nitric oxide synthase-deficient skeletal muscle of children with Duchenne muscular dystrophy.* Proc Natl Acad Sci U S A, 2000. **97**(25): p. 13818-23.
106. Wehling, M., M.J. Spencer, and J.G. Tidball, *A nitric oxide synthase transgene ameliorates muscular dystrophy in mdx mice.* J Cell Biol, 2001. **155**(1): p. 123-31.

107. Watchko, J.F., T.L. O'Day, and E.P. Hoffman, *Functional characteristics of dystrophic skeletal muscle: insights from animal models.* J Appl Physiol, 2002. **93**(2): p. 407-17.
108. Rock, K.L., et al., *The sterile inflammatory response.* Annu Rev Immunol, 2010. **28**: p. 321-42.
109. Ryan, G.B. and G. Majno, *Acute inflammation. A review.* Am J Pathol, 1977. **86**(1): p. 183-276.
110. Macarthur, M., G.L. Hold, and E.M. El-Omar, *Inflammation and Cancer II. Role of chronic inflammation and cytokine gene polymorphisms in the pathogenesis of gastrointestinal malignancy.* Am J Physiol Gastrointest Liver Physiol, 2004. **286**(4): p. G515-20.
111. Vestweber, D., *Novel insights into leukocyte extravasation.* Current Opinion in Hematology, 2012. **19**(3): p. 212-217.
112. Cannon, J.G., *Inflammatory Cytokines in Nonpathological States.* News Physiol Sci, 2000. **15**: p. 298-303.
113. Vilcek, J. and M. Feldmann, *Historical review: Cytokines as therapeutics and targets of therapeutics.* Trends Pharmacol Sci, 2004. **25**(4): p. 201-9.
114. Fernandez, E.J. and E. Lolis, *Structure, function, and inhibition of chemokines.* Annu Rev Pharmacol Toxicol, 2002. **42**: p. 469-99.
115. Ono, S.J., et al., *Chemokines: roles in leukocyte development, trafficking, and effector function.* J Allergy Clin Immunol, 2003. **111**(6): p. 1185-99; quiz 1200.
116. Laing, K.J. and C.J. Secombes, *Chemokines.* Dev Comp Immunol, 2004. **28**(5): p. 443-60.
117. Chen, Y.W., et al., *Expression profiling in the muscular dystrophies: identification of novel aspects of molecular pathophysiology.* J Cell Biol, 2000. **151**(6): p. 1321-36.
118. Farini, A., et al., *T- and B-lymphocytes depletion has a great effect on the fibrosis of the dystrophic skeletal muscles in the scid/mdx mouse.* Neuromuscular Disorders, 2007. **17**(9-10): p. 804-804.
119. Evans, N., et al., *Disregulated intracellular signaling and inflammatory gene expression during acute disease onset in Duchenne muscular dystrophy.* Am. J Phys Med and Rehab, 2009. **88**(6): p. 502-522.
120. Karin, M. and Y. Ben-Neriah, *Phosphorylation meets ubiquitination: the control of NF-[kappa]B activity.* Annu Rev Immunol, 2000. **18**: p. 621-63.
121. Karin, M. and A. Lin, *NF-kappa B at the crossroads of life and death.* Nature Immunology, 2002. **3**(3): p. 221-227.
122. Messina, S., et al., *Activation of NF-kappaB pathway in Duchenne muscular dystrophy: relation to age.* Acta Myol, 2011. **30**(1): p. 16-23.
123. Ehrhardt, C. and S. Ludwig, *A new player in a deadly game: influenza viruses and the PI3K/Akt signalling pathway.* Cell Microbiol, 2009. **11**(6): p. 863-71.
124. Peter, A.K. and R.H. Crosbie, *Hypertrophic response of Duchenne and limb-girdle muscular dystrophies is associated with activation of Akt pathway.* Experimental Cell Research, 2006. **312**(13): p. 2580-2591.
125. Peter, A.K., et al., *Myogenic Akt signaling upregulates the utrophin-glycoprotein complex and promotes sarcolemma stability in muscular dystrophy.* Hum Mol Genet, 2009. **18**(2): p. 318-27.
126. Xiong, Y., Y. Zhou, and H.W. Jarrett, *Dystrophin glycoprotein complex-associated Gbetagamma subunits activate phosphatidylinositol-3-kinase/Akt signaling in skeletal muscle in a laminin-dependent manner.* J Cell Physiol, 2009. **219**(2): p. 402-14.
127. Langenbach, K.J. and T.A. Rando, *Inhibition of dystroglycan binding to laminin disrupts the PI3K/AKT pathway and survival signaling in muscle cells.* Muscle Nerve, 2002. **26**(5): p. 644-53.

128. Papadakis, K.A. and S.R. Targan, *The role of chemokines and chemokine receptors in mucosal inflammation.* Inflamm Bowel Dis, 2000. **6**(4): p. 303-13.
129. Ye, R.D., *Regulation of nuclear factor kappaB activation by G-protein-coupled receptors.* J Leukoc Biol, 2001. **70**(6): p. 839-48.
130. Kottlors, M. and J. Kirschner, *Elevated satellite cell number in Duchenne muscular dystrophy.* Cell Tissue Res, 2010. **340**(3): p. 541-8.
131. Seale, P., et al., *Pax7 is required for the specification of myogenic satellite cells.* Cell, 2000. **102**(6): p. 777-86.
132. Zammit, P.S., et al., *Pax7 and myogenic progression in skeletal muscle satellite cells.* J Cell Sci, 2006. **119**(Pt 9): p. 1824-32.
133. Zammit, P.S., *All muscle satellite cells are equal, but are some more equal than others?* J Cell Sci, 2008. **121**(Pt 18): p. 2975-82.
134. Heslop, L., J.E. Morgan, and T.A. Partridge, *Evidence for a myogenic stem cell that is exhausted in dystrophic muscle.* J Cell Sci, 2000. **113 (Pt 12)**: p. 2299-308.
135. Grange, R.W. and J.A. Call, *Recommendations to define exercise prescription for Duchenne muscular dystrophy.* Exerc Sport Sci Rev, 2007. **35**(1): p. 12-7.
136. Spiegel, S. and S. Milstien, *Sphingosine-1-phosphate: an enigmatic signalling lipid.* Nat Rev Mol Cell Biol, 2003. **4**(5): p. 397-407.
137. Gangoiti, P., et al., *Control of metabolism and signaling of simple bioactive sphingolipids: Implications in disease.* Prog Lipid Res, 2010. **49**(4): p. 316-34.
138. Bartke, N. and Y.A. Hannun, *Bioactive sphingolipids: metabolism and function.* Journal of Lipid Research, 2009. **50**: p. S91-S96.
139. Zheng, W., et al., *Ceramides and other bioactive sphingolipid backbones in health and disease: lipidomic analysis, metabolism and roles in membrane structure, dynamics, signaling and autophagy.* Biochim Biophys Acta, 2006. **1758**(12): p. 1864-84.
140. Ponnusamy, S., et al., *Sphingolipids and cancer: ceramide and sphingosine-1-phosphate in the regulation of cell death and drug resistance.* Future Oncol, 2010. **6**(10): p. 1603-24.
141. Gault, C.R., L.M. Obeid, and Y.A. Hannun, *An overview of sphingolipid metabolism: from synthesis to breakdown.* Adv Exp Med Biol, 2010. **688**: p. 1-23.
142. Nilsson, A. and R.D. Duan, *Absorption and lipoprotein transport of sphingomyelin.* Journal of Lipid Research, 2006. **47**(1): p. 154-71.
143. Vesper, H., et al., *Sphingolipids in food and the emerging importance of sphingolipids to nutrition.* J Nutr, 1999. **129**(7): p. 1239-50.
144. Duan, R.D. and A. Nilsson, *Metabolism of sphingolipids in the gut and its relation to inflammation and cancer development.* Prog Lipid Res, 2009. **48**(1): p. 62-72.
145. Holthuis, J.C., et al., *The organizing potential of sphingolipids in intracellular membrane transport.* Physiol Rev, 2001. **81**(4): p. 1689-723.
146. Adams, J.M., et al., *Ceramide content is increased in skeletal muscle from obese insulin-resistant humans.* Diabetes, 2004. **53**(1): p. 25-31.
147. Stoica, B.A., et al., *Ceramide-induced neuronal apoptosis is associated with dephosphorylation of Akt, BAD, FKHR, GSK-3 beta, and induction of the mitochondrial-dependent intrinsic caspase pathway.* Molecular and Cellular Neuroscience, 2003. **22**(3): p. 365-382.
148. Bourbon, N.A., J. Yun, and M. Kester, *Ceramide directly activates protein kinase C zeta to regulate a stress-activated protein kinase signaling complex.* J Biol Chem, 2000. **275**(45): p. 35617-23.
149. Rosen, H., et al., *Sphingosine 1-phosphate receptor signaling.* Annu Rev Biochem, 2009. **78**: p. 743-68.
150. Maines, L.W., et al., *Suppression of ulcerative colitis in mice by orally available inhibitors of sphingosine kinase.* Dig Dis Sci, 2008. **53**(4): p. 997-1012.

151. Fyrst, H., et al., *Natural sphingadienes inhibit Akt-dependent signaling and prevent intestinal tumorigenesis.* Cancer Res, 2009. **69**(24): p. 9457-64.
152. Zhang, P., et al., *Dietary sphingomyelin inhibits colonic tumorigenesis with an up-regulation of alkaline sphingomyelinase expression in ICR mice.* Anticancer Res, 2008. **28**(6A): p. 3631-5.
153. Zhang, Y., et al., *Crucial role of alkaline sphingomyelinase in sphingomyelin digestion: a study on enzyme knockout mice.* J Lipid Res, 2011. **52**(4): p. 771-81.
154. Duan, R.D., *Physiological functions and clinical implications of sphingolipids in the gut.* J Dig Dis, 2011. **12**(2): p. 60-70.
155. Bartke, N. and Y.A. Hannun, *Bioactive sphingolipids: metabolism and function.* Journal of Lipid Research, 2009. **50 Suppl**: p. S91-6.
156. Bjorklund, S., et al., *Effects of sphingosine 1-phosphate on calcium signaling, proliferation and S1P2 receptor expression in PC Cl3 rat thyroid cells.* Mol Cell Endocrinol, 2005. **231**(1-2): p. 65-74.
157. Baltgalvis, K.A., et al., *Effects of prednisolone on skeletal muscle contractility in mdx mice.* Muscle Nerve, 2009. **40**(3): p. 443-54.
158. Creekmore, A.L., et al., *Changes in gene expression and cellular architecture in an ovarian cancer progression model.* PLoS One, 2011. **6**(3): p. e17676.
159. Sabbadini, R.A., et al., *The effects of sphingosine on sarcoplasmic reticulum membrane calcium release.* J Biol Chem, 1992. **267**(22): p. 15475-84.
160. Ghosh, N., R. Sabbadini, and S. Chatterjee, *Identification, partial purification, and localization of a neutral sphingomyelinase in rabbit skeletal muscle: neutral sphingomyelinase in skeletal muscle.* Mol Cell Biochem, 1998. **189**(1-2): p. 161-8.
161. Danieli-Betto, D., et al., *Sphingosine 1-phosphate protects mouse extensor digitorum longus skeletal muscle during fatigue.* Am J Physiol Cell Physiol, 2005. **288**(6): p. C1367-73.
162. Takagi, A., et al., *Increased Leakage of Calcium-Ion from the Sarcoplasmic-Reticulum of the Mdx Mouse.* Journal of the Neurological Sciences, 1992. **110**(1-2): p. 160-164.
163. Woods, C.E., et al., *The action potential-evoked sarcoplasmic reticulum calcium release is impaired in mdx mouse muscle fibres.* Journal of Physiology-London, 2004. **557**(1): p. 59-75.
164. Blouin, J.S., et al., *High-frequency submaximal stimulation over muscle evokes centrally generated forces in human upper limb skeletal muscles.* Journal of Applied Physiology, 2009. **106**(2): p. 370-377.
165. Vollestad, N.K., *Measurement of human muscle fatigue.* J Neurosci Methods, 1997. **74**(2): p. 219-27.
166. Hardiman, O., *Dystrophin deficiency, altered cell signalling and fibre hypertrophy.* Neuromuscul Disord, 1994. **4**(4): p. 305-15.
167. Chamberlain, J.S., et al., *Dystrophin-deficient mdx mice display a reduced life span and are susceptible to spontaneous rhabdomyosarcoma.* FASEB J, 2007. **21**(9): p. 2195-204.
168. Syriga, M. and M. Mavroidis, *Complement system activation in cardiac and skeletal muscle pathology: friend or foe?* Adv Exp Med Biol, 2013. **735**: p. 207-18.
169. Romagnani, S., *Cytokines and chemoattractants in allergic inflammation.* Mol Immunol, 2002. **38**(12-13): p. 881-5.
170. Baker, C., et al., *SERPINA3 (aka alpha-1-antichymotrypsin).* Front Biosci, 2007. **12**: p. 2821-35.
171. Palming, J., et al., *Plasma cells and Fc receptors in human adipose tissue-lipogenic and anti-inflammatory effects of immunoglobulins on adipocytes.* Biochemical and Biophysical Research Communications, 2006. **343**(1): p. 43-48.

172. Sweetwyne, M.T. and J.E. Murphy-Ullrich, *Thrombospondin1 in tissue repair and fibrosis: TGF-beta-dependent and independent mechanisms.* Matrix Biol, 2012. **31**(3): p. 178-86.
173. De Luna, N., et al., *Role of thrombospondin 1 in macrophage inflammation in dysferlin myopathy.* J Neuropathol Exp Neurol, 2010. **69**(6): p. 643-53.
174. Turk, R., et al., *Muscle regeneration in dystrophin-deficient mdx mice studied by gene expression profiling.* BMC Genomics, 2005. **6**: p. 98.
175. Kumar, A. and A.M. Boriek, *Mechanical stress activates the nuclear factor-kappaB pathway in skeletal muscle fibers: a possible role in Duchenne muscular dystrophy.* FASEB J, 2003. **17**(3): p. 386-96.
176. Villalta, S.A., et al., *IFN-gamma promotes muscle damage in the mdx mouse model of Duchenne muscular dystrophy by suppressing M2 macrophage activation and inhibiting muscle cell proliferation.* J Immunol, 2011. **187**(10): p. 5419-28.
177. Loh, K.C., et al., *Sphingosine-1-phosphate enhances satellite cell activation in dystrophic muscles through a S1PR2/STAT3 signaling pathway.* PLoS One, 2012. **7**(5): p. e37218.
178. Ferreira, L.F., et al., *Sphingomyelinase depresses force and calcium sensitivity of the contractile apparatus in mouse diaphragm muscle fibers.* J Appl Physiol, 2012. **112**(9): p. 1538-45.
179. Call, J.A., et al., *Adaptive strength gains in dystrophic muscle exposed to repeated bouts of eccentric contraction.* J Appl Physiol, 2011. **111**(6): p. 1768-77.
180. Call, J.A., et al., *Progressive resistance voluntary wheel running in the mdx mouse.* Muscle Nerve, 2010. **42**(6): p. 871-80.
181. Bennett, A.F., *Thermal dependence of muscle function.* Am J Physiol, 1984. **247**(2 Pt 2): p. R217-29.

Appendices

Appendix A. Preliminary Data

Methods

The previous study was used to identify specific genetic markers pertaining to the inflammatory response in C57BL6 and mdx mice. Mice were fed an AIN 76A diet with or without 0.01% dietary sphingolipids for 3 weeks starting at an age of 3 weeks. After treatment, mice were euthanized, TA muscles were collected, pooled, and mRNA was extracted to be run on an Affymetrix mouse 2.0A mouse gene chip, with two chips per treatment group. VBI services provided hybridization and data analysis of the gene chip. Gene chip data were evaluated to determine significant fold changes between treatment groups (>2.0, <0.5). Genes selected were run through GeneTrail Advanced Gene Set Enrichment Analysis to identify inflammatory related genes ($p<0.05$). To confirm fold changes observed by microarray analysis, qRT-PCR was performed. RNA extraction, qRT-PCR methods, and primer set optimization were performed as described in Chapter 3.

Results/Discussion

Microarray analysis revealed 53 genetic markers of inflammation that were differentially expressed in TA samples. A classification of these markers can be seen in table A.1. Of these, 16 were verified through qRT-PCR. From the microarray, numerous genetic markers were increased in mdx, but were decreased by sphingolipid treatment (i.e. Acp5, C1qa, C1qb). Verification by qRT-PCR revealed some similar changes (Acp5, C1qa) as seen in the microarray, while others were different from the microarray (C1qb, Serpina3n). Of note, the control used was a C57BL6, whereas the data presented in Chapter 4 reflects a C57BL10 control. Due to a small sample number, statistical analysis could not be performed.

Table A.1. Classification of detected inflammatory markers.

Class	Observed Genes

Complement System	12
Cytokine and Receptors	8
Chemokine and Receptors	8
Lymphoid and Myeloid Markers	22
Vascular Response/Permeability	2
Antioxidant	1
Total	**53**

Table A.2. Functions of the 16 Selected Markers

Classification	Function
Complement System	
Complement component 1, q subcomponent, alpha (C1qa)	Complement activation-classical pathway, complement and coagulation cascades, innate immune signaling
Complement component 1, q subcomponent beta polypeptide (C1qb)	Complement activation-classical pathway, complement and coagulation cascades, innate immune signaling
Complement component 1, q subcomponent, C chain (C1qc)	Complement activation-classical pathway, complement and coagulation cascades, innate immune signaling
CD59a antigen (CD59a)	Complement and coagulation cascades, hematopoietic cell lineage

Complement factor D (adipsin) (Cfd)	Complement and coagulation cascades, platelet activation and degranulation, hemostasis, immune signaling
Complement factor properdin (Cfp)	Complement activation-alternative pathway, complement and coagulation cascades, immune response
Serine (or cysteine) peptidase inhibitor, clade A, member 3N (Serpina3n)	Complement and coagulation cascades, platelet activation and degranulation, hemostasis
Cytokines and Receptors	
Arachidonate 5-lipoxygenase activating protein (Alox5ap)	Il-5 signaling pathway, production of leukotriene
Chemokines and Receptors	
Chemokine (C-C motif) ligand 2 (Ccl2)	Chemokine signaling pathway
Chemokine (C-C motif) ligand 8 (Ccl8)	Chemokine signaling pathway, cytokine-cytokine receptor interaction
Chemokine (C-C motif) receptor 5 (Ccr5)	Chemokine signaling pathway, GPCR signaling and binding, endocytosis
Lymphoid and Myeloid Markers	

Acid phosphatase 5, tartrate resistant (Acp5)	lysosomal activity, osteoclast differentiation, metabolism of vitamins and cofactors
Fc receptor, IgE, high affinity I, gamma polypeptide (Fcer1g)	Fc epsilon RI signaling pathway, NK cell mediated cytotoxicity, hemostasis
Lymphocyte antigen 86 (Ly86)	Lymphocyte activation, innate immune response
Vascular Response/Permeability	
Fibronectin 1 (Fn1)	Platelet activation and degranulation, focal adhesion, regulation of actin cytoskeleton
Thrombospondin 1 (Thbs1)	Platelet activation and degranulation, focal adhesion, integrin cell surface interactions

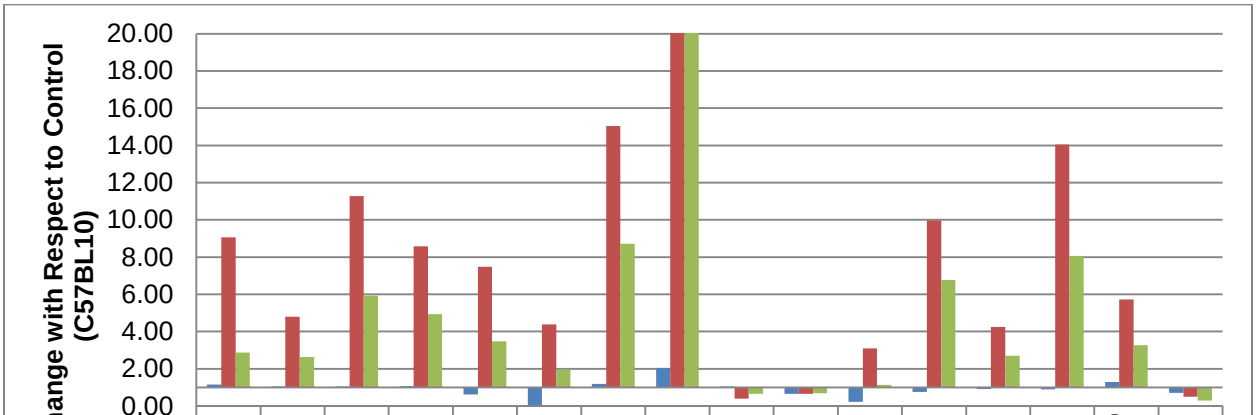

	Acp5	Alox5ap	C1qa	C1qb	C1qc	Ccl2	Ccl8	Ccr5	Cd59a	Cfd	Cfp	Fcer1g	Fn1	Ly86	Serpina3n	Thbs1
WT+S	1.14	1.04	1.05	1.06	0.62	0.06	1.18	2.04	1.04	0.65	0.23	0.76	0.92	0.90	1.29	0.70
MDX	9.06	4.79	11.2	8.58	7.49	4.39	15.0	56.7	0.40	0.66	3.09	9.97	4.25	14.0	5.72	0.51
MDX+S	2.87	2.64	5.93	4.93	3.48	1.96	8.72	28.5	0.66	0.69	1.13	6.77	2.70	8.06	3.27	0.29

Figure A.1. Microarray results of selected genes. Relative to a C57BL6 control

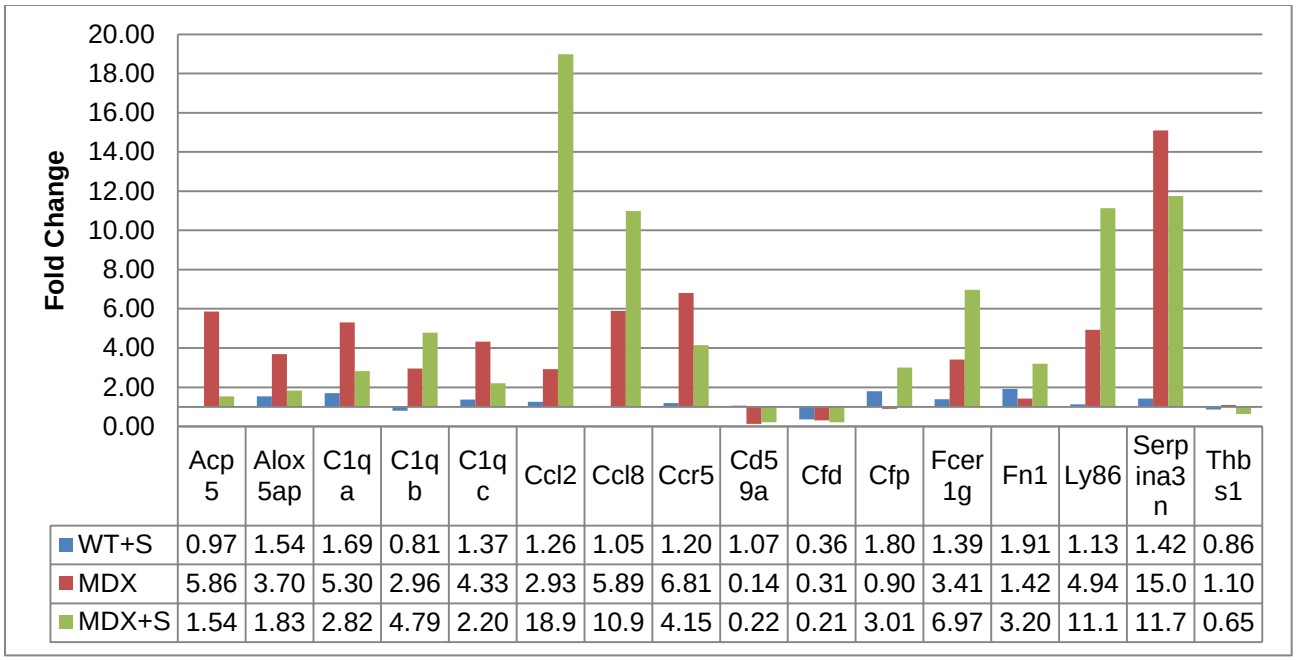

	Acp5	Alox5ap	C1qa	C1qb	C1qc	Ccl2	Ccl8	Ccr5	Cd59a	Cfd	Cfp	Fcer1g	Fn1	Ly86	Serpina3n	Thbs1
WT+S	0.97	1.54	1.69	0.81	1.37	1.26	1.05	1.20	1.07	0.36	1.80	1.39	1.91	1.13	1.42	0.86
MDX	5.86	3.70	5.30	2.96	4.33	2.93	5.89	6.81	0.14	0.31	0.90	3.41	1.42	4.94	15.0	1.10
MDX+S	1.54	1.83	2.82	4.79	2.20	18.9	10.9	4.15	0.22	0.21	3.01	6.97	3.20	11.1	11.7	0.65

Figure A.2. qRT-PCR results of selected genes. Relative to a C57BL6 control.